Title
Electrolyte Engineering to Improve Capacity and Rechargeablility in the Lithium-Oxygen Battery

Author
Burke, Colin M

Publication Date
2018

Peer reviewed|Thesis/dissertation

Electrolyte Engineering to Improve Capacity and Rechargeablility in the Lithium-Oxygen Battery

By

Colin M. Burke

A dissertation submitted in partial satisfaction of the

requirements for the degree of

Doctor of Philosophy

in

Chemical Engineering

in the

Graduate Division

of the

University of California, Berkeley

Committee in charge:

Professor Bryan D. McCloskey, Chair
Professor Nitash P. Balsara
Professor Angelica M. Stacy

Summer 2018

Electrolyte Engineering to Improve Capacity and Rechargeablility
in the Lithium-Oxygen Battery

by
Colin M. Burke

Abstract

Electrolyte Engineering to Improve Capacity and Rechargeability
in the Lithium-Oxygen Battery

by

Colin M. Burke

Doctor of Philosophy in Chemical Engineering

University of California, Berkeley

Professor Bryan D. McCloskey, Chair

A primary goal in rechargeable battery research is developing batteries with higher specific energies, with motivations including increasing electric vehicle range and enabling new deep space technologies. One such option, the nonaqueous lithium-oxygen (Li-O_2) battery, consists of a lithium negative electrode, a lithium salt and ether-based electrolyte, an electrolyte-soaked porous carbon positive electrode, and a gaseous oxygen headspace, and operates via the electrochemical formation (discharge) and decomposition (charge) of lithium peroxide (Li_2O_2). With an estimated theoretical specific energy of 3330 Wh/kg active material (Li_2O_2), more than four times that of current lithium-ion positive electrode materials, and a relatively low cost of battery components, the nonaqueous lithium-oxygen (Li-O_2) battery has garnered significant research attention over the past decade.

Unfortunately, critical challenges have been identified that prevent the realization of a high-capacity, rechargeable Li-O_2 battery. The ultimate discharge product, Li_2O_2, is insoluble in the most stable nonaqueous electrolytes and is a wide-band gap insulator, so during discharge it forms as a solid on the cathode's carbon support and electronically passivates it, preventing further discharge after only a small amount of Li_2O_2 has formed. Li_2O_2 and its electrochemical intermediates also undergo irreversible side reactions with the nonaqueous electrolytes and carbon positive electrodes studied to-date, causing poor battery rechargeability.

In this work, the nonaqueous electrolyte of the Li-O_2 was engineered toward addressing these challenges and achieving a high-capacity, rechargeable Li-O_2 battery. Toward increasing achievable discharge capacity, the ability of electrolytes to induce solubility of the intermediate to Li_2O_2 formation, lithium superoxide (LiO_2), was studied, as this enables a solution mechanism of growth whereby Li_2O_2 grows in large, aggregated structures, allowing more Li_2O_2 to form before cathode passivation. First, the effect of the lithium salt anion on LiO_2 solubility was studied. To do so, a typical lithium battery salt,

lithium bis(trifluoromethane) sulfonimide (LiTFSI), was partially exchanged for the more strongly electron-donating lithium nitrate ($LiNO_3$) in Li-O_2 battery electrolytes. During galvanostatic conditions, a correlation between $LiNO_3$ concentration and discharge capacity was observed. Titrations and scanning electron microscopy of cathodes extracted from discharged batteries confirmed Li_2O_2 formation in aggregated structures in cells that partially employed $LiNO_3$ as an electrolyte, indicative of an increase in the solution mechanism with the addition of $LiNO_3$. The increase in LiO_2 solubility was attributed via ^{7}Li NMR to a lower free energy of Li^+ in the electrolyte as a result of the addition of the strongly electron donating NO_3^- in the lithium solvation shell. Differential electrochemical mass spectrometry (DEMS) showed similar oxygen evolution on charge with and without $LiNO_3$, indicating no deleterious effect on cell rechargeability with the addition of $LiNO_3$.

Second, as anion selection induces the solution mechanism by lowering the free energy of Li^+ in solution, non-Li alkali metal cations and alcohols were studied as methods of inducing the solution mechanism by lowering the free energy of the superoxide anion (O_2^-) in solution. Galvanostatic cycling of Li-O_2 batteries containing non-Li alkali metal salts showed a small increase in the achievable discharge capacity, attributed to the softer acidity of non-Li alkali metal cations more favorably solvating the soft base O_2^-. However, gas analysis of a sodium-oxygen battery with a small amount of Li^+ salt added to the battery electrolyte showed Li^+ quickly scavenges any non-Li alkali metal cation-associated O_2^-, and the resultant LiO_2 quickly disproportionates into the insoluble Li_2O_2. It is therefore anticipated that an increase in Li-O_2 battery capacity upon the addition of non-Li alkali metal cations is only expected at high currents, when oxygen reduction rates are sufficiently high to allow some O_2^- to temporarily avoid Li^+ in solution. Ppm quantities of methanol, ethanol, and 1-propanol were added to ether-based Li-O_2 battery electrolytes as analogues to water, which has been previously shown to induce the solution mechanism due to its strong Lewis acidity lowering the free energy of O_2^- in solution. The additives induced a two-fold increase in battery capacity, though with little trend in the capacity as a function of the additive's Acceptor Number. These results highlight the complexity of interactions between the constituent species in an electrolyte in terms of their Lewis basicities, Lewis acidities, and other physicochemical properties.

While the formation of Li_2O_2 in large aggregated structures increases the achievable discharge capacity, an electrolyte-soluble redox mediator is required to oxidize aggregated Li_2O_2 on charge and shuttle electrons back to the electrode surface. The rechargeability of Li-O_2 batteries containing redox mediators in the presence of water impurities, which are likely difficult to eliminate in practical lithium-air batteries, was studied. Specifically, the effect of water contamination in the electrolyte on the promising redox mediator lithium iodide (LiI) was studied. DEMS and titrations of cathodes extracted from discharged batteries confirmed recent reports that lithium hydroxide (LiOH) formed as the dominant discharge product via a 4 e^-/O_2 process. However, isotopic labeling and DEMS were used to show LiOH is not reversibly oxidized back to

its reactants (Li^+, O_2, H_2O). Rather, titrations, scanning electron microscopy (SEM), energy-dispersive X-ray spectroscopy (EDX), and galvanostatic cycling of batteries under an argon atmosphere showed charge current in batteries containing both LiI and H_2O is a complex mixture of side reactions and redox shuttling.

With LiOH identified as an undesirable discharge product, the mechanism for Li_2O_2 degradation to LiOH in the presence of LiI and H_2O was studied. Galvanostatic cycling of lab-scale Li-O_2 batteries containing LiI and H_2O in DME and dimethyl sulfoxide (DMSO) showed that DMSO prevents Li_2O_2 degradation to LiOH. Cyclic voltammetry of these electrolytes showed DMSO exhibits a higher potential for iodide oxidation than DME, indicating iodide-mediated H_2O_2 reduction is more difficult in DMSO than DME. The ability of an additive to reduce H_2O_2 is therefore identified as a key consideration in Li_2O_2's stability in the presence of water impurities. A tangential important finding during this study was the difficulty in selection of an appropriate reference electrode for studying redox mediators in Li-O_2 batteries, as electrodes with too high of a lithium intercalation voltage will chemically oxidize the redox mediator, while electrodes with too low of a lithium intercalation voltage exhibit spontaneous oxygen consumption in a Li-O_2 battery.

Table of contents

List of figures

List of tables

Acknowledgments

I gratefully acknowledge the Department of Energy Vehicle Technologies Office and the NASA Space Technology Research Fellowship for funding my research endeavors.

I am thankful for the many collaborators who have shared their time, equipment, and ideas with me the last few years, especially Vikram Pande, Dr. Abhishek Khetan, Professor Venkat Viswanathan, Dan Addison, Dr. Vincent Giordani, Dylan Tozier, Professor Julia Greer, Dr. Robert Black, Ivan Kochetkov, Professor Linda Nazar, Dr. John Lawson, Dr. Vadim Lvovich, Bill Bennett, Dr. Rocco Viggiano, Dr. Don Dornbusch, Dr. Pedro Arrechea, Dr. Justin Haskins, Dr. Thilanga Liyana Arachchi, Dr. Eve Papajak, Dr. Lauren Abbott, Dr. Bala Gadaguntla Radhakrishnan, Dr. Mohit Mehta, and Dr. Hieu Pham.

Thank you Professor Angy Stacy, Professor Alex Bell, Professor Enrique Iglesia, and Professor Nitash Balsara for serving on my qualifying exam committee, and thank you Professor Clay Radke, Professor Wenjun Zhang, Dr. Colin Cerretani, and Esayas Kelkile for mentoring me as a graduate student instructor.

Thank you Carlet Altamirano and Joseph Nolan for diligent administrative support. Thank you Eric Granlund and the rest of the College of Chemistry machine shop for meticulous and timely work on parts for our instruments.

I am grateful for my colleagues in the McCloskey Lab. Thank you Jessica Nichols and Sara Renfrew for your partnership in starting our lab, and for helpful research discussions, along with Dr. Francis Richey, Dr. Hilda Buss, Dr. Kristian Knudsen, Kyle Diederichsen, and Joe Papp. Thank you to all of the labmates and visiting scholars who provided friendship over the years. Thank you Chris Dekmezian, Charles Wan, and Howie Nguyen for working with me as undergraduate researchers.

Thank you Professor Bryan McCloskey for empowering me as a researcher, for teaching me electrochemistry, and for nurturing my chemical intuition.

Thank you Professor Catherine Brinson for providing my first experiences with research at Northwestern University, and thank you Dr. Karl Putz, Dr. Charles Wood, and Dr. Marc Palmeri for your guidance and encouragement.

Thank you to my friends, especially Marty, Matt, Kari, Blaine, Bennett, Perry, Jon, Karl, Barb, Greg, and Robert, for sharing in joie de vivre, and thank you Mom, Dad, Brian, Kevin, Jenn, Jenn, Evie, James, and Connor for your love and support.

Lastly, and most importantly, thank you Laura for your laughter, compassion, and love.

Chapter 1: Introduction to the lithium-oxygen battery

Portions of this chapter are adapted from Ref. 1 with permission from The Royal Society of Chemistry.[1]

1.1 Motivation

The state-of-the-art rechargeable battery for high specific energy and high energy density applications is the lithium-ion battery. Shown in Figure 1.1a, the conventional lithium-ion battery consists of a graphite negative electrode and a lithium transition metal oxide positive electrode separated by an electrolyte of lithium salt in carbonate solvents, and operates via reversible lithium intercalation between the two solid electrodes. As such, the lithium-ion battery's specific energy – energy stored per mass – and energy density – energy stored per volume – are given by the lithium storage capacity of its electrodes. Commercially available lithium-ion batteries have more than three times the specific energy and energy density of previous rechargeable battery chemistries, such as nickel-metal hydride and silver-zinc, and as a result have revolutionized personal electronics and fully electric vehicles.[2]

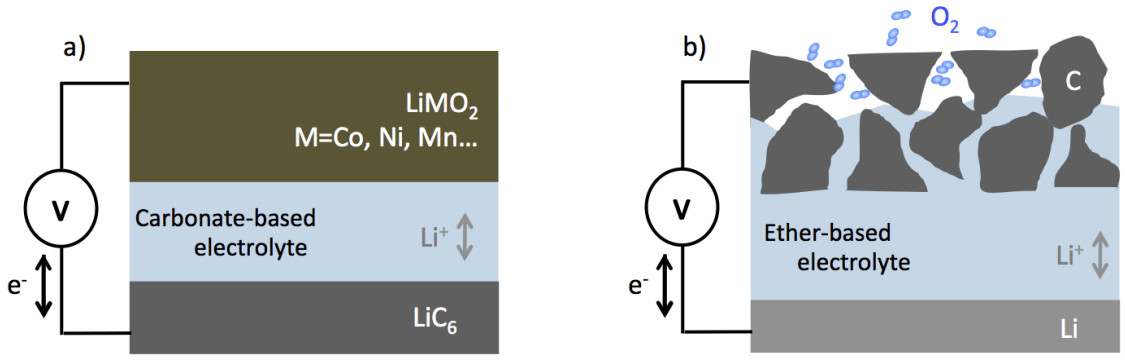

Figure 1.1. a) Schematic of the conventional lithium-ion battery b) Schematic of the conventional lithium-oxygen battery

A current focus in rechargeable battery research is identifying new materials or chemistries that could enable higher specific energy, higher energy density, and lower cost batteries than currently available lithium-ion batteries.[2-3] These research directions are primarily driven by the understanding that, while still maintaining sufficient lifetime, safety, and power performance, a drastic reduction in battery cost and increase in battery energy density will be necessary to increase market penetration of electric vehicles.[4] Improvements in specific energy, energy density, and cost would be welcomed for other technologies as well, including portable electronic devices, drones, and even space technology. As listed in NASA's 2015 Space Power and Energy Storage Technology Roadmap, "the primary sub-goal for any space energy storage technology is to provide power at the highest possible specific energy with sufficient durability in the mission environment and, in the case of rechargeable storage, sufficient cycle life." Of the

possible energy storage technologies, it lists that, "batteries that can safely store very large amounts of energy in small, low-mass packages enable the next generation of deep-space EVA suits that require advanced life support, communications, and computing equipment. All other missions are enhanced by having additional electrical power available without a mass penalty."[5]

As a result, multiple research directions are now being pursued in hopes of advancing beyond the limits imposed by conventional lithium-ion electrode materials.[6] In the lithium-ion field, new high-energy electrode materials, such as silicon anodes[7] and high voltage cathodes,[3, 8] are being developed. New battery chemistries, including lithium–oxygen, lithium-sulfur, and magnesium-ion, are being explored due to their active cathode materials' high theoretical specific energies compared to lithium-ion cathode materials. Table 1.1 provides a comparison of the electrochemical performance of lithium sulfide (Li_2S), lithium peroxide (Li_2O_2), and various lithium-based metal oxides used as lithium-ion battery cathode materials.[2, 9-18]

Table 1.1
Reprinted from Ref. 1 with permission from The Royal Society of Chemistry.[1]

Table 1 A comparison of capacity, voltage and energy (disregarding weight of non-active battery components) of selected Li-based cathode materials for energy storage

Active cathode material	Approximate reversible Li extraction/ insertion[a] (x)	Theoretical specific capacity[b] (mA h g^{-1})	Average discharge potential (V *vs.* Li/Li^+)	Typical voltage operating window (V *vs.* Li/Li^+)	Approximate theoretical specific energy (mW h g^{-1})
$Li_{(1-x)}CoO_2$	0.6	164	3.8	4.2–3.7	625
$Li_{(1-x)}Mn_{1.5}Ni_{0.5}O_4$ (high-voltage spinel)	1	147	4.7	5.0–3.0	690
$Li_{(1-x)}Ni_{0.8}Co_{0.15}Al_{0.05}O_2$ (LiNCA)	0.7	195	3.8	4.2–2.0	740
$Li_{(1-x)}Ni_{0.33}Mn_{0.33}Co_{0.33}O_2$ (NMC333)	0.6	166	3.8	4.3–2.0	620
$Li_{(1.2-x)}Mn_{0.55}Ni_{0.15}Co_{0.10}O_2$ (LMR-NMC)	0.85	267	3.65	4.7–2.0	970
$Li_{(2-x)}O_2$	2	1168	2.8	4.5–2.0	3330
$Li_{(2-x)}S$	2	1168	2.15	2.5–1.5	2510

[a] Exact Li extraction, and therefore approximate specific energy, is a function of the upper operating voltage limit and rate of extraction employed.
[b] Calculated using the Li extraction provided in the second column. Values extracted/inferred from ref. 1, 3, 9, 12 and 14–16.

Among the 'beyond Li-ion' battery cathode materials, Li_2O_2, the main discharge product of a nonaqueous lithium–oxygen (Li-O_2) battery, has the highest theoretical specific energy. With two electrons extracted per Li_2O_2 and an approximate average discharge potential of 2.8 V vs. Li^+/Li, the approximate theoretical specific energy is 3330 Wh/kg active material. This is more than four times that of current lithium-ion positive electrode materials, e.g., 625 Wh/kg active material for $LiCoO_2$, approximating 0.6 electrons extracted per $LiCoO_2$ and an average discharge potential of 3.8 V vs. Li^+/Li.[1] As a result, and in combination with the relatively low cost of the battery's active materials, the Li-O_2 battery has attracted significant research attention over the past decade.[19-22]

It should be noted that although the values reported in Table 1 provide the impetus for Li–O_2 and lithium-sulfur (Li–S) research activity, more sophisticated treatments of realistic practical battery energy densities suggest only modest specific energy improvement, and no volumetric energy density improvement, may be achievable with fully developed Li–O_2 batteries over advanced lithium-ion batteries (e.g., those

using LMR-NMC and Li metal as the electrode materials).[23] Tempering estimates are engineering considerations including the possible need for onboard storage of O_2 (a closed-system, lithium-oxygen battery) rather than O_2 directly from air (an open-system, lithium-air battery) to avoid water and carbon dioxide impurities that are detrimental to cell performance,[24-26] as well as the use of a pure lithium metal negative electrode, which hinges on the same engineering of reversible, dendrite-free lithium metal stripping and plating that would enable lithium metal to be used in lithium-ion batteries. Of course, this conclusion is contingent on the successful development of LMR-NMC and other high-energy Li-ion electrode materials, which are currently limited by fundamental challenges that result in voltage and capacity fade during extended cycling.[16, 18] Additionally, it is difficult to estimate some critical parameters for a practical Li-O_2 battery, such as separator thickness, electrolyte volume to positive electrode ratio, and carbon electrode mass and porosity, as we still work to study and address fundamental electrochemical challenges. Thus, while tempered from initial estimates, a modest increase in specific energy via low-cost active materials motivates the study of the lithium-oxygen battery.

1.2 The lithium-oxygen battery

Originally discovered by Abraham et al. and later more fully developed by Bruce et al. and McCloskey et al.,[27-30] the current conception of the nonaqueous lithium-oxygen battery is depicted in Figure 1.1b. The battery consists of a lithium negative electrode, a lithium salt and ether-based electrolyte, an electrolyte-soaked porous carbon positive electrode, and a gaseous oxygen headspace, and operates via the electrochemical formation and decomposition of lithium peroxide, Li_2O_2. Discharging the battery results in lithium oxidation at the lithium anode (reaction 1.1) coupled with oxygen reduction at the positive electrode to form Li_2O_2 on the carbon surface (reaction 1.2). Applying a charging current to the battery results in Li_2O_2 oxidation to gaseous oxygen at the carbon positive electrode and lithium plating at the lithium negative electrode.

$$\mathrm{Li(s)} \leftrightarrow \mathrm{Li^+ + e^-} \qquad U_0 = 0\ \mathrm{V\ vs.\ Li^+/Li} \qquad (1.1)$$

$$\mathrm{2Li^+ + 2e^- + O_2(g)} \leftrightarrow \mathrm{Li_2O_2(s)} \qquad U_0 = 2.96\ \mathrm{V\ vs.\ Li^+/Li} \qquad (1.2)$$

The ideal overall reversible cell reaction is therefore:

$$\mathrm{2Li(s) + O_2(g)} \leftrightarrow \mathrm{Li_2O_2(s)} \qquad U_0 = 2.96\ \mathrm{V\ vs.\ Li^+/Li} \qquad (1.3)$$

U_0 is the half-cell standard equilibrium potential of the reaction. The replacement of a conventional lithium-ion's transition metal oxide cathode with gaseous oxygen significantly decreases active material cost and gives the lithium-oxygen battery its high theoretical specific energy, motivating its study.

1.3 Challenges

While researchers have found various organic solvents and cathode materials that exhibit the desired Li_2O_2 electrochemistry as the major process on both discharge and

charge,[29-32] even the most stable of these combinations currently result in low attainable discharge capacities, or small specific energies, and poor rechargeability at the cell level. Thus, even before addressing the engineering challenges of O_2 sourcing and lithium metal reversibility as described in the motivation, three more fundamental electrochemical challenges, involving lithium peroxide at the carbon positive electrode, need to be addressed, as shown in Figure 1.2, in order to achieve high-practical specific energy, rechargeable lithium-oxygen batteries.

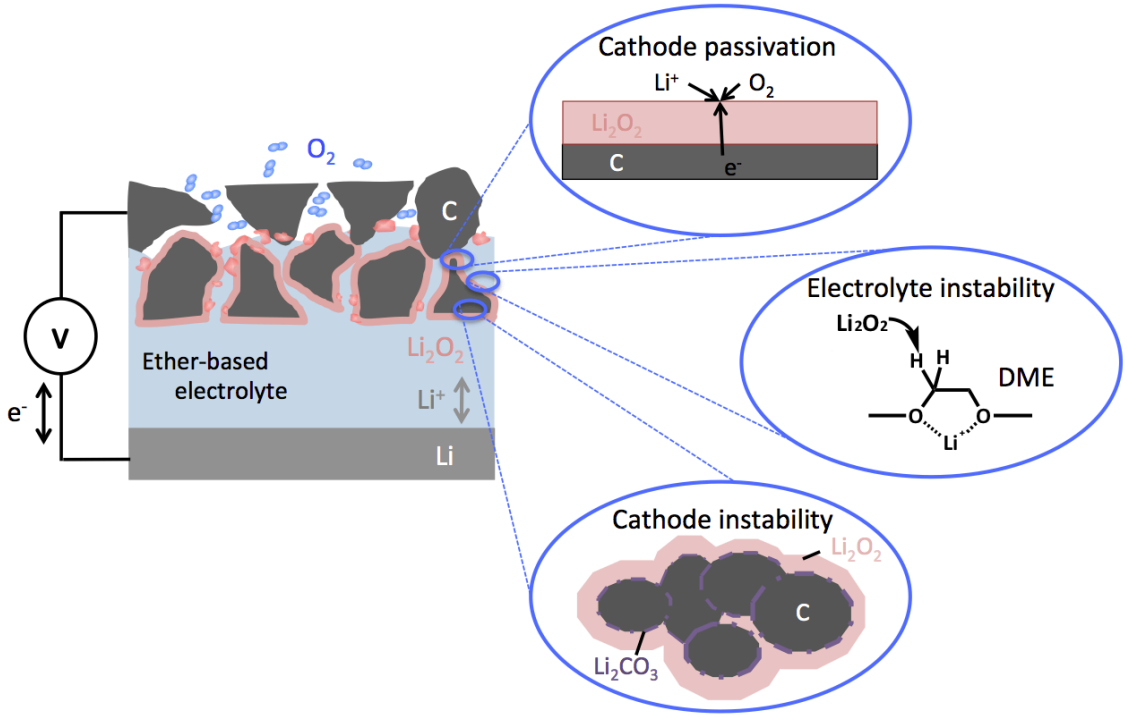

Figure 1.2. Three critical challenges at the positive electrode of the lithium-oxygen battery. Adapted from from Ref. 1 with permission from The Royal Society of Chemistry.[1]

First, no organic solvent-based electrolyte studied to-date has shown sufficient stability for a commercially viable battery. Researchers quickly discovered carbonate-based electrolytes like those employed in lithium-ion batteries promote irreversible lithium alkyl carbonate ($LiRCO_3$, with R being either Li or a small organic moiety, such as $–CH_3$ or $–C_2H_5$) formation,[30] but even the most stable solvents, ethers[29] and amides[33], participate in irreversible side reactions in the presence of Li_2O_2 and/or its electrochemical intermediates.[1] This decomposition has been shown to form solid, insoluble, and oxidatively strong side products, such as Li_2CO_3, at the positive electrode, leading to increasing charge overpotentials and subsequently exacerbated decomposition.[34-35]

Second, all porous carbons studied to-date, while cheap and high surface area, show decomposition in the presence of Li_2O_2 in operating cells. McCloskey et al. showed that Li_2O_2-induced reactions with a ^{13}C carbon cathode led to $Li_2{}^{13}CO_3$ formation during

charge, leading to rising charge overpotentials and exacerbated decomposition.[34] While noble metals and typical oxygen catalysts are more inert to Li_2O_2, they have been shown to catalyze side reactions,[36] with carbon's poor dissociation of O_2 actually desired to reduce the formation of parasitic side processes.[36-37]

Third, Li_2O_2 is a wide-band gap insulator and is insoluble in the most stable solvents, like ethers.[38] Therefore, in these electrolytes, Li_2O_2 forms as a conformal coating on the porous carbon scaffolding, and, after only a small amount of Li_2O_2 has formed, i.e., a small discharge capacity has been achieved, the Li_2O_2 electronically passivates the cathode, preventing further discharge. This results in small practical capacities, and thus a small energy per mass of cell components.[39]

These fundamental electrochemical challenges at the oxygen cathode limit the technology readiness level of the lithium-oxygen battery, as they prevent the realization of even lab-scale cells that have high capacities and long cycle lives, which are necessary before addressing engineering challenges like oxygen purification and storage for scale-up to low-mass battery packs. Thus, there is a need for electrolyte and cathode selection and engineering to achieve a high-capacity, rechargeable lithium-oxygen battery.

1.4 Outline of dissertation

This dissertation details my experimental studies in electrolyte engineering to address these fundamental electrochemical challenges at the positive electrode in the lithium-oxygen battery.

Chapter 2 outlines our experimental setups, with emphasis on considerations necessary in scaling performance behavior from lab-scale batteries.

Chapters 3 and 4 discuss methods for increasing discharge capacity by inducing solubility of lithium superoxide, LiO_2, the intermediate to lithium peroxide formation, on discharge. This enables a solution mechanism of growth whereby Li_2O_2 grows in large, aggregated structures, allowing more Li_2O_2 to form before cell death. Chapter 3 discusses how the appropriate selection of a lithium salt anion can induce LiO_2 solubility and increase discharge capacity without adversely affecting rechargeability. Chapter 4 discusses efforts to broaden this understanding of interactions to other electrolyte additives.

One difficulty with making lithium peroxide in large, aggregated structures on discharge is that Li_2O_2 – which is the final discharge product, as lithium superoxide, LiO_2, is an unstable intermediate – is still an insulator and is insoluble in the electrolytes. As such, Chapters 5 and 6 will discuss work related to redox mediation in the lithium-oxygen battery. Chapter 5 discusses the implications of combining the otherwise promising redox mediator lithium iodide with ppm quantities of water in the otherwise nonaqueous electrolyte, as it causes lithium hydroxide, LiOH, formation. Chapter 6 extends this water contamination work toward an understanding of the interactions leading to LiOH formation, and discusses the importance of selecting an appropriate reference electrode when studying redox mediators.

Chapter 7 contains a summary and is followed by the references for all chapters.

Chapter 2: Characterizing performance of Li-O_2 batteries

Portions of the descriptions of experimental methods are adapted from Burke, C. M.; Pande, V.; Khetan, A.; Viswanathan, V.; McCloskey, B. D., Enhancing Electrochemical Intermediate Solvation through Electrolyte Anion Selection to Increase Nonaqueous Li–O_2 Battery Capacity. *Proc. Natl. Acad. Sci. U. S. A.* **2015,** *112* (30), 9293-9298[40] and adapted with permission from Burke, C. M.; Black, R.; Kochetkov, I. R.; Giordani, V.; Addison, D.; Nazar, L. F.; McCloskey, B. D., Implications of 4 e– Oxygen Reduction via Iodide Redox Mediation in Li–O2 Batteries. *ACS Energy Letters* **2016,** *1* (4), 747-756.[41] Copyright 2016 American Chemical Society.

2.1 Considerations when characterizing lab-scale lithium-oxygen cells

As discussed in Chapter 1, new electrolytes and electrode materials are needed to solve the lithium-oxygen battery's fundamental electrochemical challenges. These challenges include electronic passivation of the cathode as well as electrochemical and chemical instabilities of both the electrolyte and carbon electrode in the presence of lithium peroxide and its intermediates.

If a lithium-oxygen battery were built to scale, at an acceptable weight and volume and with acceptable materials, the four main criteria, after safety, to assess whether a new electrolyte or electrode material improves the battery performance would be power, specific energy/energy density, electrical efficiency, and cycling stability. These could all be gleaned from the voltage response of a cell discharging and charging at a constant current, as shown in Figure 2.1.

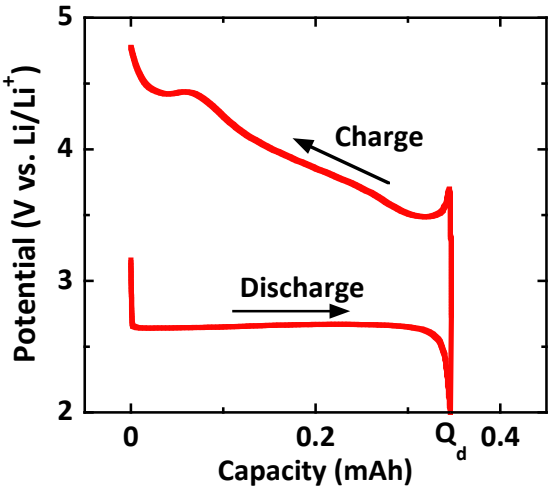

Figure 2.1. Voltage response of a lithium-oxygen cell galvanostatically discharging (bottom line left to right) to a cutoff of 2 V and then charging (top line right to left) to an identical capacity. The cell contains an XC72 carbon positive electrode and 1 M LiTFSI in dimethoxyethane (DME) as the electrolyte. This cell is presented with gas analysis in Figure 3.9.

For a cell discharging at constant current, the power, P, of a lithium-oxygen cell is given by:

$$P = IV_d \qquad (2.1)$$

where V_d is the voltage at any given time during discharge, as seen in Figure 2.1, and I is the constant current being drawn.
The achievable energy, E, from a lithium-oxygen cell is given by:

$$E = Q_d V_d \qquad (2.2)$$

where Q_d is the achievable discharge capacity before the voltage drops precipitously, calculated via:

$$Q_d = It_d \qquad (2.3)$$

where I is the constant current being drawn for t time until the voltage decrease. In our work, Q_d is measured as the capacity at which the cell voltage reaches a 2 V cutoff, as seen in Figure 2.1. In general, a precipitous fall in a battery's voltage corresponds to the inability of the battery's desired chemical reaction to support the applied constant current. This inability could be a result of charge transport issues or the full depletion of active materials, including active material transport limitations (e.g., oxygen diffusion). In the lithium-oxygen electrochemistry, the observed precipitous fall in voltage following the desired oxygen reduction reaction would continue until the cathode operating voltage falls out of the electrochemical stability window of the electrolyte (~1 V vs. Li/Li^+), meaning the electrolyte would decompose reductively if the discharge were not stopped at 2 V. As introduced in Chapter 1, the sudden voltage decline, i.e., sudden exponential increase in discharge overpotential as observed in Figure 2.1, of the lithium-oxygen batteries studied herein is a result of Li_2O_2 forming as a thin film on the carbon electrode surface, which then electronically passivates the electrode and prevents further Li_2O_2 growth.[39] The sudden exponential increase in overpotential is ascribed to a critical thickness through which electrons can no longer tunnel – as a resistor model would predict a linear increase in overpotential – and has been confirmed experimentally via measurements of charge transfer as a function of Li_2O_2 thickness via outer-sphere redox shuttles.[42] Chapter 3 discusses methods for increasing the achievable discharge capacity in order to increase achievable energy.

The electrical efficiency of a lithium-oxygen cell is given by the difference between the voltages of discharge and charge plateaus. As the area under the discharge curve is the energy supplied by the cell, and the area under the charge curve is the energy required to charge the cell, operating voltages on both discharge and charge as close to the open circuit voltage (~2.85 V) as possible are desired to ensure an electrically efficient battery. As shown in Figure 2.1, the typical Li-O_2 battery does not exhibit a stable voltage plateau on charge, but rather a steadily increasing overpotential. As introduced in Chapter 1, this is a result of oxidatively stable decomposition products like Li_2CO_3 forming on the electrode surface, driving the overpotential up to > 4V in order to

oxidize them.[34] Hence, there is a need for stable electrolytes and materials that do not degrade to these stable or any other side products.

Cycling stability is given by the quantity and quality (maintenance of power, energy, and electrical efficiency) of discharges and charges that can be achieved before the cell fails, i.e., can no longer sustain a discharge or charge current within the electrochemical stability window of the electrolyte. Figure 2.1 shows a cell's first cycle, so the voltage repsonse of additional cycles would be compared to Figure 2.1. This provides a measure of the lifetime of the cell.

Academic battery researchers aim to characterize the viability of new electrolytes or materials by testing these criteria in situ in small, unoptimized lab-scale cells and scaling up the findings to realistic, optimized cell configurations with various scaling factors, including electrode surface area, mass loading, and thickness. Unfortunately, these four criteria are not sufficient to characterize new electrolytes and electrode materials in lab-scale lithium-oxygen cells. Numerous undesired side reactions, both electrochemical and chemical, make it difficult to correctly measure power, energy, electrical efficiency and cyclability. For example, due to the reactive nature of the reduced oxygen species, voltage plateaus on discharge or charge exhibited by lithium-oxygen cells may correspond to undesired reactions. This means that electrochemical signatures that appear to be related to the reversible, desired Li-O_2 electrochemistry could actually be partially a result of unwanted side reactions. Additionally, if the discharging and/or charging is actually related to a modest amount of electrolyte and/or cathode degradation, the use of an unrealistically large volume of electrolyte in our lab-scale cells may still allow us to achieve many "cycles", even though we are just slowly degrading our constituent components over each cycle. In other words, while the voltage response of a lithium-oxygen cell cycling at constant current such as in Figure 2.1 presents some of the challenges inherent the lithium-oxygen electrochemistry, as described above, measuring voltage response alone is not sufficient to fully understand the cell's electrochemistry when comparing new materials and electrodes.

Consequently, the lithium-oxygen electrochemistry necessitates unique characterization tools to assess new electrolytes and electrode materials. These include a lab-scale battery design that uses a small ratio of electrolyte volume to positive electrode surface area and quantitative accounting for stability on the first few cycles of discharge and charge via pressure monitoring, differential electrochemical mass spectrometry (DEMS), ^{1}H nuclear magnetic resonance spectroscopy (NMR), and chemical titrations of discharge products. Characterization techniques like X-ray diffraction (XRD), scanning electron microscopy (SEM), and other spectroscopic techniques can provide useful qualitative information, as well.

Also worth noting, Li_2O_2 forms on the carbon electrode surface and its thickness and growth morphology depend on numerous factors, including the chemical composition of the electrolyte, the chemical composition of the electrode, electrode porosity and tortuosity, oxygen diffusivity in the electrolyte, actual electrode surface area (as opposed to an electrode's projected surface area), and current density. Therefore, it is difficult to compare intrinsic power, energy, electrical efficiency, and cyclability from lab to lab. In this work, capacities will simply be listed as mAh, rather than normalizing capacities to the carbon electrode weight or geometric area (mAh/mg or mAh/cm^2, respectively). Relevant carbon black composition, carbon black loading, cathode

geometrical surface areas, and current densities will be provided with the measurements described herein.

2.2 Lab-scale cell design

The lithium-oxygen cells used in our laboratory were developed by McCloskey et al. and were used extensively in their lithium-oxygen work.[30] Shown in Figure 2.2, a typical cell consists of a 7/16" diameter lithium foil negative electrode, a 1/2" diameter glass fiber separator soaked with electrolyte, a 12mm diameter positive electrode of high surface area carbon on stainless steel mesh, and 80 μL of an electrolyte, typically a lithium salt or combination of lithium salts in a nonaqueous organic solvent (a common example being lithium bis(trifluoromethanesulfonyl) imide (LiTFSI) in 1,2-dimethoxyethane (DME)). A 1 mm tall, 1/2" OD 0.43" ID stainless steel ring is added to provide additional headspace. These cell parts are compressed between two stainless steel current collectors in a fused silica cylinder. A Swagelok body (not shown in Figure 1) encases and tightens the two current collectors together to a uniform headspace, and a perfluoroelastomer O-ring in each current collector is compressed against the silica housing to provide a hermetic seal. The top current collector is that for the positive electrode and has two soldered 1/16" OD stainless steel capillaries that extend to the bottom face in order to sample gases into and out of the cell. The cells are prepared in an argon glovebox with less than 0.1 ppm water to limit impurities, which have been found to have a large effect on the electrochemistry.[24-26] The capillaries are capped prior to removal from the glovebox for attachment to the testing systems.

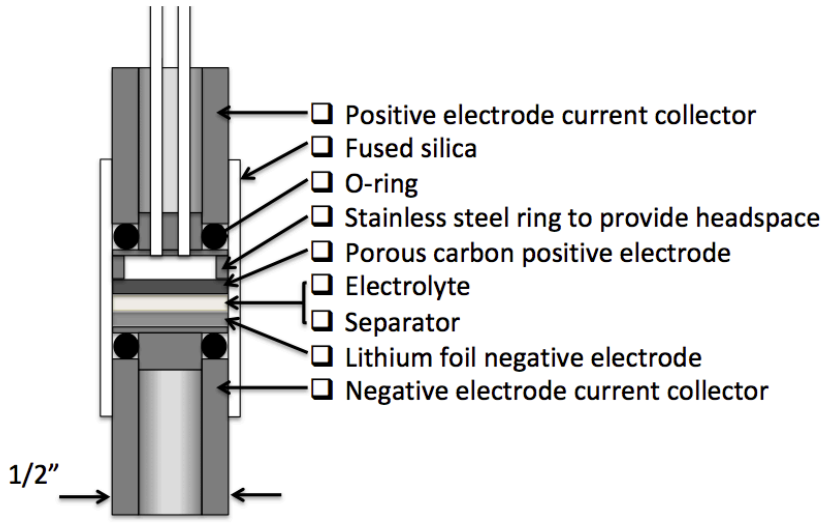

Figure 2.2. A schematic of the hermetically sealed Li-O_2 cell used in our lab. Adapted from Ref. 30.[30]

The typical carbon positive electrodes used in this work were prepared as described previously.[32] A mixture of 3:1 w:w ratio of Vulcan XC72 to PTFE binder in isopropanol (IPA) and water (4:1 water:IPA; and 15 mL total for 400 mg C) was sonicated for 30 seconds and homogenized for 6 minutes. A Badger model 250 air-sprayer was used to spray the slurry onto a ~4.5" x 4.5" piece of stainless steel mesh, which was rinsed with IPA and acetone and dried at 150°C for ten minutes prior to use. After letting the carbon air-dry, 12 mm diameter cathodes were punched out, rinsed with IPA and acetone, and dried at 150 °C under vacuum for at least 12 hours. The cathodes were then transferred, while hot, into the glove box, and stored on a hot plate at 200 °C immediately prior to use.

2.3 Gas analysis via cell pressure monitoring and differential electrochemical mass spectrometry (DEMS)

The testing systems used for our Li-O_2 cells are modeled after systems built at IBM.[30] Two different systems were constructed at UC Berkeley by my colleagues and me (Figure 2.3): one system with pressure monitoring capability only, and one system with both pressure monitoring and differential electrochemical mass spectrometry (DEMS). The pressure monitoring system can test five cells at once, while the DEMS can test two.

Figure 2.3. (*Left*) Two-channel pressure monitoring and differential electrochemical mass spectrometry (DEMS) battery cell testing system. (*Right*) Five-channel pressure monitoring battery cell testing system.

For electrical measurements, each cell's stainless steel current collectors are fastened into brass current collectors. These are connected to a Biologic VMP3 potentiostat allowing us to measure open circuit voltage, galvanostatically discharge and charge, perform cyclic voltammetry, perform electrochemical impedance spectroscopy, and more.

Simultaneously, for gas analysis, the cell capillaries from the cathode current collector are connected to 1/16" OD stainless steel capillaries on the system with Swagelok fittings. Figure 2.4 shows the process flow diagram of one channel, i.e., where one cell can be attached and cycled, as well as the connection of these channels to a vacuum pump, included in both systems, and an additional connection via a leak valve to a vacuum chamber and residual gas analyzer, included in the DEMS.

Opening the inlet valve allows gas to flow into the headspace. Upstream gas cylinders, tubing, and valves enable flowing pure oxygen, argon, isotopically enriched $^{18,18}O_2$, carbon dioxide, nitrogen, hydrogen, and other gases as needed. The cell is prefilled with argon from assembly in the glovebox. Opening the purge valve, which is connected to vacuum via more stainless steel capillary tubing, a cross connector, and a typically open (see DEMS discussion below) solenoid valve, would evaporate highly volatile electrolytes, like dimethoxyethane (DME). Thus, to exchange the argon headspace with, for example, oxygen in order to discharge, the purge valve is left closed and the 6-way valve is toggled between position A and position B. In position A, the cell is isolated, and a 500 μL loop (high-precision sample loop for high-performance liquid chromatography) is connected to vacuum and thus evacuated. In position B, the cell is reconnected to the 500 μL loop, and consequently a portion of the cell headspace fills the loop. Toggling to A then evacuates this portion of the cell headspace, and, as the inlet valve remains open, more argon flows in, returning the cell to the line pressure. From calibration, eight cycles are necessary to fully exchange, within detection limits, the headspace of a typical cell with a gas of interest.

Closing both the inlet and purge valves with the 6-way valve in position B allows pressure monitoring of the cell via the in-line pressure transducer (P1 in Figure 2.4). This enables pressure decay during discharge, as oxygen is consumed, and pressure rise during charge, as O_2, CO_2, H_2, and other gases are evolved.

In order to quantify the moles of gas consumed and evolved, the volumes of each testing channel and the volume of our cell were calibrated via an ideal gas approximation. First, we attached a known volume loop (e.g., another 500 μL high-precision sample loop for high-performance liquid chromatography) in place of the cell with the channel in position B. Second, we opened both the solenoid valve and the purge valve in order to evacuate both the cross and the channel. Third, we closed the purge valve and filled the channel with argon. After recording the pressure, we then closed the solenoid valve and then opened the purge valve to expand that gas into the full volume of the channel (in position B, everything between the inlet and purge valves, minus the cell) plus the known loop plus the cross (in position B everything between the purge valve and the solenoid valve). In the case of the DEMS, the leak valve was closed. Approximating the gas as ideal, the following equation then applies:

$$P_{initial}\left(V_{channel} + V_{loop}\right) = P_{final}(V_{channel} + V_{loop} + V_{cross}) \qquad (2.4)$$

where $P_{initial}$ is the pressure measured before volume expansion, P_{final} is the pressure measured after volume expansion, and $V_{channel}$, V_{loop}, and V_{cross} are the volumes of those sections as described above. By measuring a set of loops of various known volumes (as well as a set of various initial pressures for statistical fidelity), we calculated both the channel volume and the cross volume. Knowing these values, we replaced the known volume loop with a dry cell, i.e., a cell as described above but with no electrolyte, and performed a similar volume expansion to calculate the volume of the cell. We then subtracted the electrolyte volume (e.g., 80 μL), and added the dry cell volume and channel volume to obtain the volume in position B between the inlet and purge for a typical cell. This is the volume then used to calculate the moles of gas consumed or evolved, approximating the gas as ideal, as we are typically operating at ambient

temperature and 0-1.5 atm pressure. Cells are discharged and charged with both the inlet and purge valves closed and the 6-way valve in position B. Knowing the cell and channel volumes and the ambient temperature via a nearby thermocouple, the pressure change measured by the in-line pressure transducer, P1 in Figure 2.4, can be converted to a change in moles of gas.

Electrolyte and cathode decomposition cause deviation from the ideal lithium-oxygen electrochemistry, as the constituent substances of lithium, oxygen, electrons, and/or lithium peroxide participate in unwanted side reactions with the electrolyte and cathode to form irreversible side products. As the ideal electrochemistry is two electrons per oxygen molecule (e^-/O_2), any deviation from that value points toward electrolyte or cathode instabilities, i.e., poor rechargeability. Pressure monitoring allows a direct and real-time e^-/gas measurement.

To directly measure e^-/O_2 and to identify and quantify other gases evolved, we use the setup in Figure 2.4 in differential electrochemical mass spectrometery (DEMS) mode.

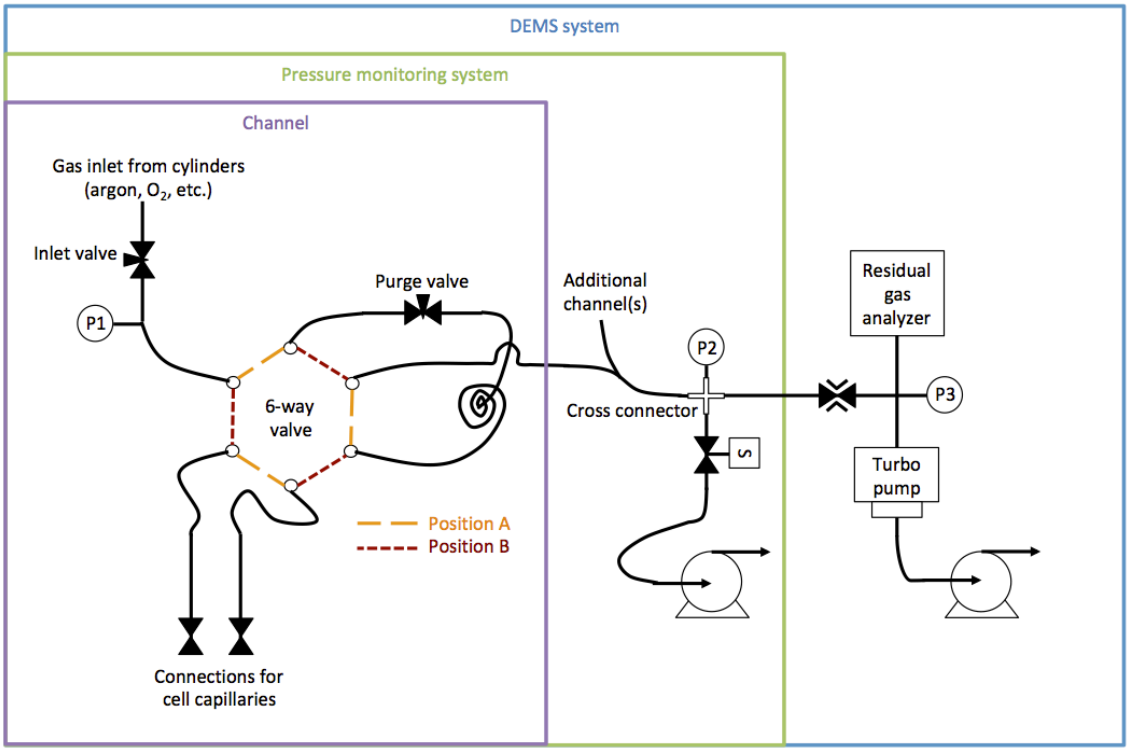

Figure 2.4. Process flow diagram of the pressure monitoring system and differential electrochemical mass spectrometer (DEMS) system. Not shown for both systems is the set of gas cylinders and selector valves to flow in a desired gas (argon, O_2, $^{18,18}O_2$, CO_2, H_2, N_2, etc.). Shown is one cell's channel; additional channel(s) are connected to the cross connector as labeled. The right arm of the cross on the DEMS system is connected to a leak valve to a vacuum chamber with a residual gas analyzer, whereas the left arm of the cross on the pressure monitoring system is connected to additional channels.

For this mode, a leak valve connects the right arm of the cross connector to a vacuum chamber containing a residual gas analyzer. Before charging, the cell headspace is exchanged for pure argon. Throughout charging, the 6-way valve is electronically actuated to pulse from A to B to A every couple minutes, sending gas from the cell headspace – predominantly argon, with small quantities of gases like oxygen, carbon dioxide, and hydrogen being evolved from the cell – via the 500 μL loop to the cross connector. Meanwhile, the solenoid valve (S in Figure 2.4) is electronically closed. The gas from the cell headspace therefore sits in the cross and leaks slowly into the chamber with the residual gas analyzer. This allows us to identify the gases being evolved from the cell.

To quantify the moles of gases evolved by the cell as identified by the residual gas analyzer, we prepared mixtures of gases of interest (for the Li-O_2 battery, typically oxygen, hydrogen, and carbon dioxide) at small concentrations in argon, approximating the gases as ideal and using pressure to calculate the concentrations. We then leaked these gases to the residual gas analyzer (RGA) and measured their ratios to the argon signal. We thus had a calibration for an actual ratio of oxygen to argon vs. the mass spectrometer's measured ratio of oxygen to argon. (Of note, we first measured the 36:40 signal ratio of our pure argon, and from then on used the 36 peak to extrapolate an argon 40 peak, as the argon 40 signal, the dominant isotope of our dominant gas, would overwhelm our RGA.) Before charging a cell, while the cell is sitting at open circuit, we pulse the cell sufficiently – usually a minimum of eight times – to establish a reliable baseline for all mass signals of interest (typically 32 for O_2, 44 for CO_2, and 2 for H_2). The baseline was then subtracted from the values measured during charging. This corrected signal for each gas was then compared to the argon mass signal, and converted to an estimated actual ratio via the calibration. Knowing the volume of the 500 μL loop, the pressure of the gas in the 500 μL loop when it is briefly in position B via the pressure transducer P1, and the ambient temperature via a nearby thermocouple, we are able to calculate the total moles of gas in the 500 μL loop. Using ratios of the gases to argon via the mass spec and calibrations, we can then calculate the molar composition of the gas in the 500 μL loop. After charging has been completed, the cell is pulsed at least eight times to remove all of the evolved gases from the cell headspace, and usually eight times to reestablish and confirm the baseline. Throughout the DEMS process, the inlet valve is left open to a supply of argon gas to resupply the cell as gas is pulsed out. Of note, $^{18,18}O_2$ gives the same signal as ^{36}Ar. As a result, the baseline 36 signal was used to extrapolate the argon 40, and then during charging, the 36 signal was used, minus the baseline. Additionally, each cell run on the DEMS is run alongside an identical cell operating under pressure rise, i.e., with both inlet and purge valves closed and the 6-way valve in position B. This is performed to ensure the total moles of gas evolved calculated from the DEMS matches the total moles of gas calculated via pressure rise.

By comparing the coulometry from the potentiostat with this regular gas quantification, e^-/O_2 values can be determined throughout a battery's discharge or charge. Additionally, the exact amount of oxygen evolved on charge (OER) can be compared with the amount consumed on discharge (ORR), giving another metric of rechargeability, as OER/ORR should approach unity. These values give important insight into the battery's rechargeability. For example, in a discharging battery, an e^-/O_2 value of 2.00 indicates the near perfect formation of Li_2O_2 on discharge (reaction 2.6). A subsequent

value of 2.50 e^-/O_2 on charge indicates 20% of electrons are going into a non-oxygen evolving reaction. Therefore, DEMS allows us to quantify the rechargeability of each cell during cell cycling.

Based on error propagation of volume calibrations and DEMS gas calibrations, typical e^-/O_2 values are within +/- 0.01 e^-/O_2. Cells containing significant water quantities formed hydrogen at open circuit via reaction with the lithium anode, and correcting the pressure decay on discharge for this pressure rise at open circuit typically led to a reduction in precision to +/- 0.1 e^-/O_2.

Of note, as described in Chapters 5 and 6 in further detail, e^-/O_2 can be a misleading metric for Coulombic efficiency in some instances. Chapters 5 and 6 describe the 4 e^-/O_2 formation of LiOH. This implies the four electron reduction reaction:

$$4Li^+ + 4e^- + O_2 + 2H_2O \rightarrow 4LiOH \quad (2.5)$$

However, as shown by Tulodziecki et al., LiOH is likely formed via the two electron formation of Li_2O_2, followed by the chemical reactions of Li_2O_2 with water to form LiOH and the consumption of H_2O_2 via iodide, followed finally by the reduction of triiodide back to iodide:[43]

$$2Li^+ + 2e^- + O_2 \rightarrow Li_2O_2 \quad (2.6)$$

$$Li_2O_2 + 2H_2O \rightarrow 2LiOH + H_2O_2 \quad (2.7)$$

$$H_2O_2 + 3I^- + 2Li^+ \rightarrow 2LiOH + I_3^- \quad (2.8)$$

$$I_3^- + 2e^- \rightarrow 3I^- \quad (2.9)$$

Overall, these electrochemical and chemical reactions sum to reaction 2.5, but the electrochemical step is still a 2 e^-/O_2 process, rather than a typical 4 e^-/O_2 reduction process such as typically observed on platinum electrodes. In other words, the presence of other compounds within a Li-O_2 battery can change the observed e^-/O_2 values, as well as the ultimate products formed, even if the electrochemical step is still 2 e^-/O_2.

2.4 Discharge product identification and quantification via chemical titrations

Other quantitative measures of rechargeability in the Li-O_2 battery are chemical titrations for the amount of Li_2O_2 on carbon cathodes extracted from cells at various states of discharge and charge. The titration protocol used here follows that developed previously.[32]

To prepare cathodes for titration, immediately upon completion of the desired discharge and/or charge, cell headspaces are replaced with argon and the cells are capped and brought into an argon glovebox. The cathode and separator are extracted from each battery and placed in a 20 mL septum vial. Vacuum is pulled on this vial for roughly 3 minutes to remove residual electrolyte before tightening the septum and removing the vial from the glovebox for titration of the contents.

The titrations begin with the injection of 2 mL of ultrapure water (18.2 MΩ cm, Millipore) through the septum to react Li_2O_2 into LiOH and H_2O_2.

$$Li_2O_2 + 2H_2O \rightarrow 2LiOH + H_2O_2 \qquad (2.7)$$

The protocol then proceeds with two chemical titrations. First, an acid/base titration is performed to quantify LiOH and any basic decomposition products present in the cell. Two drops of phenolphthalein are added as an indicator, and a standardized solution of 0.005 M hydrochloric acid is used as a titrant, with a pink to clear transition at the endpoint.

$$LiOH + HCl \rightarrow LiCl + H_2O \qquad (2.10)$$

Second, an iodometric titration is immediately performed to quantify H_2O_2. An aqueous solution of 0.01 M potassium iodide and 3.5 M sulfuric acid are added in excess (typically 1mL each) along with a drop of molybdate-based catalyst solution to form I_2 in aqueous solution.

$$H_2O_2 + 2KI + H_2SO_4 \rightarrow I_2 + K_2SO_4 + 2H_2O \qquad (2.11)$$

The molybdate-based catalyst solution is an aqueous solution of ammonium molybdate, ammonium hydroxide, and ammonium nitrate.[32] Standardized 0.01 M sodium thiosulfate is then used as a titrant for I_2, with a yellow to clear transition at the endpoint.

$$I_2 + 2Na_2S_2O_3 \rightarrow Na_2S_4O_6 + 2NaI \qquad (2.12)$$

An aqueous starch solution is typically added near the endpoint to complex with the remaining I_2 to create a more apparent dark blue to clear transition at the endpoint.

On cycled cathodes, the acid/base titration picks up basic decomposition products in addition to the LiOH formed from the reaction of water and Li_2O_2 in the septum vial, so the iodometric titration is typically taken for the Li_2O_2 yield. The Li_2O_2 percent yield is typically defined as the amount of Li_2O_2 formed during discharge, as quantified via an iodometric titration, to the amount of Li_2O_2 expected from coulometry, assuming an ideal $2e^-/Li_2O_2$ process.[32] Controls of pure commercial Li_2O_2 powder were performed to verify the titrations' accuracy.

A comparison of Li_2O_2 yields to e^-/O_2 values for cells at various states of discharge and charge gives important insight into the formation, subsequent side reactions, and oxidation of lithium peroxide.[32] For example, a near perfect 2.00 e^-/O_2 value on discharge coupled with a less ideal 80% Li_2O_2 yield after discharge indicates the dominant formation of Li_2O_2 on discharge followed by chemical degradation of Li_2O_2 to other products, such as lithium formate (HCO_2Li) and lithium fluoride (LiF) via electrolyte solvent and salt decomposition.

2.5 Qualitative spectroscopic characterization techniques

Ex situ spectroscopic characterization techniques can provide useful information about lithium-oxygen cell performance as well. Techniques like X-ray diffraction

(XRD),[30] Raman spectroscopy,[30] X-ray photoelectron spectroscopy (XPS),[34] and Fourier-transform infrared spectroscopy (FTIR)[26] can be used to identify discharge products and decomposition products. Of note, however, these characterization techniques are all locally quantitative at best, i.e., they characterize random spots on a lab-scale electrode, rather than macroscopic performance of a battery material. They are useful in identifying possible reaction products and decomposition pathways, but gas analysis and chemical titrations should be used as the quantitative measurements for cell rechargeability.[9, 32] Intricacies can complicate their use as well, such as amorphous Li_2O_2 not visible via XRD,[9] and decomposition of polyvinylidene fluoride (PVDF) binder in the carbon cathode showing similar peaks to lithium superoxide (LiO_2) in Raman spectroscopy.[44]

Scanning electron microscopy (SEM) is useful to investigate changes in Li_2O_2 morphology.[25, 40, 45] Energy-dispersive X-ray spectroscopy (SEM EDX) can also be used to identify discharge products.[41, 46]

^{1}H nuclear magnetic resonance spectroscopy (NMR) can be used to determine decomposition products in the electrolyte,[47] as well as the pKa of ppm levels of water in different nonaqueous electrolytes.[43] ^{7}Li NMR can be used to determine the lithium environment in an electrolyte, as discussed in Chapter 3. NMR procedures for this work are detailed in Chapter 3, Chapter 4, and Chapter 6.

Chapter 3: Influence of electrolyte anion on Li-O_2 discharge capacity

This work is adapted from Burke, C. M.; Pande, V.; Khetan, A.; Viswanathan, V.; McCloskey, B. D., Enhancing Electrochemical Intermediate Solvation through Electrolyte Anion Selection to Increase Nonaqueous Li–O_2 Battery Capacity. *Proc. Natl. Acad. Sci. U. S. A.* **2015,** *112* (30), 9293-9298.[40]

Abstract

Among the 'beyond Li-ion' battery chemistries, nonaqueous Li-O_2 batteries have the highest theoretical specific energy and as a result have attracted significant research attention over the past decade. A critical scientific challenge facing nonaqueous Li-O_2 batteries is the electronically insulating nature of the primary discharge product, lithium peroxide, which passivates the battery cathode as it is formed, leading to low ultimate cell capacities. Recently, strategies to enhance solubility to circumvent this issue have been reported, but rely upon electrolyte formulations that further decrease the overall electrochemical stability of the system, thereby deleteriously affecting battery rechargeability. In this study, we report that a significant enhancement (greater than four-fold) in Li-O_2 cell capacity is possible by appropriately selecting the salt anion in the electrolyte solution. Using ^{7}Li nuclear magnetic resonance, we confirm that this improvement is a result of enhanced Li^+ stability in solution, which in turn induces solubility of the intermediate to Li_2O_2 formation. Using this strategy, the challenging task of identifying an electrolyte solvent that possesses the anti-correlated properties of high intermediate solubility and solvent stability is alleviated, potentially providing a pathway to develop an electrolyte that affords both high capacity and rechargeability. To confirm the experimental results, an Ising model was developed with collaborators to predict Li^+ stability as a function of its solvation shell composition. We believe the model and strategy presented here will be generally useful to enhance Coulombic efficiency in many electrochemical systems (e.g., lithium-sulfur batteries) where improving intermediate stability in solution could induce desired mechanisms of product formation.

3.1 Introduction

The lithium-oxygen (Li-O_2) battery has garnered significant research interest in the past ten years due to its high theoretical specific energy (~3500 Wh/kg_{Li2O2}) compared to current state-of-the-art lithium-ion (Li-ion) batteries (~625 Wh/kg_{LiCoO2}).[9, 20-22] Consisting of a lithium anode and an oxygen cathode, the nonaqueous Li-O_2 battery operates via the electrochemical formation and decomposition of lithium peroxide (Li_2O_2). The ideal overall reversible cell reaction is therefore:

$$2\mathrm{Li} + \mathrm{O_2} \leftrightarrow \mathrm{Li_2O_2} \quad (2e^- \text{ process}) \; U_0 = 2.96\,\mathrm{V} \quad (3.1)$$

One challenge preventing the realization of the Li-O_2 battery's high theoretical specific energy is that the discharge product, Li_2O_2, which is generally insoluble in aprotic organic electrolytes, is an insulator.[38-39, 48-49] Thus, on discharge, Li_2O_2 forms as a conformal coating on the cathode's carbon support, as shown in Figure 3.1a. As such, it electronically passivates the cathode, resulting in practical capacities much smaller than

theoretically attainable.[50] For a cell discharging at constant current, this is exhibited by a sudden exponential drop in voltage – or exponential increase in overpotential – as shown in Figure 2.1 and Figure 3.2, and is ascribed to a critical thickness of Li_2O_2 through which electrons can no longer tunnel.[39]

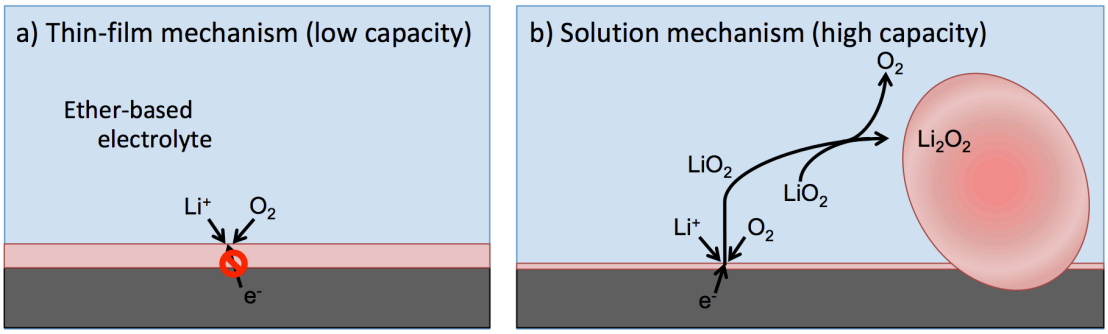

Figure 3.1. Possible discharge mechanisms in the nonaqueous lithium-oxygen battery. The thin film mechanism is dominant in typical ether-based electrolytes. The solution mechanism is induced by increasing solubility of the lithium superoxide intermediate in solution.

Recently, two reports have described the engineering of electrolytes to circumvent this passivation and improve Li-O_2 battery discharge capacity. Aetukuri et al. suggests that adding ppm quantities of water to a DME-based electrolyte increases the solubility of intermediates during Li_2O_2 formation.[25] This increased solubility allows a reduced oxygen species shuttling mechanism that promotes deposition of Li_2O_2 aggregated toroid structures, as shown in Figure 3.1b. Of note, these structures are typically platelet-shaped, but are often referred in the literature as toroids, so we will use both terms interchangeably. The diffusion of the intermediates away from the electrode surface allows the surface to remain electronically accessible to Li^+ and O_2, promoting more Li_2O_2 growth before the surface film meets a critical thickness, thereby leading to an increase in cell capacity. This increase in cell capacity with water content in the electrolyte is also consistent with reports by Gasteiger and coworkers.[51-52] Aetukuri et al. reasons that this increase could be attributed to water's significantly higher Gutmann Acceptor Number (AN) than DME, as the AN is a measure of a solvent's Lewis acidity, and thus quantifies its ability to efficiently solubilize negatively charged species, such as the potential discharge product intermediate, superoxide (O_2^-).[53] Johnson et al. presents a related analysis, showing that an electrolyte solvent with a higher Gutmann Donor Number (DN), a measure of Lewis basicity,[54] is more likely to induce toroid formation due to increased Li^+ solvation efficiency, allowing solubility of O_2^-.[45] Johnson et al. further confirmed the presence of O_2^- ions in Li^+-bearing high DN solvents using surface enhanced Raman spectroscopy, with others also confirming soluble O_2^- formation. [45, 55-57]

While water and certain organic solvents increase cell capacity via this solution mechanism, there is evidence that both decrease electrolyte stability. Water impurities in Li-ion electrolytes are known to enhance parasitic electrochemical side reactions, and Aetukuri et al. and Cho et al. showed that adding ppm quantities of water in Li-O_2 batteries leads to a decrease in electrolyte stability and irreversible reactions with the

lithium anode.[24-25] Furthermore, using quantitative measures of battery rechargeability, high DN solvents, such as DMSO and N-methyl pyrrolidone, have been observed to be less stable than low DN solvents, such as acetonitrile and DME. [58] Recently, Khetan et al. showed using thermodynamic analysis that an organic solvent's ability to induce the solution mechanism is anti-correlated with its stability towards nucleophilic attack.[59] Thus, Li-O_2 cells would benefit from an appropriately engineered electrolyte that both induces Li_2O_2 intermediate solubility and maintains or exceeds present electrolyte stability.

In this report, we describe the importance of the lithium salt anion in enhancing the solvation of electrochemically-formed intermediate species during Li-O_2 battery discharge, thereby enhancing discharge capacity. We present a study on two common Li-O_2 battery salts, lithium bis(trifluoromethane) sulfonimide (LiTFSI) and lithium nitrate ($LiNO_3$), dissolved in 1,2-dimethoxyethane (DME). These salts were selected because Schmeisser et al. found that $TFSI^-$ and NO_3^- anions provided different DN in ionic liquids with common cations (NO_3^--containing ILs having higher DN than $TFSI^-$-containing ILs).[60] We also specifically selected NO_3^- because of its reported positive influence on Li-O_2 battery rechargeability compared to the more commonly used $TFSI^-$.[61-62] We found that electrolytes containing a high concentration of NO_3^- exhibited higher donicity, as verified using ^{7}Li NMR, and provided an increase in battery capacity greater than four-fold compared to a battery employing a $TFSI^-$ electrolyte, while not decreasing battery rechargeability, as measured using quantitative oxygen consumption and evolution. In order to theoretically quantify this enhancement, collaborators at Carnegie Mellon University and RWTH Aachen University developed an Ising model to describe the solvation shell of Li^+. This analysis shows the origin of this enhanced solution process is due to the formation of ion pairs (Li^+-NO_3^-) in a DME solvent. The theoretical analysis further predicted that ion-pair formation and the associated enhancement in capacity would not be observed when DMSO is used as a solvent, which was then confirmed experimentally. We generalize this analysis to provide a rational basis for selection of electrolyte (solvent + salt) combinations for use in Li-O_2 batteries. We believe these results will have profound implications not only for Li-O_2 batteries, where a practical outcome of the solubility is an enhancement in battery capacity, but for other electrochemical systems (e.g., lithium-sulfur batteries) in which intermediate solvation may induce desired mechanisms of product formation.

3.2 Experimental methods

Materials. Lithium nitrate (BioUltra) and lithium bromide (ReagentPlus) were purchased from Sigma-Aldrich and were dried under vacuum in a heated glove box antechamber at 150°C for 24 hours before use. Lithium bis(trifluoromethane) sulfonimide (LiTFSI), 1,2-dimethoxyethane (DME), and dimethyl sulfoxide (DMSO) were purchased from BASF and used as received. Whatman QM-A glass fiber filters were purchased from VWR. Poly(tetrafluoroethylene) (PTFE, 60 wt% dispersion in H_2O) was purchased from Sigma-Aldrich. Vulcan XC72 was purchased from Fuel Cell Store and was filtered through a 60-mesh screen prior to use. T316 stainless steel 120 mesh, with wire diameter 0.0026", was purchased from TWP Inc. Research-grade oxygen and argon were purchased from Praxair. 99% $^{18}O_2$ was purchased from Sigma-Aldrich. All electrolyte,

cell, and NMR sample preparation was completed in an argon-filled glove box with <0.1 ppm O_2 and <0.1 ppm H_2O. Lithium foil with a thickness of 0.01" was purchased from FMC Lithium. 99% Lithium chloride (BioUltra) was purchased from Sigma-Aldrich. 99.9% deuterium oxide (D_2O) was purchased from Cambridge Isotope Laboratories, Inc.

Cathode preparation. Cathodes of XC72 carbon on stainless steel mesh were prepared via the spray-coating method described in Chapter 2.

Carbon loading. Cell capacities depend on carbon loading. To keep carbon loading consistent, the cathodes used for any particular data set, such as the capacity measurements displayed in Figure 3.2 or the cathode morphology images in Figure 3.3, were all from the same batch of spray-coated cathodes. As a control, the capacity measurements presented in Figure 3.2 were repeated with a second batch of cathodes. All capacities changed proportionally (a slight increase for all cases), with the capacity of the cell using 0.5M $LiNO_3$/0.5M LiTFSI in DME maintaining just over a three-fold increase from the capacity of the cell employing 1M LiTFSI in DME. Cathodes contained on average 1.5-2 mg carbon/cm^2 electrode projected area.

Cell preparation. The Li-O_2 cells used followed the same Swagelok design as described previously[30] and described in detail in Chapter 2. All cells employed a 7/16" diameter lithium foil, a 1/2" diameter Whatman QM-A glass fiber separator, a 12mm diameter cathode of Vulcan XC72 carbon on stainless steel mesh, and a 1mm thick, 1/2" diameter stainless steel ring. The QM-A separators, like the cathodes, were rinsed with IPA and acetone and dried under vacuum at 150°C under vacuum for at least 12 hours before being transferred to the glove box and stored on a hot plate at 200°C. Each battery contained 80 µL of electrolyte.

Scanning electron microscopy. Discharged cathodes were characterized via scanning electron microscopy immediately after discharge. After replacing discharged cells' headspaces with argon, the cells were transferred into the glove box, and the cathodes were removed. The cathodes were each rinsed with two 1 mL aliquots of DME and were subsequently dried under vacuum for at least five minutes in the glove box antechamber. The cathodes were then sealed in septa vials, removed from the glove box, and taken to the SEM. Immediately before imaging, the cathodes were removed from the argon-filled septa vials, placed on carbon tape on the SEM holder, and inserted into the SEM. From discharge completion to SEM insertion was typically one hour. From removing the cathodes from the septa vials to insertion into the SEM was typically less than 30 seconds. SEM was performed on a JEOL JSM-7500f.

Titration. The Li_2O_2 titration protocol used here followed that described previously[32] and described in detail in Chapter 2. Of note, no titratable I_2 was observed from titrations on the separator alone, confirming the following two points: a) no NO_2^- that may have formed at the Li metal anode is present in the separator, and therefore NO_2^- does not result in a falsely higher Li_2O_2 yield as measured using the iodometric titration (NO_2^- also oxidizes I^-); b) Li_2O_2 only forms on the cathode and not the separator.

Nuclear magnetic resonance spectroscopy. ^{7}Li and ^{23}Na nuclear magnetic resonance spectroscopy measurements were completed on a Bruker AM-400 magnet with a 5mm Z-gradient broad brand probe. Reference samples, those employing a chloride salt in D_2O, were prepared outside the glove box and were flame-sealed in melting point capillaries. Electrolyte samples were prepared inside the glove box and were placed, along with a reference capillary, in a Wilmad screw-cap NMR tube. All reference

samples were 3M of the chloride salt in D_2O. For the ^{23}Na NMR, 0.2M $NaClO_4$ was added. These molarities were taken from Schmeisser et al.[60] ^{23}Na NMR spectra are not reported here because of the poor solubility of $NaNO_3$ in DME. NMR spectra of only the reference and only the sample were taken to verify the identity of each peak.

3.3 Results and discussion

To characterize the effects of the electrolyte salt anion on discharge performance, Li-O_2 cells were prepared with electrolytes of varying concentrations of $LiNO_3$ and LiTFSI salts, totaling 1.0M Li^+, in DME.

Figure 3.2a presents representative galvanostatic discharge profiles of these Li-O_2 cells as a function of the $LiNO_3$ salt concentration. The inset in Figure 3.2a shows the average cell capacity for each $LiNO_3$ salt concentration. Cell capacity increases more than four-fold over the $LiNO_3$ concentration range studied, clearly indicating the substantial effect of the Li^+ counterion on cell capacity.

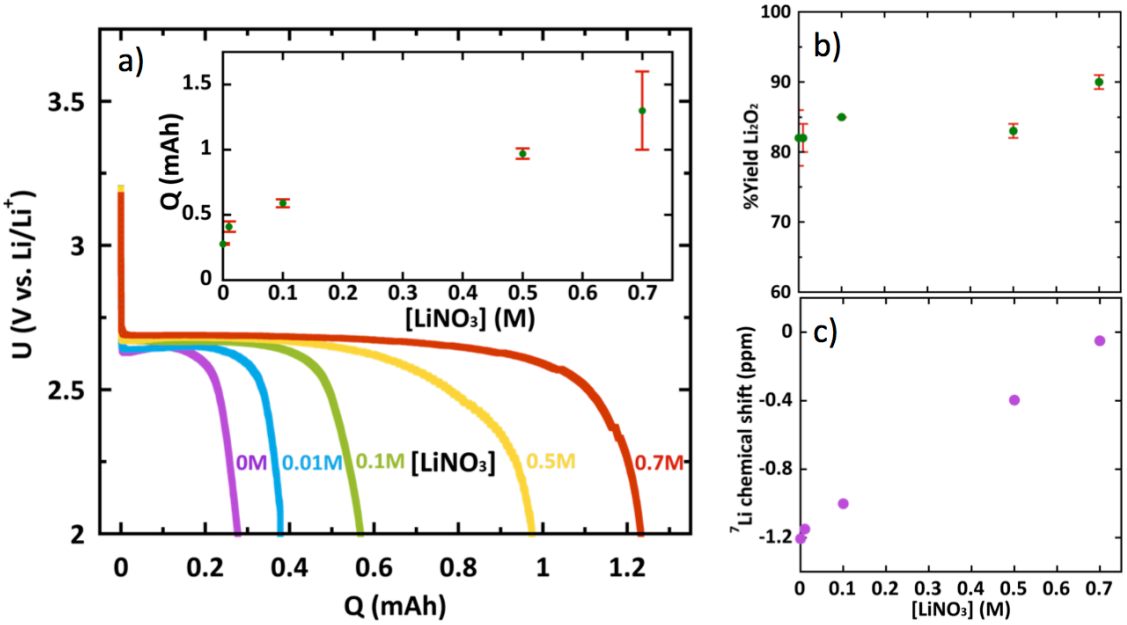

Figure 3.2. a) Representative galvanostatic discharge profiles of Li-O_2 cells (450 μA/cm^2 under a 1.5 atm O_2 atmosphere to a 2V cutoff). Inset shows capacity dependence on $LiNO_3$ concentration. **b)** Li_2O_2 discharge yield as a function of $LiNO_3$ concentration. **c)** ^7Li chemical shift of sample electrolyte solutions, versus a 3 M LiCl in D_2O standard, as a function of electrolyte $LiNO_3$ concentration. A less negative chemical shift represents a shift downfield. A 1.0M Li^+ concentration was used for all electrolytes (DME used as the solvent), while the LiTFSI/$LiNO_3$ ratio was varied. The $LiNO_3$ concentration for each cell is provided in the figure. As an example, the cell labeled '0.1M $LiNO_3$' contained 0.1M $LiNO_3$ and 0.9M LiTFSI. Error bars are one standard deviation of multiple experiments.

Scanning electron microscopy (SEM) was performed on discharged cathodes to investigate changes in Li_2O_2 morphology, and hence changes in discharge mechanism, with increased $LiNO_3$ concentration. Figure 3.3 presents SEM images of a pristine cathode (Figure 3.3a) and images of cathodes from cells of identical electrolyte compositions as those studied in Figure 3.2, but discharged at 45 μA/cm^2 (Figure 3.3b-f). When comparing Figure 3.3a-c, the pristine, 0M $LiNO_3$, and 0.01M $LiNO_3$ cathodes appear indistinguishable. This implies a conformal coating of discharge product on the 0M $LiNO_3$ and 0.01M $LiNO_3$ cathodes, and is consistent with previous reports for 1M LiTFSI in DME.[25, 37]

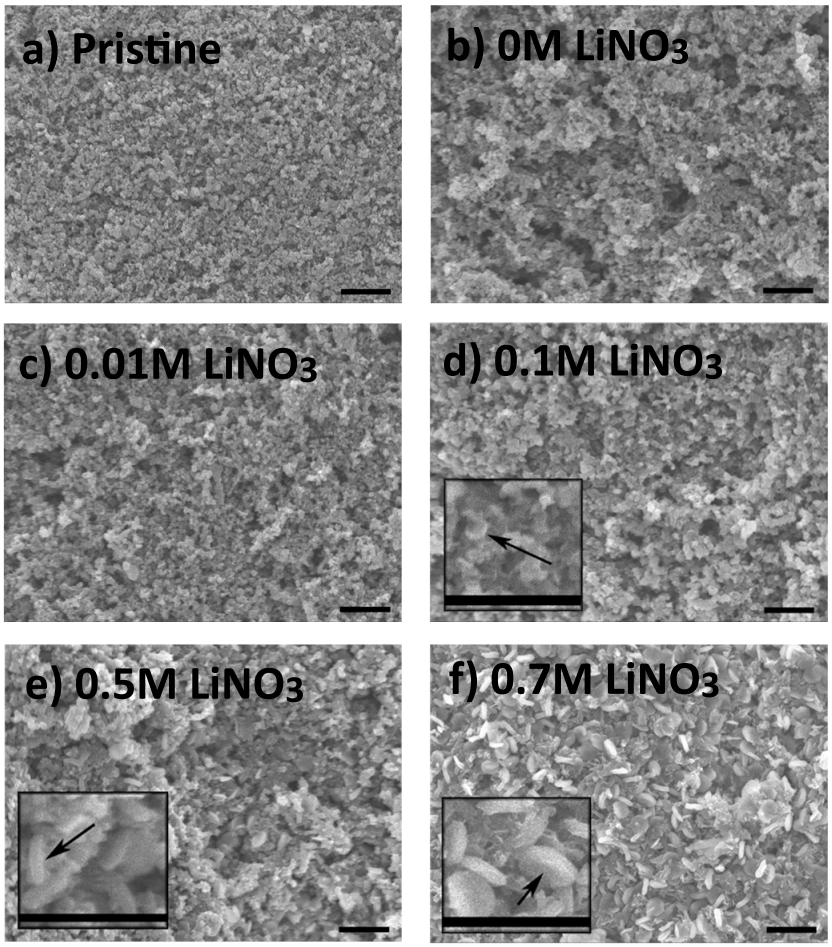

Figure 3.3. a) Scanning electron microscope (SEM) image of pristine XC72 carbon cathode prior to discharge. **b-f)** Discharged cathodes in cells employing 1M total Li^+ concentration, with 0M $LiNO_3$ (1M LiTFSI), 0.01M $LiNO_3$, 0.1M $LiNO_3$, 0.5M $LiNO_3$, 0.7M $LiNO_3$, respectively. Cells were discharged at 45 μA/cm^2 to 0.9 mAh/cm^2 or a 2 V cutoff voltage, but all cells had at least 0.5 mAh/cm^2 capacity. Scale bars are 1μm.

A conformal coating of discharge product is indicative of a predominant thin film Li_2O_2 surface deposition mechanism. Originally outlined by Laoire et al., this mechanism is described by the following elementary steps [63-64]:

$$Li^+ + e^- + O_2^* \leftrightarrow LiO_2^* \qquad (3.2)$$

$$Li^+ + e^- + LiO_2^* \leftrightarrow Li_2O_2^* \qquad (3.3a)$$

and/or

$$2LiO_2^* \leftrightarrow Li_2O_2^* + O_2 \qquad (3.3b)$$

where '*' denotes a species adsorbed to the cathode/Li_2O_2 surface. Importantly, in the DME/LiTFSI electrolyte, lithium superoxide (LiO_2) is insoluble and therefore remains adsorbed to the electrode surface, where a second charge transfer step (reaction 3.3a) or a disproportionation reaction (reaction 3.3b) results in the conformal Li_2O_2 coating observed in Figure 3.3b and c. [9, 37, 63-66]

As the $LiNO_3$/LiTFSI ratio increases, the discharge morphology perceptibly changes. As seen in Figure 3.3d, when using 0.1M $LiNO_3$, nodular morphologies appear on the cathode surface. Increasing the $LiNO_3$ concentration to 0.5M and 0.7M finds these structures replaced with increasingly larger toroid structures, as seen in Figure 3.3e and f, respectively.

Of note, in preparing the electrolytes, we found the solubility limit of $LiNO_3$ in DME is approximately 1M. The capacity variability of the 0.7M $LiNO_3$/0.3M LiTFSI cell in Figure 3.2 is likely due to concentration polarization effects in the electrolyte, as 0.7M begins to approach the solubility limit of $LiNO_3$ in DME, such that $LiNO_3$ precipitation at the anode may occur. The $LiNO_3$ concentration range (<0.7M) we report was limited by this effect. Notably, we did not observe a maximum in capacity at any capacity less than saturation. Iliksu et al. recently reported a downturn in capacity above 0.7M $LiNO_3$, implying an optimal concentration of $LiNO_3$ below the solubility limit.[67] However, above 0.7M $LiNO_3$ we observed a large range of observed capacities that disallowed the assignment of any capacity trend. Some cells in this concentration range exhibited visible salt precipitation, which likely resulted in the observed capacity irreproducibility.

As described previously, the toroid morphology observed in Figure 3.3d-f is indicative of a solution mechanism of Li_2O_2 growth proceeding through solubility of the LiO_2 intermediate.[25, 45, 68] The solvation of LiO_2 into lithium cations and the redox active superoxide anion, O_2^-, follows the equilibrium reaction [25]:

$$LiO_2^* \leftrightarrow Li^+(sol) + O_2^-(sol) \qquad (3.4)$$

Solvated O_2^- can then diffuse in solution to a growing Li_2O_2 toroid, where it combines with Li^+ to form adsorbed LiO_2^* on the toroid surface. LiO_2^* subsequently undergoes disproportionation according to reaction 3.3b, leading to the formation of Li_2O_2 on the toroid surface, as shown in Figure 3.1b.[25] The observed toroid formation on discharged cathodes from cells employing high $LiNO_3$/LiTFSI ratios supports the enhancement of this solution mechanism with increasing $LiNO_3$ concentration.

In further support of the solution mechanism, increasingly larger toroid structures were observed as current density decreased in cells employing 0.5M $LiNO_3$ (0.5M

LiTFSI) (Figure 3.4). This observation is consistent with previous reports where Li_2O_2 toroid formation was correlated to the enhancement of the solution Li_2O_2 formation mechanism at low currents.[25, 45, 68]

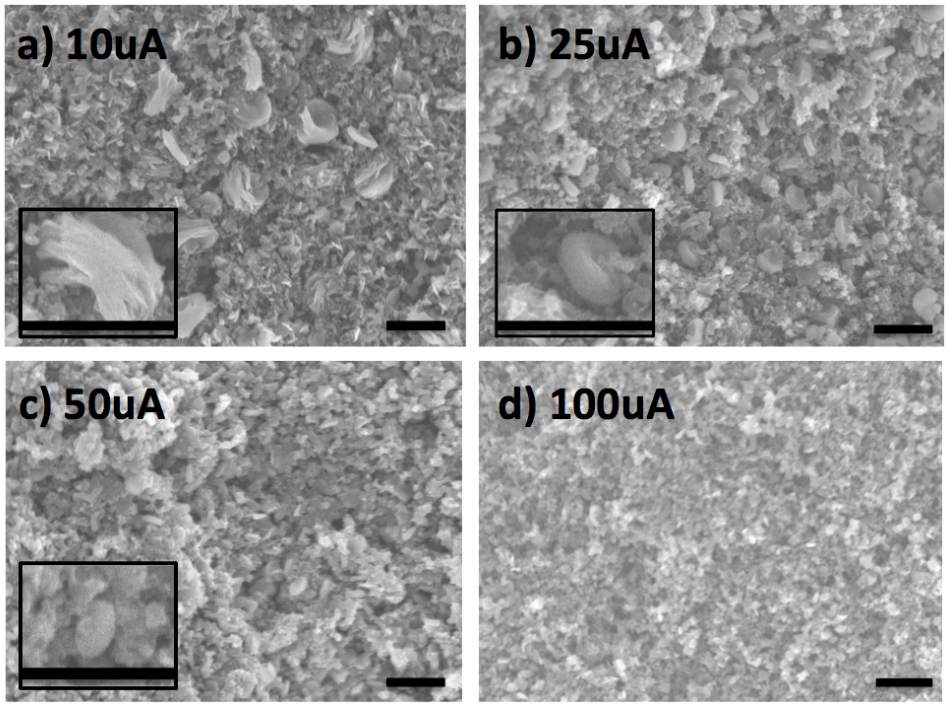

Figure 3.4. Scanning electron microscope images of carbon cathodes from cells employing 0.5M $LiNO_3$/0.5M LiTFSI in DME discharged to 1 mAh capacity at currents of **a)** 10 μA, **b)** 25 μA, **c)** 50 μA, and **d)** 100 μA. Total electrode area was 1.1 cm^2 (12 mm diameter).

With the solubility mechanism confirmed, it was important to check that the increased solubility was indeed due to DN effects of NO_3^- and not another experimental artifact, in particular water contamination. As a first control, the key experiments were repeated with new electrolyte solutions that used lithium nitrate powder that had been dried a second time under vacuum in a heated glove box antechamber at 150°C for 24 hours. All repeated experiments gave consistent results with their original counterparts. As a second control, water levels in the electrolytes were measured via Karl Fischer titration. All electrolytes had less than 70 ppm water, although the 1M LiTFSI (0M $LiNO_3$) had <10 ppm water content. Therefore, a battery employing an electrolyte of 1M LiTFSI in DME with 70 ppm of water was discharged at 450 mA/cm^2 to 2 V, analogous to the batteries in Figure 3.2. As observed in Figure 3.5, this battery saw an increase in capacity of 40% compared to a battery with 1M LiTFSI in DME, much smaller than the four-fold increase displayed in Figure 3.2 from the cell employing the 0.3M LiTFSI/0.7M $LiNO_3$ electrolyte.

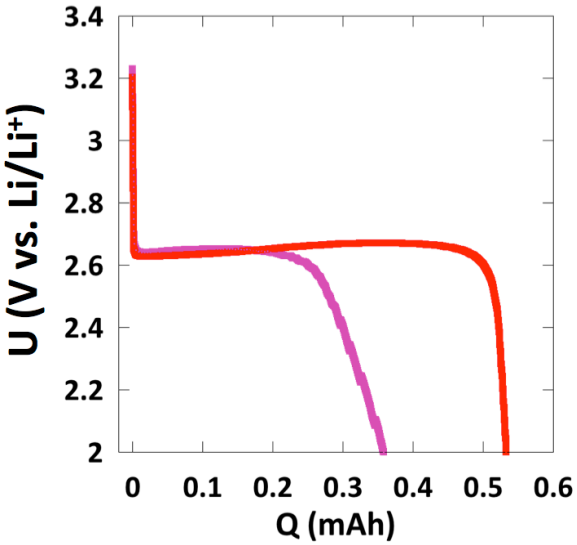

Figure 3.5. Galvanostatic discharge of a cell employing nominally anhydrous (<10 ppm H_2O, purple curve) and 70 ppm H_2O added (red curve) to 1M LiTFSI in DME. A small water impurity in the $LiNO_3$ salt led to a linear increase in H_2O content with $LiNO_3$ concentration, with a maximum water content of 70 ppm H_2O in the 0.7M $LiNO_3$ cell. A 40% increase in capacity is observed when 70 ppm H_2O is added to a 1M LiTFSI cell. A greater than 400% increase was observed in the 0.7N $LiNO_3$ cell compared to the anhydrous 1M LiTFSI cell (Figure 3.2a in the main text).

Of note, we find that Li_2O_2 yield, as measured using an established peroxide titration technique,[32] is generally unaffected by the electrolyte compositions studied here (Figure 3.2b), although a slightly higher Li_2O_2 yield may be observed at high $LiNO_3$ concentrations.

With a change in anion clearly inducing a solution Li_2O_2 growth mechanism, it can be reasoned that the NO_3^- anion is affecting LiO_2 solubility via enhanced Li^+ solvation. The electrolyte anion can affect the overall electrolyte's donicity (quantified by the Gutmann Donor number (DN), a measure of Lewis basicity[54]), in turn affecting its ability to solubilize LiO_2 through enhanced solvation of Li^+. We used ^{7}Li NMR to probe the electron donicity felt by Li^+ ions in our $LiNO_3$/LiTFSI in DME electrolytes as a proxy measurement of the relative effect of the anion on electrolyte DN.

Using NMR as a proxy for DN is a well-known technique, with Erlich et al. first proposing ^{23}Na NMR as an effective measurement for a solvent's DN. [69] Erlich et al. reasoned that a downfield ^{23}Na shift resulted from stronger interaction between the solvation shell molecules and the cation, thereby decreasing the cation's shielding. The environment of Li^+ in $LiNO_3$/LiTFSI in DME electrolytes cannot be determined via ^{23}Na NMR, though, as adding $NaClO_4$ to the electrolytes causes a white precipitate to crash out of solution (likely $NaNO_3$, as dissolving $NaClO_4$ in an anhydrous solvent containing $LiNO_3$ has been proposed as a method for making anhydrous $LiClO_4$ [70]).

We reason that ^{7}Li NMR, in place of ^{23}Na NMR, can serve as a reasonable proxy of the relative donicity of Li^+ electrolytes in a single solvent. A representative ^{7}Li NMR

spectrum of a 0.5M LiTFSI/0.5M $LiNO_3$ in DME electrolyte versus our standard external standard of 3M LiCl in D_2O is shown in Figure 3.6.

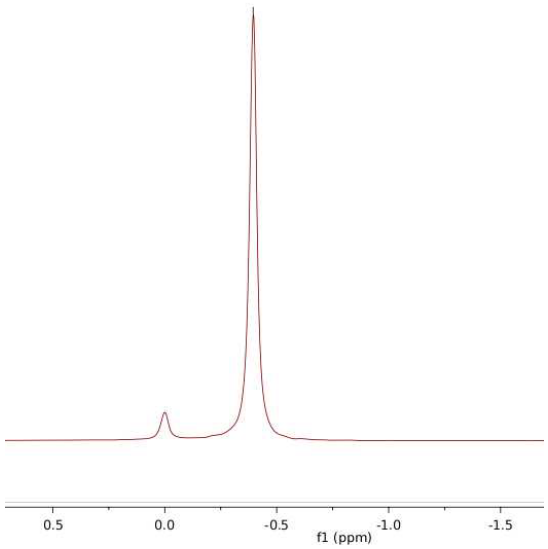

Figure 3.6. Representative ^7Li NMR spectrum on 0.5M LiTFSI/0.5M $LiNO_3$ in DME. The chemical shift at 0 ppm corresponds to the Li shift of LiCl in D_2O, whereas the chemical shift at -0.39 ppm corresponds to the Li shift in the electrolyte.

Figure 3.2c shows the ^7Li chemical shift, referenced to an external standard of LiCl in D_2O, of each $LiNO_3$/LiTFSI in DME electrolyte. As $LiNO_3$ concentration increases, the ^7Li peak shifts downfield, or becomes less shielded. Cahen et al. showed that the ^7Li chemical shift of a lithium salt may display a concentration dependence, contingent, to a first approximation, on the DN of the solvent and the DN of the anion.[71] The DN of an electrolyte containing a low DN solvent and high DN anion, like Br^- (DN=33.7) in acetonitrile (DN=14.1), exhibits an anion concentration dependence (DN values from Linert et al.[72]). Conversely, electrolytes comprised of a high DN solvent with a relatively low DN anion, like ClO_4^- (DN=8.44) in dimethyl sulfoxide (DN=29.8), do not exhibit a DN dependence on anion concentration. These trends agree with Linert et al., who found via solvatochromic dyes that the effective DN of an electrolyte depended on an interplay between the DN of the solvent, DN of the anion, and AN of the solvent.[72] For example, if the solvent's DN was larger than the anion's DN, then the electrolyte comprising the two had a DN similar to its solvent's DN.

If $LiNO_3$ indeed has a higher DN than DME, then increasing the concentration of $LiNO_3$ will increase the number of NO_3^- interacting with any particular Li^+, which, in turn, will lead to an increase in the electrolyte's DN. Thus, we reason that the presence of a concentration dependence on ^7Li chemical shift indicates NO_3^- serving an active role in the electrolyte's donicity, and the increasingly downfield shift of ^7Li with increasing $LiNO_3$ concentration represents increasing donicity. In contrast, Figure 3.7 shows that indeed $LiNO_3$/LiTFSI salts in the high DN solvent dimethyl sulfoxide do not exhibit a

substantial change in ^{7}Li shift with increasing $LiNO_3$ concentration, and, as therefore expected, no statistically significant capacity increase is observed in DMSO-based electrolytes as the $LiNO_3$/TFSI ratio increases.

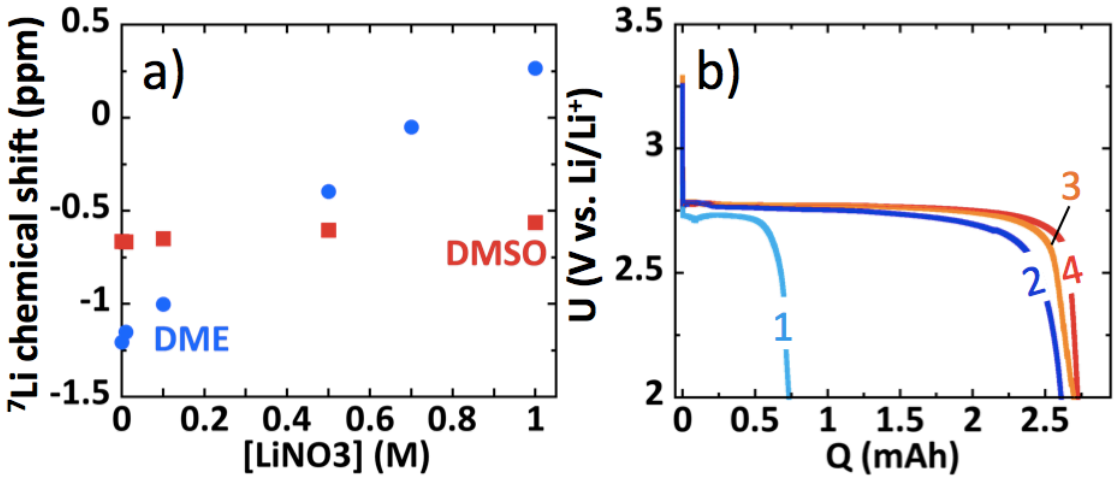

Figure 3.7. a) ^{7}Li chemical shift of DMSO and DME-based electrolytes, versus a 3 M LiCl in D_2O reference, as a function of electrolyte $LiNO_3$ concentration. A less negative chemical shift represents a shift downfield. **b)** Discharge profiles (45 μA/cm^2, 2 V cutoff) as a function of $LiNO_3$ concentration for DMSO and DME-based electrolytes. A 1.0M Li^+ concentration was used for all cell electrolytes, while the LiTFSI/$LiNO_3$ ratio was varied. Labels correspond to discharges of cells using the following electrolytes: **1.** 1 M LiTFSI in DME, **2.** 0.5 M $LiNO_3$:0.5M LiTFSI in DME, **3.** 1 M LiTFSI in DMSO, and **4.** 0.5 M $LiNO_3$:0.5M LiTFSI in DMSO.

To confirm the general correlation between enhanced Li^+ solvation and Li-O_2 battery capacity, another high DN anion, Br^-, was studied. As expected, similar trends in ^{7}Li NMR chemical shifts and Li-O_2 battery capacity are observed between 0.5M/0.5M LiBr/LiTFSI and similar $LiNO_3$/LiTFSI concentrations in DME and DMSO-based electrolytes (Figure 3.8). The LiBr-containing electrolytes had <10 ppm water content measured via Karl Fischer titration.

We note, however, that extreme care must be taken when using NMR techniques to compare and quantify solvent DNs, particularly between dislike solvent classes, such as protic and aprotic solvents, as was discussed by Gal and Laurence.[73] Additionally, we recognize that ^{7}Li has comparable, and thus offsetting, diamagnetism and paramagnetism, meaning anisotropic factors can contribute significantly to the observed chemical shifts, unlike in the more commonly used ^{23}Na NMR for measuring solvent DNs.[71] For the current study, our interest is only in the relative changes of the Li^+ chemical environment as a function of anion composition in a single aprotic solvent (both for DME and DMSO), such that ^{7}Li NMR provides useful qualitative, if not quantitative, values for comparison.

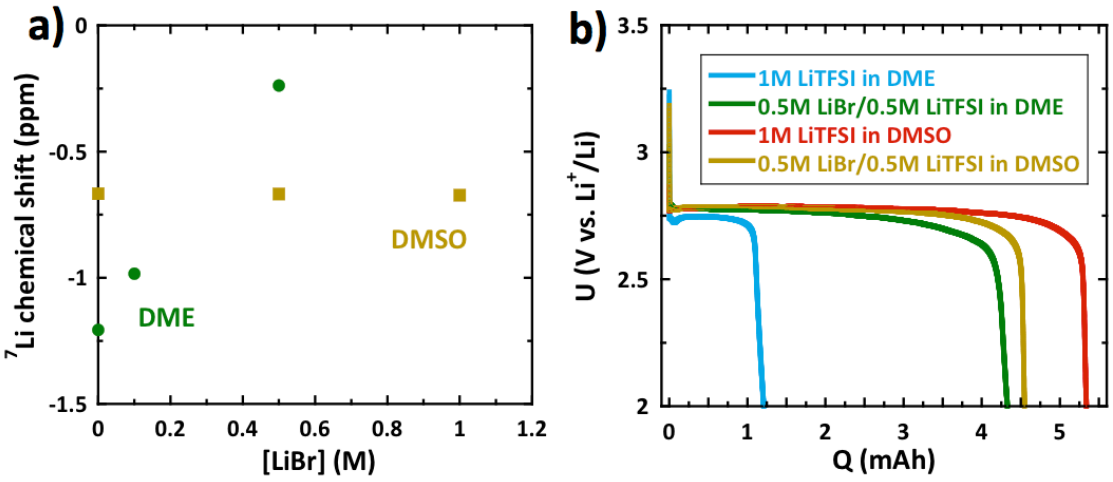

Figure 3.8. a) ^{7}Li chemical shift of DMSO and DME-based electrolytes, versus a 3M LiCl in D_2O reference, as a function of LiBr concentration. A less negative chemical shift represents a shift downfield. Analogous to Figure 3.7a) in the main text, 0.5M Br^- causes a noticeable downfield shift in the ^{7}Li in DME, but not in DMSO. **b)** Discharge profiles (45 μA/cm^2, 1.5 atm O_2 atmosphere, 2 V cutoff), as a function of LiBr concentration for both DMSO and DME-based electrolytes. A 1.0 M Li^+ concentration was used for all cell electrolytes, with LiTFSI as the supporting salt. The LiBr concentration for each cell is provided. Analogous to NO_3^- in Figure 3.7b) in the main text, 0.5M Br^- provides over a three-fold increase in capacity in a DME-based electrolyte, but not in a DMSO-based electrolyte.

For a quantitative basis for the role played by the electrolyte anion, collaborators at Carnegie Mellon University and RWTH Aachen University developed a revised thermodynamic model for the solution electrochemical process. The solution mediated electrochemical growth of Li_2O_2 is triggered by the dissolution reaction given in reaction 3.4. The free energy change involved in this dissolution reaction is given by:

$$\Delta G_{sol} = G_{Li^+_{sol}} + G_{O^-_{2,sol}} - G_{LiO^*_2} \qquad (3.5)$$

where $G_{Li^+_{sol}}$ is the free energy of the Li^+ ions in the electrolyte, $G_{O^-_{2,sol}}$ is the free energy of O_2^- ions in the electrolyte and $G_{LiO^*_2}$ is the free energy of the adsorbed LiO_2 on the Li_2O_2 surface during discharge. To understand the role of salt anion on the equilibrium of the dissolution reaction, the stabilization of the solvated intermediates in the presence of the anion was explored by calculating the free energy of Li^+ ions. To a first approximation, the free energy of the Li^+ ions and thus the free energy of LiO_2 dissolution is largely dependent on the species that are present in Li^+ first solvation shell.[74-75] A modified Ising model[76] for the site occupancy in the solvation shell of Li^+[77] was developed by calculating interaction energies for the various ions with Li^+. The model uses inputs of the anion DN, solvent AN, solvent DN, and $LiNO_3$ concentration and is solved via the mean field approximation to calculate the occupancy of the Li^+ solvation shell for each of our electrolytes, the resultant average free energy of Li^+ (Figure 3.S1), and the resultant expected rate enhancement of the solution mechanism via

$$r_S \sim \exp\left(\frac{-\Delta G_{sol}}{kT}\right) \qquad (3.6)$$

The model shows that at 0.5M $LiNO_3$/0.5M LiTFSI, we would expect a ~4 fold enhancement in the rate of the solution process, in excellent agreement with experiment (Figure 3.S2). The model can be generalized to map out the entire electrolyte design space with a contour map of the Li^+ stabilization as a function of varying DN of solvent and anion. Please refer to Burke et al., *PNAS* 2015 for more information on the model.

With the ability of NO_3^- to induce the solution mechanism confirmed experimentally and computationally, differential electrochemical mass spectrometry (DEMS) was used, as described previously,[30, 32] to quantify the reversibility of the electrochemical reactions (Figure 3.9).

Figures 3.9a and 3.9d present galvanostatic discharge-charge profiles for cells employing 1M LiTFSI and 0.5M $LiNO_3$/0.5M LiTFSI. Discharge, or oxygen reduction reaction (ORR), overpotentials are similar between the two electrolytes. The cell employing $LiNO_3$ salt, however, exhibited a higher initial charge overpotential, which likely arises from an electronic transport limitation to Li_2O_2 toroid decomposition, although further studies are necessary to confirm this hypothesis. Figure 3.10 shows that for cells charged from the same discharge capacity, this initial charge overpotential does increase with increasing $LiNO_3$ concentration. As discussed in Chapters 5 and 6, this invites the use of an additive redox mediator to allow charge transfer during charge to occur through the electrolyte rather than the electronically insulating Li_2O_2 toroid.

Figures 3.9b and 3.9e show oxygen consumption as a function of capacity during discharge and charge for these two cells. On both discharge and charge, both cells show nearly identical e^-/O_2, indicating nearly equivalent degrees of reversibility. Figures 3.9c and 3.9f display gas evolution on charge from DEMS. Oxygen was clearly the dominant gas evolved for both cells, and in nearly identical quantities, with oxygen comprising 92% of the gases evolved from the 0M $LiNO_3$ (1M LiTFSI), and 93% of the gases from the 0.5M $LiNO_3$ (0.5M LiTFSI) cell. The ratio (OER/ORR) of the amount of oxygen evolved during charge (oxygen evolution reaction, OER) to the amount of oxygen consumed during discharge (ORR), an important metric of reversibility, is statistically equal for a cell employing 1M LiTFSI and a cell employing 0.5M $LiNO_3$/0.5M LiTFSI (OER/ORR ~0.82). Small quantities of carbon dioxide and hydrogen were evolved from each cell toward the end of charging, with the 0M $LiNO_3$ evolving slightly more carbon dioxide. The 0.5M $LiNO_3$ cell evolved slightly more hydrogen. Overall, DEMS shows that NO_3^- induces the solution mechanism without deleteriously affecting the battery stability.

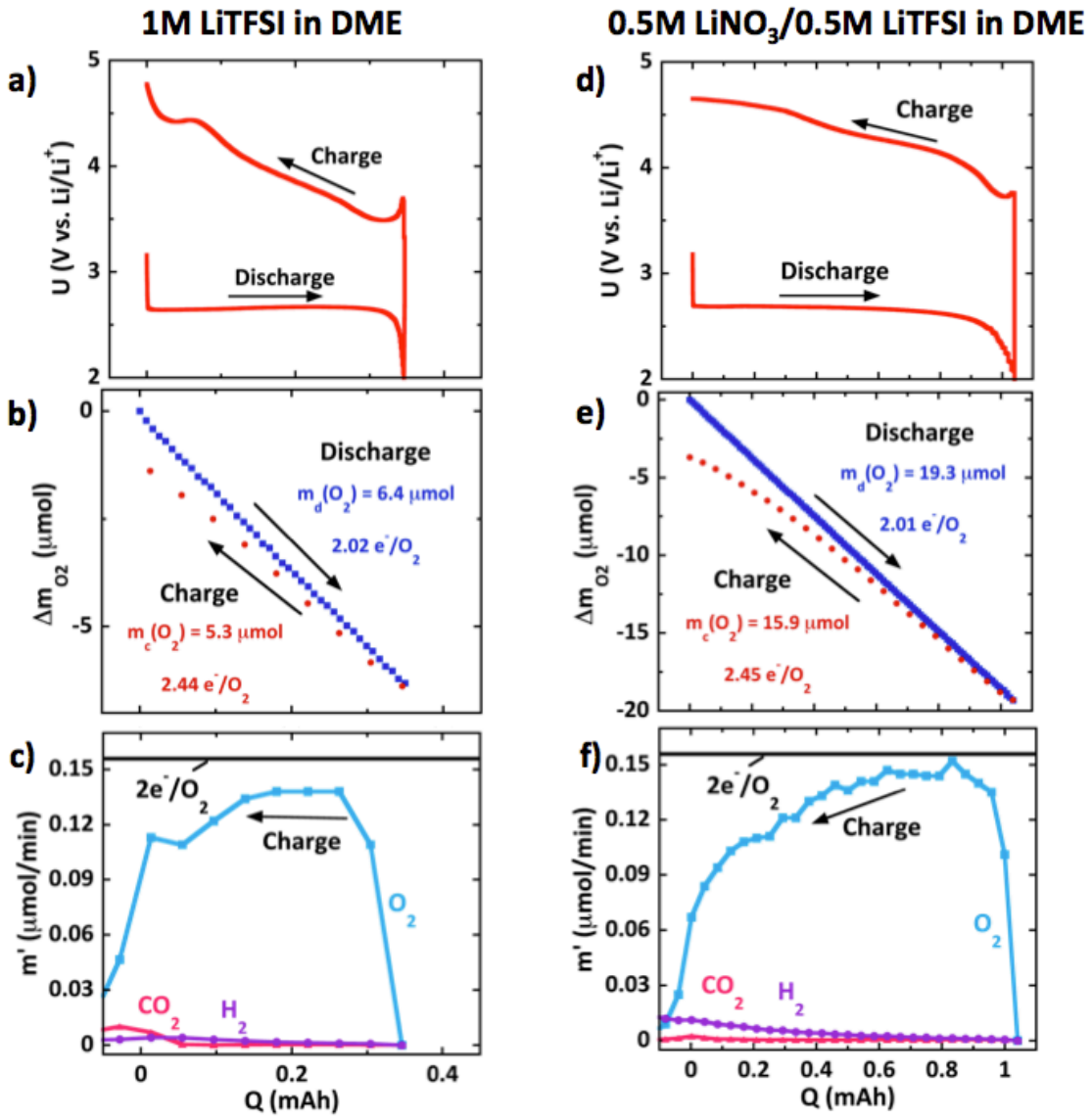

Figure 3.9. a, d) Galvanostatic discharge-charge curves for cells employing **a-c)** 1M LiTFSI in DME and **d-f)** 0.5M $LiNO_3$/0.5M LiTFSI in DME. **b, d)** Oxygen consumption during discharge and evolution during charge. **c, f)** Gas evolution rates for H_2, CO_2, and O_2 during cell charge. These were the only gases found to evolve during charge.

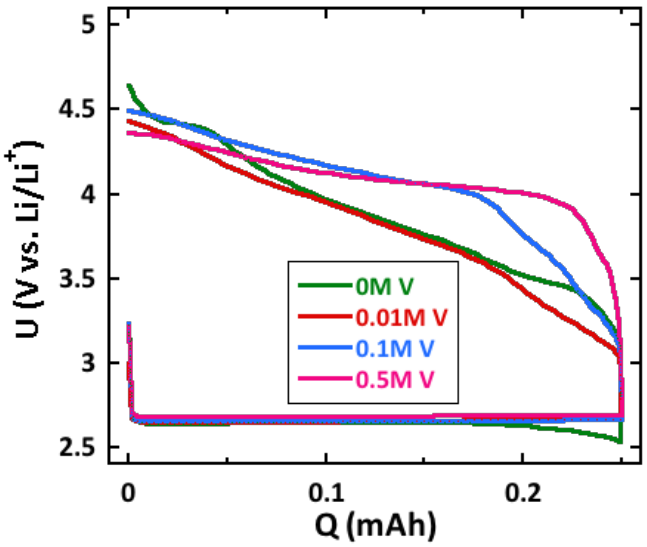

Figure 3.10. Representative discharge-charge profiles of cells of various $LiNO_3$ concentrations. All cells were discharged at 450 μA/cm^2 to 0.23 mAh/cm^2. A 1.0M Li^+ concentration was used for all cell electrolytes, while the LiTFSI/$LiNO_3$ ratio was varied. The $LiNO_3$ concentration for each cell is provided in the figure legend.

DEMS further showed only $^{18}O_2$ is evolved on charge after a discharge under $^{18}O_2$ of a cell employing 0.5M $LiN^{16}O_3$/0.5M LiTFSI, confirming that NO_3^- does not participate in the electrochemical reaction other than to induce solubility of the intermediates, i.e., NO_3^- does not act as a oxygen transfer catalyst via a redox reaction involving a reduced form like NO_2^-. This result agrees with a similar experiment using pure LiTFSI-based electrolytes,[37] implying that electroactive O_2 remains associated during both Li_2O_2 formation and oxidation. Note that this does not preclude NO_2^-, formed via the reduction of NO_3^- at the lithium metal negative electrode, from acting as a redox mediator toward Li_2O_2 via the couple NO_2^-/NO_2, as has been recently reported.[78]

3.4 Conclusion

In conclusion, we have demonstrated Li^+ counterion influence on promoting the solubility of electrochemical intermediates during a Li-O_2 battery discharge without further compromising electrolyte stability. Specifically, Li-O_2 batteries employing electrolytes of $LiNO_3$ and LiTFSI in DME display increasing capacity and increasing toroid formation with increasing $LiNO_3$ concentration. We ascribe intermediate solubility to enhanced stability of Li^+ in solution by anions with higher effective donor numbers than that of the solvent, thereby also allowing increased stability of the electrochemically formed anion, O_2^-, in solution.

The addition in $LiNO_3$ does not deleteriously affect cell rechargeability, evidenced via DEMS gas analysis, so this strategy can be easily combined with current efforts to identify novel, stable electrolytes. For example, collaborators at the private company Liox and the California Institute of Technology showed that the use of a

eutectic mixture of alkali metal nitrate salts as the electrolyte, without any organic solvent and operated at elevated temperature to melt the salt for ionic conductivity, showed superior reversibility to our typical 1M LiTFSI in DME electrolyte.[46] The carbon cathode still degraded in the presence of lithium peroxide, but this represents a significant step forward toward a practical electrolyte that both induces the solution mechanism and is stable with lithium peroxide.

Further, a generalized Ising model was developed to predict Li^+ solvation sphere occupation and the resulting stability of Li^+ in electrolytic solutions. We envision this strategy for intermediate stabilization to be generally applicable to numerous nonaqueous systems in which stabilization of desired intermediates may lead to improved electrochemical efficiency. For example, in Li-S batteries, polysulfide intermediate speciation could potentially be controlled by simply tuning the Li^+ anion, perhaps providing a route for increasing sulfur utilization.

3.5 Acknowledgments

The computational work described was performed by Vikram Pande and Professor Venkatasubramanian Viswanathan at Carnegie Mellon University and Dr. Abhishek Khetan at RWTH Aachen University, and is greatly appreciated. Special thanks to Alan Luntz, Dan Addison, Jeffrey Reimer, Hilda Buss, Jessica Nichols, and Christopher Dekmezian for helpful discussions and guidance on characterization of the materials studied here. The work at UC Berkeley was supported in part by previous work performed through the Laboratory Directed Research and Development Program of Lawrence Berkeley National Laboratory under U.S. Department of Energy Contract No. DE-AC02-05CH11231, and support for CMB was provided through the Vehicle Technologies Office under FOA DE-FOA-0000991 and start-up funds through the Department of Chemical and Biomolecular Engineering at UC Berkeley. The work at Carnegie Mellon University was supported through start-up funds through the Department of Mechanical Engineering at Carnegie Mellon University. A. K. thankfully acknowledges the funding for his doctoral studies by the Deustche Forschungsgemeinschaft (DFG).

3.6 Supporting information

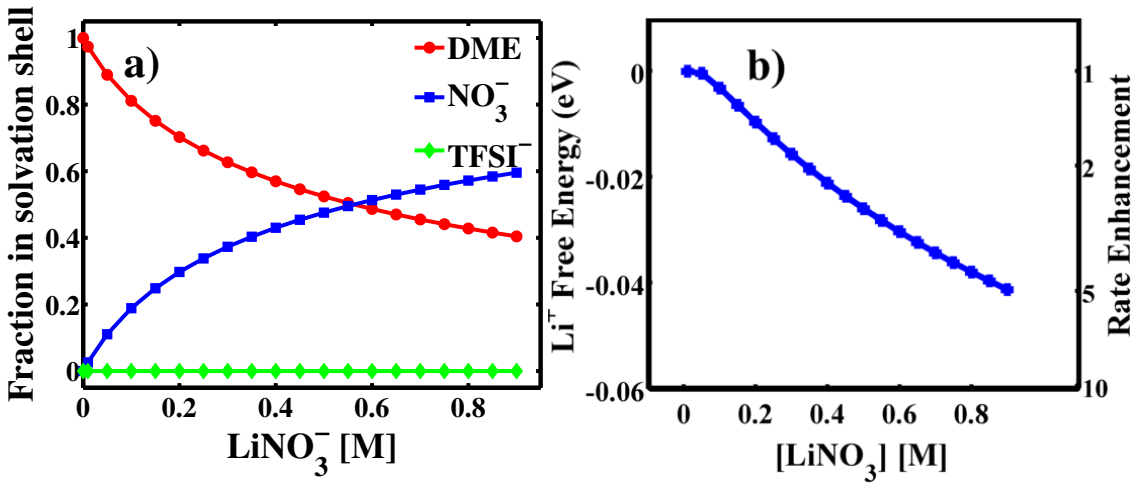

Figure 3.S1 a) The occupation of the solvent (red line), $TFSI^-$ (green line) and NO_3^- (blue line) in the Li^+ solvation shell and **b)** the Li^+ solvation energy (eV) as a function of the concentration of the NO_3^- anion. The rate enhancement of the solution process, $r_S \sim \exp\left(\frac{-\Delta G_{sol}}{kT}\right)$, is marked on the right y-axis of b). The Li^+ free energy is normalized relative to that of the case with 1M LiTFSI. There is a rate enhancement, r_S, by a factor of ~4 as the concentration of NO_3^- is increased from 0.1M to 0.5M. Prepared by Vikram Pande and Professor Venkatasubramanian Viswanathan at Carnegie Mellon University and Dr. Abhishek Khetan at RWTH Aachen University.

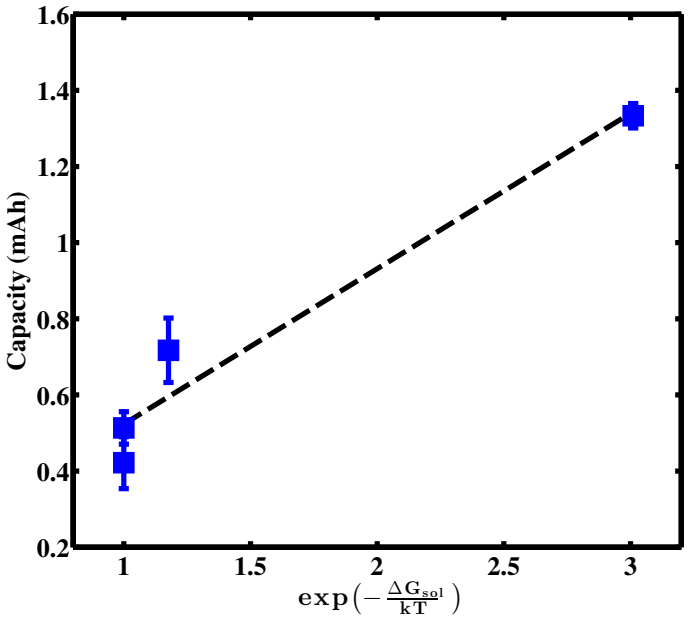

Figure 3.S2. Plot showing the linear correlation between capacity (mAh) obtained from experiments (from Figure 3.2a inset) and rate enhancement of the solution process $r_S \sim \exp\left(\frac{-\Delta G_{sol}}{kT}\right)$ as evaluated from the Ising model for various concentrations of $LiNO_3$ in DME. The plot shows that the capacity varies exponentially with the Gibbs free energy of solvation of Li^+ in the electrolyte. Prepared by Vikram Pande and Professor Venkatasubramanian Viswanathan at Carnegie Mellon University and Dr. Abhishek Khetan at RWTH Aachen University.

Chapter 4: Influence of electrolyte additives on Li-O_2 discharge capacity

Abstract

The achievable discharge capacity of the lithium-oxygen (Li-O_2) battery is limited by electrode passivation due to the deposition of the ultimate discharge product, lithium peroxide (Li_2O_2), which is an electronic insulator and insoluble in the most stable, ether-based electrolytes. Recent reports have shown electrolyte engineering can increase the achievable discharge capacity by inducing solubility of the electrochemical intermediate to Li_2O_2 formation, lithium superoxide (LiO_2). In this study, we investigate the effect of the Lewis acidity of electrolyte additives toward lowering the free energy of the superoxide anion (O_2^-) in solution, increasing LiO_2 solubility and increasing achievable discharge capacity. The addition of non-Li alkali metal cations, which are expected to lower the free energy of O_2^- relative to lithium cations according to Pearson's Hard-Soft Acid-Base theory, to ether-based electrolytes results a minimal increase in achievable discharge capacity. From the addition of lithium salt to a sodium-oxygen (Na-O_2) battery, it appears that in electrolytes containing both Li^+ and non-Li alkali metal cations, Li^+ quickly scavenges any formed O_2^-. Therefore, the resultant capacity increase from the addition of non-Li alkali metal salts to a Li-O_2 battery is likely apparent only at high currents, where oxygen reduction occurs at sufficiently high rates to allow some O_2^- to temporarily avoid association with Li^+ and remain in solution as non-Li alkali metal cation-associated O_2^-, congruent with a recent report. As analogues to the strong Lewis acid water, the addition of ppm quantities of various alcohols to ether-based electrolytes show a two-fold increase in discharge capacity, but with little trend in the Lewis acidity of the alcohols. This highlights the complexity of interactions involving Lewis basicity, Lewis acidity, and other physicochemical properties of each constituent species in an electrolyte and their effect on Li-O_2 battery performance.

4.1 Introduction

A critical issue preventing the realization of a high-capacity, rechargeable lithium-oxygen (Li-O_2) battery is electrode passivation by the ultimate discharge product, lithium peroxide (Li_2O_2). Li_2O_2 is insoluble in the most stable nonaqueous electrolytes, like ethers, and is a wide-band gap insulator. In these electrolytes, Li_2O_2 is therefore conformally deposited on the cathode's carbon support during discharge (Figure 3.1a), and it electronically passivates the cathode, preventing further discharge after only a fraction of the lithium and oxygen have reacted.[39]

As discussed in Chapter 3, the electrolyte can be engineered to circumvent this cathode passivation by enabling a solution-mediated growth mechanism of Li_2O_2 (Figure 3.1b). This mechanism is predicated on the solubility of the intermediate to lithium peroxide formation, lithium superoxide (LiO_2), to its constituent ions, Li^+ and O_2^-. The diffusion of these soluble ions away from the electrode surface enables the formation of thermodynamically favored aggregated Li_2O_2 structures and simultaneously leaves the electrode surface accessible for further reaction. Two methods were originally reported to enhance LiO_2 solubility and trigger this solubility-driven growth mechanism. Johnson et

al. presented that the use of a solvent with a high Gutmann Donor Number – a measure of Lewis basicity – like dimethyl sulfoxide (DMSO), increases LiO_2 solubility by stabilizing (or lowering the free energy of) Li^+ in solution.[45] Similarly, Aetukuri et al. presented the use of ppm quantities of water (H_2O), which has a high Gutmann Acceptor Number – a measure of Lewis acidity – to stabilize (or lower the free energy of) O_2^- in solution.[25] While both methods showed increased battery capacity via the formation of aggregated Li_2O_2 structures as confirmed via SEM, neither method proved promising, as each has been shown to decrease battery rechargeability. Strongly electron donating solvents have been shown to be more susceptible to nucleophilic attack by lithium peroxide and thus are more prone to decomposition,[59] and water impurities have been shown to cause irreversible reactions with the lithium anode.[24-25]

As discussed in Chapter 3, an appropriately selected lithium salt anion can also induce the solution mechanism of Li_2O_2 growth. As electron donors, anions have been found to play a role in stabilizing cations in solution.[72] The most common lithium-oxygen electrolytes use weakly electron donating anions, like bistrifluoromethylsulfonamide ($TFSI^-$). The addition of a lithium salt with a strongly electron donating anion, like the nitrate anion (NO_3^-), induces LiO_2 intermediate solubility without the deleterious effects of water or a strongly electron donating solvent. At increasingly higher concentrations of the strongly electron donating anion, more anions enter the solvation shell of Li^+, and thus LiO_2 solubility is further enhanced and battery capacity further increased.[40]

While an appropriately selected anion can increase capacity by four times, there are inherent limitations to the method. Higher concentrations of the anion in the lithium cation solvation shell equate to salt association, so salt solubility and possibly electrolyte conductivity limit the effectiveness of anion selection. Further, anion selection works to increase solution stability of Li^+, but Li^+ is already very stable in a 1 M solution compared to the superoxide anion, O_2^-.

In this chapter, we investigated the effect of additives to a typical lithium salt/organic solvent electrolyte toward increasing achievable discharge capacity via preferential solvation of O_2^-. Non-Li alkali metal cations, like sodium, potassium and cesium, are expected to be stronger electron acceptors from the superoxide anion, O_2^-, than lithium cations, as Pearson's Hard Soft Acid Base theory suggests that increased cation size better suits electron acceptance from the soft base O_2^-.[63] This is supported by the increased solubility of sodium superoxide, NaO_2 – the major discharge product in sodium-oxygen batteries – over LiO_2 in DME.[79] Thus, adding these cations to the electrolyte is expected to increase O_2^- solubility, and as a result increase the achievable discharge capacity of lithium-oxygen batteries. Lab-scale Li-O_2 batteries containing non-Li alkali metal salts in addition to lithium salt show a minimal increase in achievable discharge capacity. From studying the addition of lithium salt to a sodium-oxygen battery, it appears that in electrolytes containing both Li^+ and non-Li alkali metal cations, Li^+ quickly scavenges any non-Li alkali metal cation-associated O_2^-. This indicates the resultant capacity increase in a lithium-oxygen cell is minimal and only apparent at high currents, as recently reported,[80] where oxygen reduction occurs quickly enough that some O_2^- temporarily avoids Li^+ and remains in solution as non-Li alkali metal cation-associated O_2^-.

In addition to non-Li alkali metal cations, we investigated the effect of ppm quantities of methanol, ethanol, and 1-propanol on the discharge capacity of ether-based

Li-O_2 toward better understanding water's role in increasing discharge capacity. Galvanostatic discharges show these alcohols provide a two-fold increase in discharge capacity, though with little trend in their Gutmann Acceptor Numbers. This work highlights the complexity of interactions between Lewis basicity, Lewis acidity, and other physicochemical properties of each constituent species.

4.2 Experimental methods

Materials. Litithium bis(trifluoromethane) sulfonimide (LiTFSI), 1,2-dimethoxyethane (DME), dimethyl sulfoxide (DMSO), Whatman QM-A glass fiber filters, poly(tetrafluoroethylene) (PTFE, 60 wt% dispersion in H_2O), Vulcan XC72, stainless steel mesh, research-grade oxygen and argon, lithium metal foil, lithium chloride (LiCl), and 99.9% deuterium oxide (D_2O) were all sourced as described in section 3.2. Lithium triflate ($LiCF_3SO_3$) was purchased from BASF and used as received. Potassium triflate (KCF_3SO_3, 98%) and cesium perchlorate ($CsClO_4$, 99.995%) were purchased from Sigma-Aldrich and used as received. Sodium triflate was purchased from Sigma-Aldrich and dried at 80 °C under vacuum for at least 12 hours prior to use. Sodium metal was purchased from GalliumSource. AvCarb P50 carbon paper was purchased from Fuel Cell Earth. Water used to contaminate the electrolytes was ultrapure (18.2 MΩ cm) via a Millipore filtration system. Methanol (anhydrous, 99.8%) and ethanol (anhydrous, 99.5%) were purchased from Sigma-Aldrich. 1-propanol (anhydrous, 99.7%, Sigma-Aldrich) was obtained from the UC Berkeley College of Chemistry Reuse Facility.

Electrolyte preparation. All electrolyte and cell preparation was carried out in an argon glove box with <0.1 ppm O_2 and <0.1 ppm H_2O. Water, methanol, ethanol, and 1-propanol were quickly and carefully added to electrolytes in the glovebox via micropipette. Water was added at a concentration of 2000 ppm by volume. Methanol, ethanol, and 1-propanol were subsequently added at the equivalent molarity as water, such that by volume, they were added closer to 4500 ppm, 6500 ppm, and 8300 ppm, respectively.

Cathode preparation. Cathodes of Vulcan XC72 carbon on stainless steel mesh were prepared via the spray-coating method described in Chapter 2. For sodium-oxygen batteries, P50 carbon paper was punched out in 11 mm diameter discs, which were subsequently rinsed with IPA and acetone prior to drying at 150 °C under vacuum for at least 12 hours. The cathodes were then transferred, while hot, into the glovebox, and stored on a hot plate at 200 °C immediately prior to use.

Cell preparation. Lithium-oxygen batteries following the Swagelok design detailed in Chapter 2 were prepared with lithium metal as the negative electrode, Whatman QM-A as a separator, Vulcan XC72 carbon on stainless steel mesh as the positive electrode, and 80 μL of electrolyte as detailed in section 3.2. Sodium-oxygen batteries were prepared similarly, with an 11 mm diameter sodium metal negative electrode, 1/2" Whatman QM-A separator, 11 mm P50 carbon paper positive electrode, and 80 μL of electrolyte.

Cell characterization. Achievable discharge capacity was measured as the capacity at which a typical cell discharging at a constant current reached a 2 V cutoff. Pressure monitoring and titrations were performed as described in Chapter 2.

Nuclear magnetic resonance spectroscopy. As described in Chapter 3, ^{7}Li nuclear magnetic resonance spectroscopy measurements were completed on a Bruker AM-400 magnet with a 5mm Z-gradient broad brand probe. Each electrolyte was placed in an NMR tube along with a sealed melting point capillary containing 3 M LiCl in D_2O as a reliable lithium reference shift.

4.3 Results and discussion

4.3.1 Non-Li alkali metal cations

To characterize the effect of non-Li alkali metal cations on achievable discharge capacity, lab-scale Li-O_2 batteries containing non-Li alkali metal cations were discharged at constant current. Figure 4.1 shows representative discharge curves for Li-O_2 batteries containing a typical electrolyte of 1 M lithium bis(trifluoromethane) sulfonimide (LiTFSI) in dimethoxyethane (DME) and 0.005 M cesium perchlorate ($CsClO_4$) or potassium triflate (KCF_3SO_3) salts discharged at a constant current of 0.2 mA/cm^2. The addition of non-Li alkali metal salts shows little effect on achievable capacity as compared to the Li^+-only electrolyte.

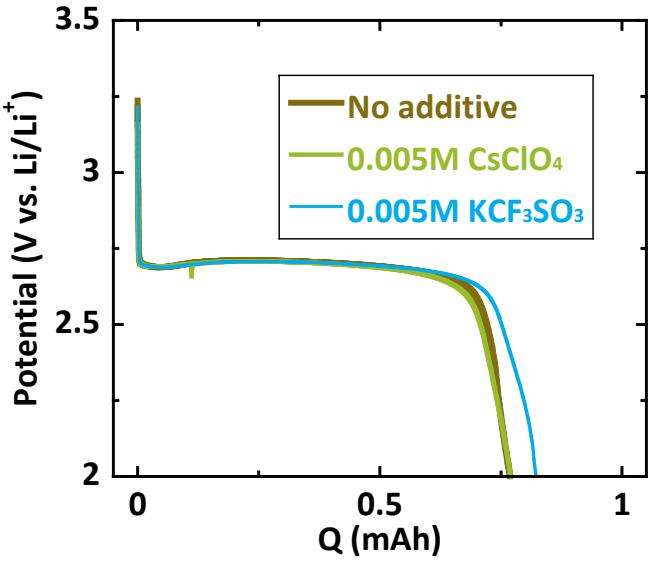

Figure 4.1 Galvanostatic discharge profiles for cells containing 1M LiTFSI in DME (brown), 1M LiTFSI in DME with 0.005M $CsClO_4$ (green), and 1M LiTFSI in DME with 0.005M KCF_3SO_3 (blue) at 0.2 mA/cm^2 to a 2 V cutoff under a constant O_2 pressure of ~1.5 atm.

The low concentrations of potassium and cesium were selected based on recent work on the addition of non-Li alkali metal cations to lithium-lithium symmetrical cells to inhibit lithium dendrite growth during electrochemical cycling.[81-82] As lithium has the lowest standard reduction potential of the alkali metals, a potassium salt electrolyte in contact with a piece of lithium metal would be expected to plate potassium on the lithium electrode while lithium dissolves into the electrolyte.

$$K^+ + e^- \leftrightarrow K \qquad U_0 = -2.931 \text{ V vs. SHE} \quad (4.1)$$

$$Cs^+ + e^- \leftrightarrow Cs \qquad U_0 = -3.026 \text{ V vs. SHE} \quad (4.2)$$

$$Li^+ + e^- \leftrightarrow Li \qquad U_0 = -3.040 \text{ V vs. SHE} \quad (4.3)$$

However, the standard reduction potentials of the larger alkali metals are sufficiently close to lithium's that, according to the Nernst equation, the non-Li salts are thermodynamically stable against lithium metal at low concentrations.[82] For a one-electron process at 25 °C, a modified Nernst equation is given by:

$$U = U_0 - 0.05916 \text{ [V]} \ln\left(\frac{a_{red}}{a_{ox}}\right) \quad (4.4)$$

where U is the effective reduction potential, U_0 is the standard reduction potential, a_{red} is the activity of the reductant, and a_{ox} is the activity of the oxidant. In this case, a_{red} is taken as unity for the solid alkali metal, and a_{ox} is approximated as the concentration of the cation that is dilute in solution. This equation can be used to estimate the concentration of a non-Li alkali metal cation at which the effective reduction potential equates the standard reduction potential of lithium, i.e., the maximum concentration of a non-Li alkali metal cation before plating onto lithium metal is thermodynamically favored. 0.005 M is a sufficiently low concentration for both K^+ and Cs^+ to expect no non-Li alkali metal plating at the lithium electrode.

Interestingly, recent reports point to the ability of larger concentrations of potassium to significantly increase the achievable discharge capacity of nonaqueous lithium-oxygen batteries. Landa-Medrano et al. showed that the addition of 0.1 M potassium triflate (KCF_3SO_3) to a 1 M lithium triflate ($LiCF_3SO_3$) in tetraglyme (TEGDME) electrolyte resulted in a three-fold increase in attainable Li-O_2 battery capacity.[80] Matsuda et al. similarly showed the addition of 50 mM KCF_3SO_3 increased the achievable discharge capacity two-fold.[83] While the Nernst equation predicts only 0.014 M potassium is stable in thermal equilibrium with lithium metal, these reports imply a kinetic barrier prevents significant potassium plating on the lithium metal negative electrode.

Furthermore, these recent reports showed that a significant capacity increase with non-Li alkali metal cations only occurs at high current densities. This is interesting, as all previous methods of inducing the solution mechanism have shown an increase in the solution mechanism with a decrease in current density, as decreasing the rate of LiO_2 production increases the likelihood of LiO_2 dissolution over immediate reduction or disproportionation to form surface Li_2O_2.[25, 40, 45] In the case of a non-Li alkali metal salt additive, an increase in the solution mechanism hinges on the electrochemical formation of the non-Li alkali metal superoxide, rather than lithium superoxide, in order to take advantage of the increased solubility of the non-Li alkali metal superoxide over LiO_2. Landa-Medrano et al. propose that high current densities enable KO_2 formation and dissolution with temporary avoidance of O_2^- with Li^+ ions.

Upon contact in solution, Li^+ immediately reacts with O_2^- to form LiO_2 and consequently Li_2O_2 upon additional charge transfer or disproportionation.[80, 84] This mechanism is supported by the addition of lithium salt to a sodium-oxygen battery.

Sodium-oxygen batteries exhibit the 1 e^-/O_2 formation of sodium superoxide, NaO_2, as their dominant discharge process. Shown in Figure 4.2, the addition of 0.1 M $LiCF_3SO_3$ to an electrolyte of 1 M $NaCF_3SO_3$ in DME in a sodium-oxygen battery exhibits a 1.95 e^-/O_2 process on discharge until it nears the capacity associated with lithium exhaustion, whereby the discharge process switches to an expected 1.08 e^-/O_2 process. This confirms that Li^+ quickly scavenges any non-Li alkali metal cation-associated O_2^- in metal-oxygen batteries containing both Li^+ and non-Li alkali metal cations.

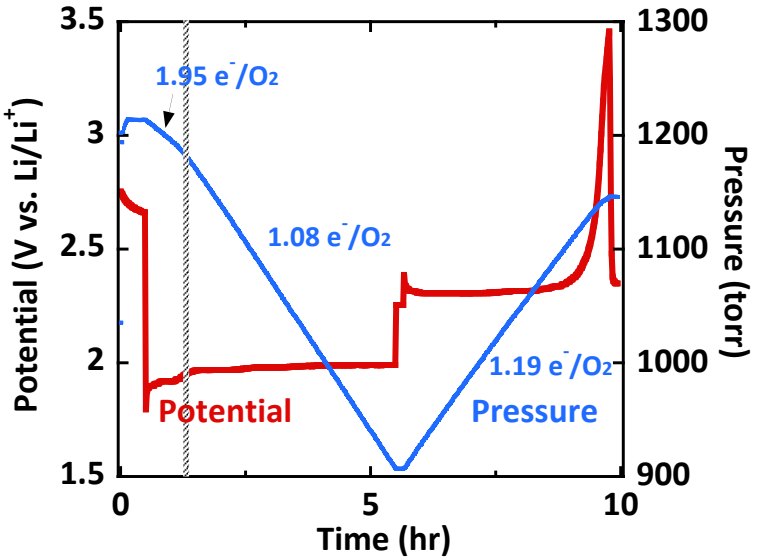

Figure 4.2 Potential and pressure profiles for a sodium-oxygen cell containing a sodium anode, P50 carbon paper cathode, and 80 µL of 1M $NaCF_3SO_3$ and 0.1M $LiCF_3SO_3$ in DME. Cell was rested at open circuit for 0.5 hr, discharged at 0.2 mA/cm^2 to 1 mAh capacity, rested at open circuit for 10 min, charged at 0.2 mA/cm^2 to 3.5 V (reached at 0.82 mAh charge capacity), and rested at open circuit for 10 min. There is sufficient lithium for 0.21 mAh (94 min) of an ideal 2 e^-/O_2 process, noted by the dotted line.

We tested similar lithium-oxygen cells in our lab to those recent reports mentioned above, particularly focusing on high current discharges where a substantive difference in capacities was observed between purely Li^+ containing electrolytes and those containing additional small K^+ or Cs^+ inclusions. Figure 4.3 shows a small increase in capacity with 0.1 M KCF_3SO_3 at higher current, though a smaller capacity increase than prior reports.[80, 83] Of note, all cells exhibited a 2.0 e^-/O_2 process on discharge, indicating little to no formation of KO_2 – a 1 e^-/O_2 product – as a final product. Toward studying even higher current densities, we performed chronoamperometry in an attempt to maximize formation of non-Li alkali metal-associated O_2^- before Li^+ scavenging. Figure 4.4 shows the resultant current and the corresponding O_2 consumption rates from monitoring cell pressure of cells discharged at 2.3 V for 10 hours. The cell without the potassium additive, displayed in Figure 4.4a, actually exhibited a larger integrated capacity of 1.20 mAh compared with 1.01 mAh for the cell with K^+, displayed in Figure

4.4b. The axes in Figure 4.4 are scaled for 2 e^-/O_2, showing that each cell also maintained a 2 e^-/O_2 process throughout discharge.

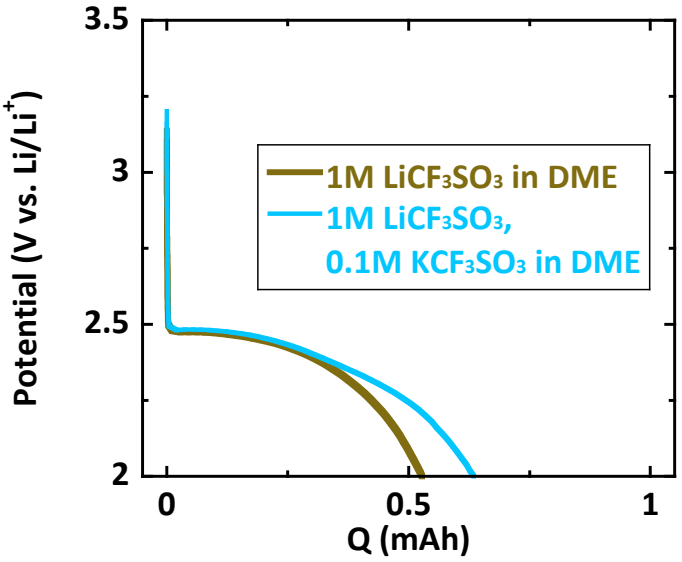

Figure 4.3 Galvanostatic discharge profiles from cells containing 1M $LiCF_3SO_3$ in DME (brown) and 1M $LiCF_3SO_3$ in DME with 0.1M KCF_3SO_3 (blue) at 2 mA/cm^2 to a 2 V cutoff under a closed headspace of O_2.

While these results are seemingly at odds with the recent literature, various experimental differences could play a role. A different lithium metal surface layer in our lab-scale cells could cause more potassium to plate out, decreasing the amount of potassium active at the cathode. Geometric factors, such as electrode surface area and the ratio of electrolyte volume to electrode surface area, could also differ. It is likely the addition of non-Li alkali metal salts modestly increases the achievable discharge capacity of Li-O_2 batteries at high current densities, although not as substantially as the inclusion of ppm quantities of water or high Lewis basicity anions (e.g., NO_3^-).

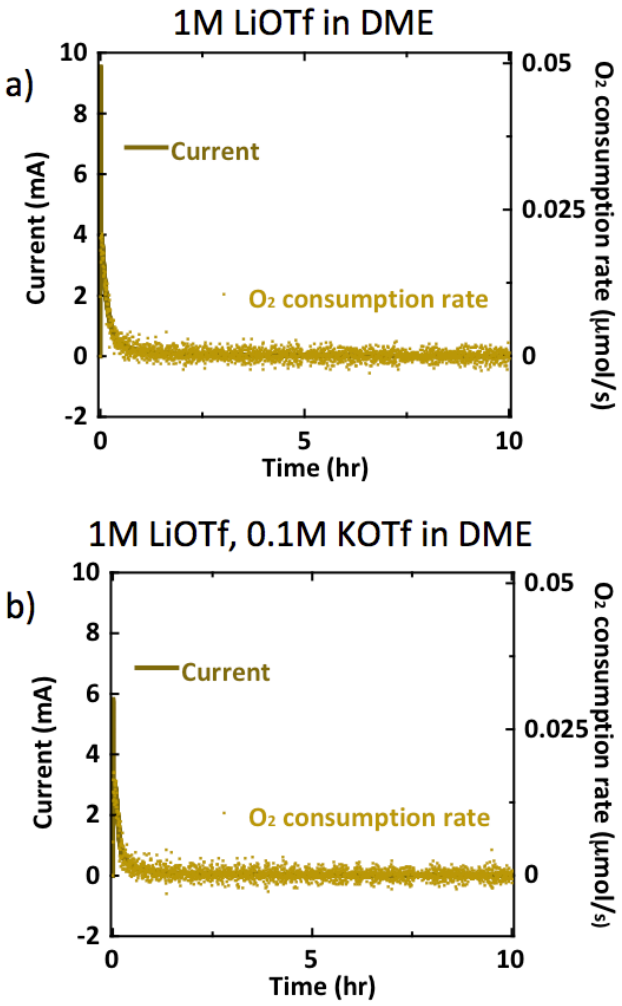

Figure 4.4 Chronoamperometry at 2.3 V under a closed O_2 headspace of cells containing **a)** 1M $LiCF_3SO_3$ (LiOTf) in DME and **b)** 1M $LiCF_3SO_3$ in DME with 0.1M KCF_3SO_3 (KOTf). Axises for current (brown line) and O_2 consumption rate (gold points) are scaled for a 2 e^-/O_2 process.

4.3.2 Alcohols

As described in the introduction, another additive considered to increase cell capacity by lowering the free energy of O_2^- in solution is water. Aetukuri et al. showed that the addition of 2000 ppm of H_2O resulted in a six-fold increase in achievable discharge capacity of a Li-O_2 battery containing an ether-based electrolyte. Aetukuri et al. argued that water's high Gutmann Acceptor Number, a measure of Lewis acidity, results in preferential solvation of O_2^- and a concomitant lowering of the free energy of O_2^- in solution.[25]

Toward investigating this mechanism, we studied the effect on Li-O_2 discharge capacity of adding ppm quantities of anhydrous methanol, ethanol, and 1-propanol to an ether-based electrolyte. Considering the chemical similarity of water and alcohols (R-OH, with R=H for water and R=alkyl substituents for alcohols), increasing the alkyl chain length correlates to decreasing Lewis acidity, or decreasing Acceptor Number, as shown in Table 4.1. Electrolytes consisting of our typical, most-stable electrolyte of 1 M lithium bis(trifluoromethane)sulfonimide (LiTFSI) in dimethoxyethane (DME) were prepared with 2000 ppm H_2O by volume or an identical molarity of anhydrous methanol, ethanol, or 1-propanol, labeled as "2000 ppm equivalent" in Table 4.1.

Table 4.1 presents the average achievable discharge capacity of lab-scale Li-O_2 batteries containing these electrolytes from galvanostatic discharges at 0.5 mA/cm^2, normalized by the milligrams of carbon in the electrode, which is a proxy for the available surface area. The alcohols induce a two-fold increase in battery capacity relative to no additives. However, water increases the capacity more than five-fold, and there is little trend in the capacity as a function of the additive's Acceptor Number. Of note, each electrolyte composition corresponded to a near 2 e^-/O_2 process, and titrations confirmed the formation of Li_2O_2 as the dominant discharge product.

Table 4.1 Discharge capacity for batteries containing 1M LiTFSI in DME and added H_2O, methanol, ethanol, or 1-propanol. The added H_2O is 2000 ppm by volume; the methanol, ethanol, and propanol were added such that equivalent moles were added as for the H_2O electrolyte (i.e., 4500 ppm, 6500 ppm, and 8300 ppm by volume, respectively). Gutmann Acceptor Numbers and Donor Numbers are from Knovel Solvents – A Properties Database.[85]

Additive to 1M LiTFSI in DME	Additive AN	Additive DN (kcal/mol)	Average capacity (mAh/mg)	Electrolyte ^{7}Li peak (ppm) referenced to 3M LiCl in D_2O
None	n/a	n/a	0.3	-1.18
2000ppm H_2O	54.8	18	1.7	-1.12
2000ppm equiv. methanol	41.5	30	0.6	-1.16
2000ppm equiv. ethanol	37.1	32	0.6	-1.16
2000ppm equiv. 1-propanol	33.7	30	0.7	-1.16

As seen in Table 4.1, the alcohols each have a higher Donor Number than water, in addition to their lower Acceptor Numbers. This could point to stronger interaction

between the alcohol and Li^+ than water and Li^+, at the expense of favorable solvation of O_2^-. This hypothesis is supported by the effect of water on achievable discharge capacity when dimethyl sulfoxide (DMSO) is used as the electrolyte solvent. DMSO is a stronger Lewis base than DME, with a Gutmann Donor Number of 29.8 kcal/mol compared to DME's 20 kcal/mol.[85] As a strong Lewis base, DMSO has been shown to strongly solvate Li^+, but it possibly also strongly solvates Lewis acid additives, like water, decreasing their interaction with O_2^-. Table 4.2 shows the addition of 2000 ppm H_2O to a DMSO-based electrolyte results in the same ultimate capacity as 2000 ppm H_2O in DME. This corresponds to a three-fold increase in capacity over an anhydrous DMSO electrolyte, whereas 2000 ppm H_2O in DME corresponds to more than a five-fold increase in capacity over an anhydrous DME electrolyte. This shows the interaction of DMSO with Li^+ and the interaction of H_2O with O_2^- are not mutually exclusive, as the ultimate capacity is less than the sum of the enhancement from just DMSO and from just 2000 ppm H_2O. Rather, the resultant capacity is at the least a complex mixture of the accepting and donating properties of each electrolyte constituent.

Table 4.2 Li-O_2 battery capacity results for dimethyl sulfoxide (DMSO)-based electrolytes. Acceptor Number and Donor Number values are from Knovel Solvents – A Properties Database.[85]

Additive to 1M LiTFSI in DMSO	Additive AN	Additive DN (kcal/mol)	Average capacity (mAh/mg)
None	n/a	n/a	0.6
2000ppm H_2O	54.8	18	1.8

In an attempt to measure the effect of the alcohols' higher Donor Numbers on Li^+ solvation, ^7Li NMR was performed, as discussed in Chapter 3. Figure 4.5 shows each electrolyte's ^7Li peak referenced to 3 M LiCl in D_2O, a reliable reference shift for lithium, contained in a sealed melting point capillary within the sample tube. The exact electrolyte peak shifts are listed in Table 4.1 as well. Only one ^7Li peak was observed for each electrolyte composition, and is indicative of the average of all Li^+ environments in the electrolyte. A downfield shift of this lithium peak relative to the reference indicates the lithium is on average interacting with stronger Lewis bases, indicating a higher apparent Donor Number of the electrolyte. There is a slight correlation between the ^7Li peak and the capacity, but the magnitude of the change (e.g., 0.06 ppm from anhydrous to 2000 ppm H_2O) is small. To compare, an electrolyte of 0.5 M $LiNO_3$/0.5 M LiTFSI in DME, which induces a capacity increase similar to 1000 ppm H_2O, exhibits an electrolyte peak shifted over 0.5 ppm further downfield than the electrolyte peak of anhydrous 1 M LiTFSI in DME. Furthermore, ^7Li peaks can be complicated by more factors than just electron density due to a relative balance in lithium's paramagnetic and diamagnetic contributions.[71] Thus, this perhaps simply highlights the difficulty in assessing Li^+ solvation from ^7Li NMR.

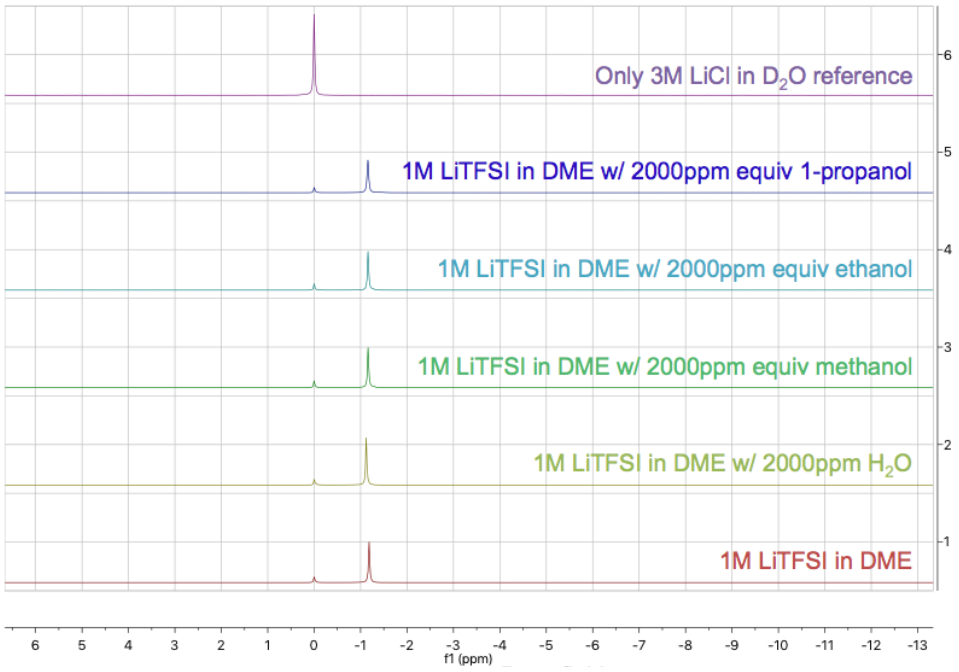

Figure 4.5 ^{7}Li NMR spectra of labeled electrolytes referenced to 3 M LiCl in D2O in a sealed melting point capillary in the NMR tube. This reference is set to 0 ppm. Downfield corresponds to more positive ppm values.

4.4 Conclusion

In conclusion, we studied the effect of adding non-Li alkali metal cations and ppm quantities of alcohols to ether-based Li-O_2 battery electrolytes on Li-O_2 discharge capacity. The addition of non-Li alkali metal salts induces a minimal increase in achievable discharge capacity in our lab-scale Li-O_2 cells. Gas analysis of the addition of lithium salt to a sodium-oxygen battery shows Li^+ quickly scavenges any non-Li alkali metal cation-associated O_2^- in electrolytes containing both Li^+ and non-Li alkali metal cations. This corroborates that a capacity increase is only expected at high currents when oxygen reduction occurs quickly enough that some O_2^- temporarily avoids Li^+ and solubilizes as non-Li alkali metal cation-associated O_2^-, as recently proposed.[80]

The addition of ppm quantities of methanol, ethanol, or 1-propanol to ether-based Li-O_2 battery electrolytes induces a two-fold increase in battery capacity. However, there is little trend in the capacity as a function of the additive's Acceptor Number, highlighting the complexity of interactions between Lewis basicity, Lewis acidity, and other physicochemical properties of each constituent species in an electrolyte.

Experimental confirmation of the ability of additive species to solvate and lower the free energy of the superoxide anion is difficult, as O_2^- forms in situ and is a short-lived species in the presence of Li^+. Through the NASA Space Technology Research Fellowship (NSTRF) program, I have worked with collaborators at NASA's Ames Research Center developing density functional theory and molecular dynamics modeling of additives' influence on the solvation of O_2^- in ether-based Li-O_2 electrolytes. Dr. John Lawson's group has recently published robust molecular dynamics models of lithium electrolytes, both in the bulk and at electrochemical interfaces, which can determine

solvation shells and double layer behavior.[86-87] Applying these models to ether-based electrolytes containing LiO_2 and either non-Li alkali cations or ppm quantities of water or alcohols could inform the important physicochemical properties of additives for preferential solvation of O_2^-.

4.5 Acknowledgments

I gratefully acknowledge Chris Dekmezian and Howie Nguyen for working with me as undergraduate researchers on the effect of non-Li alkali metal cations on Li-O_2 discharge capacity. This work was supported by a NASA Space Technology Research Fellowship.

Chapter 5: Implications of 4 e^- oxygen reduction via iodide redox mediation in Li-O_2 batteries with trace water

Adapted with permission from Burke, C. M.; Black, R.; Kochetkov, I. R.; Giordani, V.; Addison, D.; Nazar, L. F.; McCloskey, B. D., Implications of 4 e^- Oxygen Reduction via Iodide Redox Mediation in Li–O_2 Batteries. *ACS Energy Letters* **2016,** *1* (4), 747-756.[41]

Abstract

The nonaqueous lithium-oxygen (Li-O_2) electrochemistry has garnered significant attention due to its high theoretical specific energy compared to the state-of-the-art lithium-ion battery. The common active nonaqueous Li-O_2 battery cathode electrochemistry is the formation (discharge) and decomposition (charge) of lithium peroxide, Li_2O_2. In high-capacity cells, Li_2O_2 forms in large aggregated structures, but it is an insulator and insoluble in common Li-O_2 battery electrolytes and is therefore difficult to oxidize on charge. Recent research has focused on identifying small molecules that can serve as soluble redox mediators between Li_2O_2 and the electrode surface. One of the best candidates is lithium iodide, LiI, because the I^-/I_3^- redox potential is only slightly higher (~3V vs. Li/Li^+) than the equilibrium potential of Li_2O_2 oxidation to O_2 (~2.96V vs. Li/Li^+). Interestingly, recent reports suggest that the introduction of lithium iodide to an ether-based electrolyte containing water at impurity levels induces a 4 e^- oxygen reduction reaction forming lithium hydroxide, LiOH, as the dominant discharge product. We provide quantitative analysis of the influence of LiI and H_2O on the electrochemistry in a common Li-O_2 battery employing an ether-based electrolyte and a carbon cathode. We confirm, through numerous quantitative techniques, that the addition of LiI and H_2O promotes efficient 4 e^- oxygen reduction to LiOH on discharge, which is unexpected given that only 2 e^- oxygen reduction is typically observed at undoped carbon electrodes. Unfortunately, LiOH is not reversibly oxidized to O_2 on charge, where instead a complicated mix of redox shuttling and side reactions is observed.

5.1 Introduction

Due to its high theoretical specific energy, the Li-air (or O_2) battery is currently being explored as a possible alternative to lithium-ion batteries.[9, 21] In typical nonaqueous Li-O_2 cell compositions, lithium peroxide (Li_2O_2) formation and oxidation has been identified as the reversible electrochemical reaction at the carbon cathode:

$$2Li^+ + 2e^- + O_2 \leftrightarrow Li_2O_2 \quad (2e^- \text{ process}) \; U = 2.96\,V \text{ vs. } Li^+/Li \quad (5.1)$$

The forward reaction occurs on discharge and the reverse reaction occurs on charge. Unfortunately, many unsolved scientific challenges inhibit the achievement of reversible, efficient Li_2O_2 formation and oxidation, with two being particularly pressing. First, Li_2O_2 and its intermediates (O_2^- and LiO_2) are known to undergo parasitic side reactions with organic electrolytes and carbon cathodes during battery operation.[1, 29, 31, 36, 47, 56, 61, 88-93] When a realistically small electrolyte volume is used, these reactions limit Li-O_2 cell rechargeability to only a few cycles. Additionally, the products of these parasitic

reactions include solid carbonate/carboxylate species, which accumulate at the electrode surface, thereby blocking O_2 evolution from the Li_2O_2-electrolyte interface on charge.[34] As a result, the potential on charge necessarily increases to values substantially higher (>1 V higher) than the equilibrium potential for O_2 evolution from Li_2O_2, creating an energy inefficient battery. With these parasitic reactions seemingly exacerbated at high potentials, this challenge perpetuates itself. Therefore, parasitic reactions are linked with energy inefficiency and are detrimental to rechargeability.

Second, Li_2O_2 is a wide bandgap insulator and is insoluble in all studied organic electrolytes. Therefore, as it deposits on the cathode during discharge, it passivates the electrode surface, limiting Li-O_2 cell discharge capacity to a minor fraction of that necessary to compete with the specific energy of Li-ion batteries.[38-39, 42, 48-50, 94] Recent reports have elucidated strategies to partially circumvent this passivation issue by triggering a solution-based mechanism for Li_2O_2 formation.[25, 40, 45-46] However, this mechanism results in Li_2O_2 deposition in large toroids, as shown in Figure 5.1a, and perhaps Li_2O_2 deposition away from the cathode surface.[68] A fraction of Li_2O_2 therefore becomes electronically isolated from the conductive cathode surface, likely contributing to the observed large charge overpotentials.

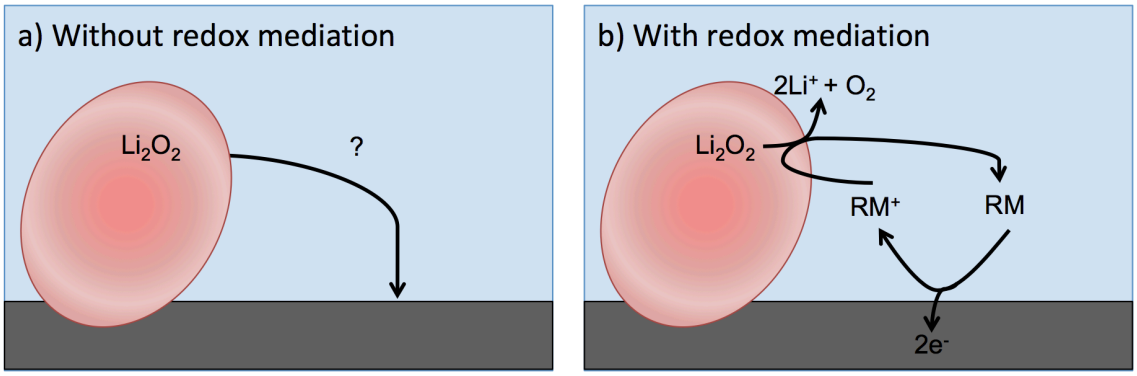

Figure 5.1. Schematics for charging lithium peroxide particles (pink) on carbon electrode (charcoal) in typical ether-based electrolytes (blue) **a)** without and **b)** with redox mediation.

Substantial research into redox mediators is being pursued to address these charge transport limitations. In the context of Li-O_2 batteries, redox mediators are small, soluble molecules with a reversible redox potential slightly above the equilibrium potential of the Li-O_2 battery (experimentally observed as ~2.85 V).[37] During charge, as shown in Figure 5.1b, the mediator oxidizes at electronically accessible sites on the cathode, diffuses to electronically isolated Li_2O_2, and accepts charge via an outer sphere electron transfer from the Li_2O_2, allowing the Li_2O_2 to be oxidized while regenerating the redox mediator.[95] The battery therefore charges near the redox potential of the mediator, which, if appropriately selected, is only slightly above the open circuit potential of the battery, rather than reaching the high potentials required to presumably drive charge transport through Li_2O_2. The lower charge potential also provides a route to reduce parasitic processes observed at high potentials. Numerous redox mediators have now been studied in Li-O_2 batteries, including tetrathiafulvalene (TTF),[96] (2,2,6,6-Tetramethylpiperidin-1-

yl)oxyl (TEMPO),[97] tris[4-(diethylamino)phenyl]amine (TDPA),[98] iron phthalocyanine (FePC),[99] and lithium iodide (LiI).[100-101]

LiI is a redox mediator of particular interest. Iodide, I^-, exhibits two redox couples in a common nonaqueous ether-based Li-O_2 electrolyte:

$$3I^- \leftrightarrow I_3^- + 2e^- \quad U = \sim 3 \text{ V vs. } Li^+/Li \qquad (5.2)$$

$$2I_3^- \leftrightarrow 3I_2 + 2e^- \quad U = \sim 3.5 \text{ V vs. } Li^+/Li \qquad (5.3)$$

The potentials listed are experimental oxidative onset potentials in dimethoxyethane, as shown in Figure 5.2 via cyclic voltammetry in lithium/porous carbon cells under an argon headspace. The first redox couple, ascribed to the I^-/I_3^- redox reaction shown in equation 5.2, is just above the Li-O_2 equilibrium potential, and I^- is stable against reduction against lithium unlike many organic redox mediators.[95, 102]

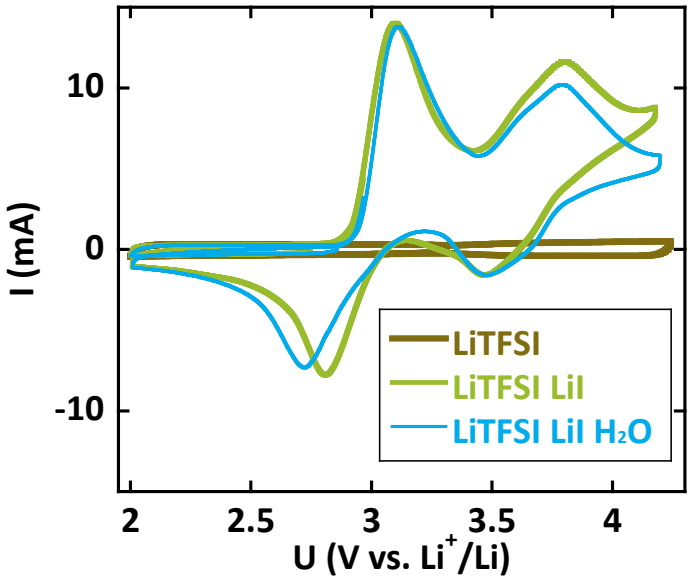

Figure 5.2. Cyclic voltammetry of cells under an argon headspace containing XC72 carbon electrodes and 0.25 M LiTFSI in DME (brown line), 0.25 M LiTFSI/0.2 M LiI in DME (green line), and 0.25 M LiTFSI/0.2 M LiI/500 ppm H_2O in DME (blue line). Each cell was reductively scanned to 2 V, anodically scanned to 4.25 V, cathodically scanned to 2 V, and returned to OCV. Sweep rate was 10 mV/s. CVs were IR corrected with electrolyte resistance via PEIS impedance. PEIS parameters were 10 mV amplitude from 100 kHz to 50 mHz, 8 points per decade. CVs clearly show I^-/I_3^- (oxidative onset at ~3.0 V) and I_3^-/I_2 (oxidative onset at ~3.5 V) redox couples.

Interestingly, recent reports indicated that in a typical nonaqueous Li-O_2 cell containing LiI and water impurities, Li_2O_2 was not the ultimate discharge product, but rather LiOH.[100-101, 103] This is interesting, as water by itself does not induce the formation of LiOH rather than Li_2O_2,[25] and possibly provides a route to reducing parasitic reactions

typically associated with Li_2O_2 formation and oxidation. Furthermore, an incredibly low voltage gap (~200 mV) between the discharge and charge voltage plateaus was observed, indicating that the cell achieved a remarkable energy efficiency.[101] LiOH oxidation to O_2 and H_2O through the action of the I^-/I_3^- redox couple (3 V vs. Li/Li^+) was reported as the active charge electrochemistry, although the I^-/I_3^- redox potential lies below the standard potential for LiOH oxidation at standard conditions (3.45 V vs. Li/Li^+). Liu et al. indicate in their motivating work that the equilibrium of water, iodide, and oxygen is complex, and the role of polyanions (iodo-oxygen species) on the LiOH oxidation mechanism is poorly understood.[101, 104-105] Therefore, while the reported electrochemistry of the I^-/I_3^- couple for Li-O_2 batteries is intriguing, the exact activity of the I^- and its oxidized states, I_3^- and I_2, towards Li_2O_2/LiOH oxidation is unclear.

In this chapter, with the help of collaborators at the University of Waterloo and the private company Liox, we present quantitative insight into the influence of LiI and H_2O on the electrochemistry of a typical nonaqueous Li-O_2 cell employing a carbon cathode. LiOH is observed as the primary discharge product, along with minor parasitic side products, when LiI and H_2O are both present in the cell, with H_2O consumed in the oxygen reduction reaction. If H_2O (which is present in impurity quantities in our study) is fully consumed during discharge, the discharge electrochemistry reverts back to the more common 2 e^- oxygen reduction reaction to form Li_2O_2. On charge, the concentrations of LiI and H_2O and the identities of the discharge products all have a dramatic influence on the observed electrochemistry and resultant voltage profiles. Isotopic labeling confirmed that O_2 evolution is only observed to occur from Li_2O_2, although reactions between Li_2O_2 and oxidized iodo species (I_3^-) can result in other product formation at low potentials (~3 V). No O_2 evolution was observed from electrochemically formed LiOH. Instead, LiOH reacts with I_2, which electrochemically forms at ~3.5V from I_3^- oxidation, to form H_2O and $LiIO_3$, the latter of which can be solubilized in water-contaminated DME. Thus, while the 4 e^- oxygen reduction activity on carbon electrodes in the presence of water impurities and I^- is intriguing, the addition of LiI and water to a Li-O_2 battery does not promote a reversible oxygen electrochemistry in the cell compositions studied.

5.2 Experimental methods

Materials and methods described below are for my contributions to this study. Li-O_2 cells with slight variations in design and material were employed by our collaborators (supporting information figures) but showed consistent results, as discussed at the beginning of section 5.3.

Materials. Lithium iodide was purchased from Sigma-Aldrich and was dried under vacuum in a heated glove box antechamber at 150 °C for 24 hours before use. Lithium bis(trifluoromethane) sulfonamide (LiTFSI) and 1,2-dimethoxyethane (DME) were purchased from BASF and used as received. PTFE (both 60 wt% dispersion in H_2O and 1 μm particle-size powder) was purchased from Sigma-Aldrich. Vulcan XC72 was purchased from Fuel Cell Store and was filtered through a 60-mesh screen. Ketjenblack® (KB) was received from Toyota. T316 stainless steel 120 mesh, with wire diameter 0.0026", was purchased from TWP Inc. Research-grade oxygen and argon were purchased from Praxair. 99% $^{18}O_2$ was purchased from Sigma-Aldrich. 90% $H_2{}^{18}O$ was purchased from Cambridge Isotopes. 99.9% deuterium oxide (D_2O) was purchased from Cambridge Isotope Laboratories, Inc. and used as received. Water used to contaminate

the electrolytes was ultrapure (18.2 MΩ cm, Millipore). All electrolyte and cell preparation was carried out in an argon glove box with <0.1 ppm O_2 and <0.1 ppm H_2O. Water was quickly and carefully added to electrolytes in the glovebox via micropipette. Lithium foil with a thickness of 0.01" was purchased from FMC Lithium.

Cathode preparation. The XC72 cathodes were prepared as described in Chapter 2. The Ketjenblack carbon cathodes were prepared via a slurry method. First, 20 mg of PTFE powder was added to 500 μL of IPA and sonicated for at least 1 hour. Second, a volume of this solution was mixed with four times its volume of ethanol and added to a vial containing lightly ground KB such that the final mixture was 85:15 w:w KB to PTFE. This mixture was sonicated and stirred for five minutes, three times each, until thick but flowing. If the mixture was too thick or started to dry out, more ethanol was added (usually about a couple of milliliters). The mixture was then spread over 12 mm diameter pieces of stainless steel mesh that had been cleaned with IPA and acetone and dried at 150°C. These were left to dry in a fume hood for 12 hours, and then were dried at 150 °C under vacuum for at least 12 hours and transferred hot to the glove box, similarly to the XC72 cathodes.

Cathode carbon loadings are identified in figure captions. Each set of data (high LiI DEMS, low LiI DEMS, titrations, etc.) used cathodes from the same batch with similar loading.

Cell assembly. Li-O_2 cells following the same hermetically sealed Swagelok design as described in Chapter 2 were built in an argon glove box with < 0.1 ppm H_2O and O_2. Cells consisted of 7/16" diameter pure lithium metal, 1/2" diameter Whatman QMA glass fiber as a separator, electrolyte, and a 12 mm diameter cathode of XC72 or KB carbon, with PTFE binder, on stainless steel mesh. Either 80 or 160 μL of electrolyte of varying concentrations of LiI, LiTFSI, and water in nominally anhydrous DME were added to each cell. Cells employing 80 μL contained one glass fiber separator; cells employing 160 μL contained two. The cells had a headspace of approximately 1.5 mL, which were discharged starting with a headspace of ~1.5 atm pure O_2, and charged starting with a headspace of ~1.2 atm Ar.

Gas quantification. To quantify oxygen consumption and gas evolution, such as shown in Figure 5.3, cells were attached to a differential electrochemical mass spectrometry (DEMS) setup with a pressure transducer within the closed cell headspace, as described in Chapter 2.

On discharge, oxygen consumption was quantified via pressure decay of a known cell headspace volume. Cells containing ≥2000 ppm of water showed a discernible pressure increase at open circuit potential due to hydrogen evolution from the water reacting with the lithium anode. Cells were left at open circuit potential for 30 minutes prior to discharge and 30 minutes after discharge to record the pressure rise. An average of these rises was subtracted from the pressure decay to obtain a corrected pressure change during discharge. Pressure rise was only ever witnessed before and after a 4 e^-/O_2 process, never before or after a 2 e^-/O_2 process, because in LiI-containing cells, a 2 e^-/O_2 process only occurred if any intentionally added water was entirely consumed during LiOH formation, obviously disallowing parasitic water reduction to evolve hydrogen at the anode. Therefore, if a battery exhibited a switch from a 4 e^-/O_2 process to a 2 e^-/O_2 process in the middle of the discharge, it was approximated that the onset of the 2 e^-/O_2 process was where pressure rise from hydrogen evolution at the anode ceased, which was

then taken into consideration during calculations of O_2 consumption in the pressure rise/decay measurements.

Of note, hydrogen evolution, and thus the reaction between water and the lithium metal electrode, is negligible for cells with low water contents (<2000 ppm). We do not see an increase in pressure over 30 minutes, with a resolution of +/- 0.2 torr. An increase in pressure of 0.2 torr over 30 minutes would correspond to a gas evolution rate of 0.001 μmol/min. The actual rate of H_2 evolution/LiOH formation at the anode will consistently decrease during discharge as water is consumed at both the anode and cathode, such that over the course of a 10 hour discharge (100 μA to 1 mAh), at most 0.6 μmol of LiOH could be formed at the lithium metal electrode.

For cells containing high water contents, the amount of LiOH formed at the lithium metal electrode is much smaller than that electrochemically formed at the positive electrode. Of the battery compositions studied, a battery containing 160 μL of electrolyte with 5000 ppm H_2O exhibited the most LiOH formation at the lithium metal electrode, as evidenced by hydrogen evolution at open circuit potential. This was confirmed via DEMS and then quantified via pressure measurements of a closed headspace. The initial rate of water consumption at the lithium metal electrode to form LiOH in these cells was 0.0088 μmol/min. Over the course of a 10-hour discharge (100 μA to 1 mAh), this corresponds to approximately 5.3 μmol of chemically-formed LiOH at the anode. We expect substantially less LiOH formation than this at the anode, as no H_2 evolution was observed after a discharge, indicating that the LiOH formation rate at the anode decreases to undetectable values during the discharge. At the cathode, these high water content batteries exhibit 37.3 μmol of LiOH formation. Thus, electrochemical formation of LiOH at the cathode is clearly the dominant source of LiOH in these high water content cells.

On charge, gas evolution was quantified by DEMS, as described in Chapter 2. Again, the cell headspace at the beginning of charge was pure argon. Whenever a cell was charged with the mass spec, an identical cell was charged with simple pressure rise measurements to verify that the gas evolution from the mass spectrometer (O_2, H_2, CO_2) matched the observed pressure rise.

Titrations for LiOH and Li_2O_2 quantification. Titrations of carbon positive electrodes for discharge product quantification were completed as described in Chapter 2.

Of note, there are three sources of base for the acid/base titration: LiOH formed as the ultimate discharge product, LiOH formed via the reaction of Li_2O_2 with water in the titration protocol, and basic decomposition products. As discussed more completely in section 5.3, on discharge, all three sources were uncoupled. The quantity of basic decomposition products was estimated as 24% of the quantity of Li_2O_2 formed, a consistent value for identical cells without lithium iodide. The quantity of LiOH formed as the discharge product was therefore the total amount of base titrated minus the quantity of basic decomposition products and the stoichiometric amount of LiOH formed from reacting the titrated value of Li_2O_2 with water. The expected values in Figure 5.4 were calculated via the observed discharge e^-/O_2 value, i.e., a 4.0 e^-/O_2 expects only LiOH formation, whereas a value of 3.0 e^-/O_2 expects both Li_2O_2 and LiOH formed in a 1:2 ratio, and a 2.0 e^-/O_2 expects only Li_2O_2 formation. On charge, the basic decomposition products and electrochemically formed LiOH cannot be decoupled, as the fate of the basic decomposition products formed during discharge is unknown on charge (i.e., they may or may not oxidize during charge).

Additionally, as the iodometric titration is based on quantitatively titrating I_2, I_2 formation from the I_3^-/I_2 redox couple at high charge voltages is a false positive that makes the titration not applicable after high charge voltages, such as in Figure 5.4 at point iv.

Charing with no prior discharge. As shown in Figure 5.5 and Figure 5.6, typical cells constructed as detailed above were charged with a headspace of ~1.2 atm Ar with no prior discharge, i.e., no prior formation of Li_2O_2. The cells were charged at constant current to an arbitrary final capacity or a 4 V cutoff.

5.3 Results and discussion

We initially investigated the impact of various H_2O and LiI electrolyte concentrations on the discharge and charge voltage profiles of the Li-O_2 cell. The voltage response for a Ketjenblack positive electrode discharged and charged (100 μA/cm^2 to a capacity of 1 mAh/cm^2) with different concentrations of LiI and H_2O in DME-based aprotic electrolyte is shown in Figure 5.S1. Only small changes are observed in the discharge voltage profile between cells with varying LiI and H_2O concentrations. On charge, the potential profile is clearly influenced by the LiI and H_2O concentrations. Generally, the higher LiI concentration cells show lower charging voltages compared to their lower LiI concentration counterparts. In fact, the 0.2M LiI, 500 ppm H_2O cell maintains a ~3 V plateau for the duration of charge, consistent with previous reports.[100-101] As a result, the energy efficiency of this cell appears outstanding, as only a ~0.25 V gap between the discharge and charge voltages is observed. High water concentrations, in addition to low LiI concentrations, appear to result in higher final charging voltages, as well. Of note, other carbon-based electrodes exhibit only small differences in overpotentials compared to Ketjenblack electrodes. In particular, XC72 carbon black, a different type of high-surface area carbon, shows similar overpotentials to Ketjenblack (e.g. Figure 5.S1 and Figure 5.7 give comparison of Ketjenblack and XC72, respectively, with 0.05M LiI), and therefore results from cells comprised of either carbon electrode can be directly compared if needed. See figure captions for the specific carbon used for that data set. Figure 5.S2 shows that graphene-based electrodes exhibit similar overpotentials as well, and thus graphene-based electrodes were not studied further.

As discussed in Chapter 2, energy efficiency is not necessarily a measure of the reversibility of Li-O_2 cells, as the discharge and charge profiles could correspond to undesired reactions. The electrochemical reactions at various lithium iodide and water concentrations were quantified via a combination of differential electrochemical mass spectrometry (DEMS), pressure decay/rise measurements in a closed cell headspace, and acid/base and peroxide titrations, as discussed in the experimental section.

Figure 5.3 shows pressure decay (discharge) and DEMS (charge) results for batteries employing 0.2 M lithium iodide and water concentrations corresponding to nominally anhydrous (< 20 ppm), 500 ppm, and 5000 ppm. 0.2 M LiI was selected for these measurements because, at modest current densities and with the given overall cell geometry, this concentration, coupled with a low water concentration, enables the low ~3 V potential throughout the entire duration of charge, as observed in Figure 5.S1 and in previous reports.[100-101] Pressure decay and DEMS allow for the direct correlation of observed oxygen consumption and evolution to the observed voltage profiles of our galvanostatic cycling.

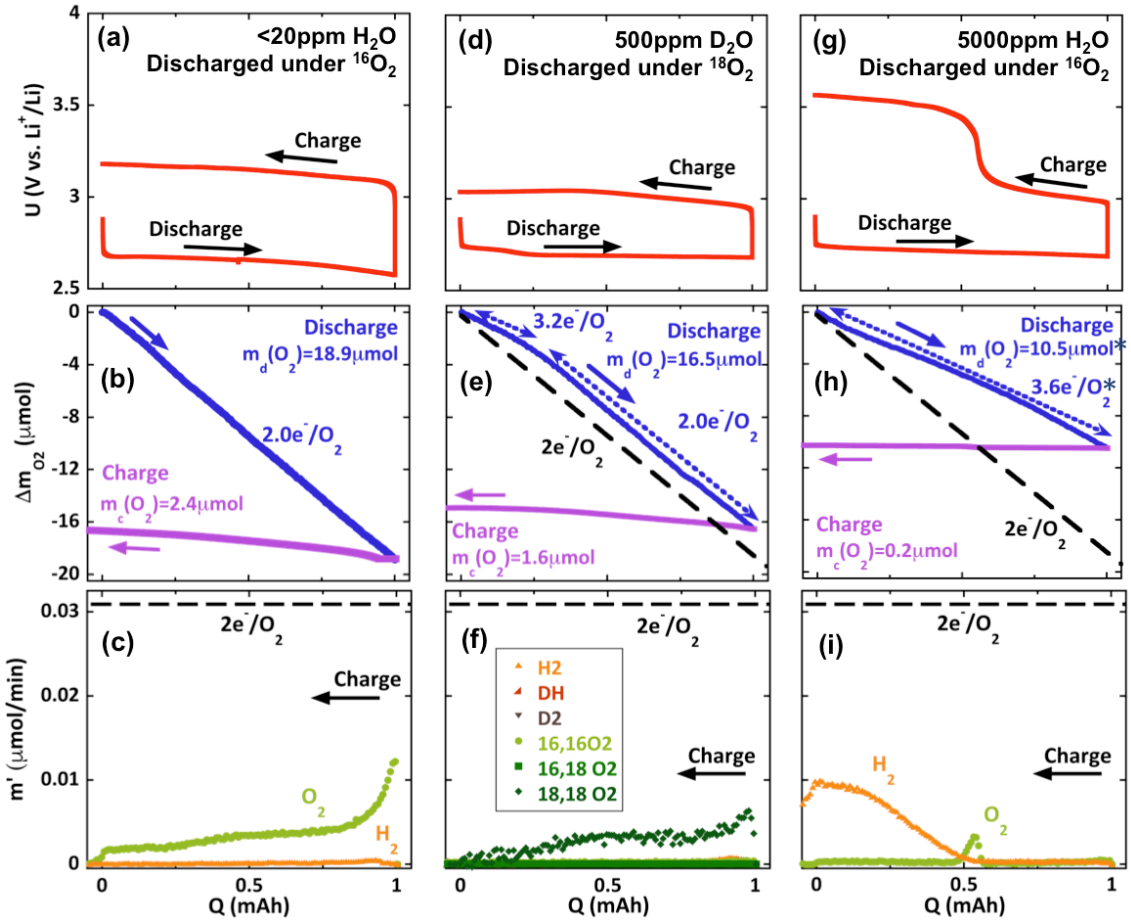

Figure 5.3. High [LiI] DEMS results. Galvanostatic discharge and charge profiles (100 μA/cm^2) with oxygen consumption and gas evolution for lithium-oxygen batteries employing a lithium anode, a cathode of ~1 mg Ketjenblack® with PTFE binder on stainless steel mesh (12mm diameter), and 160 μL of DME with 0.25 M LiTFSI and 0.2 M LiI as the electrolyte. Each column presents a battery with different added electrolyte water content: **a-c)** nominally anhydrous; **d-f)** 500 ppm D_2O, and **g-i)** 5000 ppm H_2O. The batteries were discharged under a headspace of ~1.5 atm oxygen and charged under a constant pressure headspace of ~1.2 atm argon. **b)**, **e)** and **h)** show oxygen consumption on discharge and evolution on charge. The asterisk (*) denotes a value adjusted for a hydrogen evolution rate at open circuit potential, which arises from water reacting with the lithium anode. Gas evolution on charge was quantified via DEMS. **c)**, **f)**, and **i)** show quantitative gas evolution throughout the charge.

Focusing on the discharge processes of the cells presented in Figure 5.3, all three cells exhibit oxygen consumption with rates varying between a pure 2 e^-/O_2 process and a pure 4 e^-/O_2 process depending on the cell's total water content. The nominally anhydrous battery exhibits a clear 2 e^-/O_2 process for the duration of the discharge, indicative of lithium peroxide formation as is typically observed in nonaqueous Li-O_2

cells (Figure 5.3a-c).[30] The battery containing 500 ppm water (Figure 5.3d-f) exhibits a 3.2 e^-/O_2 process for the first 0.24 mAh of discharge, and a 2 e^-/O_2 process for the remainder of the 1 mAh discharge. The initial 3.2 e^-/O_2 process indicates a mix of lithium hydroxide formation (reaction 5.4) – a 4 e^-/O_2 process – and lithium peroxide formation (reaction 5.1, from the introduction) – a 2 e^-/O_2 process.

$$4Li^+ + 4e^- + O_2 + H_2O \leftrightarrow 4LiOH \quad (4e^- \text{ process}) \quad (5.4)$$

The switch from a 3.2 e^-/O_2 process to a 2 e^-/O_2 process likely occurs once H_2O is completely consumed, as 500 ppm of water in the electrolyte volume employed (160 mL) corresponds to a capacity of 0.24 mAh for LiOH formation (as calculated from the reaction 5.4 stoichiometry), and the discharge potential noticeably drops to a lower plateau at the onset of the 2 e^-/O_2 Li_2O_2 formation process. The battery containing 5000 ppm water (Figure 5.3g-i) exhibits a near 4 e^-/O_2 process for the duration of the 1mAh discharge, indicating lithium hydroxide formation dominates at high water contents. Theoretically, as calculated from reaction 5.4, 5000 ppm water in the electrolyte volume employed (160 μL) corresponds to a capacity of 2.4 mAh for LiOH formation, so there is sufficient water to allow a 1 mAh discharge even after considering (the discernible) water consumption at the lithium anode. The presence of LiOH as a discharge product was further confirmed via X-ray diffraction (XRD) studies of the cathode, as shown in Figure 5.S3 for a cell with high LiI and H_2O content.

Quantification of both LiOH and Li_2O_2 was performed using established titrations on extracted cathodes from cells with identical composition as those studied in Figure 5.3 (Figure 5.4).[32] For a battery containing 500 ppm H_2O and 0.2 M LiI (Figure 5.3d-f), 5.8 μmol LiOH and 15.8 μmol Li_2O_2 are expected to form during the 1 mAh discharge given the amount of O_2 consumed during the 4 e^-/O_2 and 2 e^-/O_2 processes; 5.1 μmol LiOH and 11.1 μmol Li_2O_2 were titrated (Figure 5.4a-b), giving yields of 87% LiOH and 70% Li_2O_2. The Li_2O_2 yield is consistent with previous reports for nominally anhydrous Li-O_2 cells employing Ketjenblack® cathodes.[32] Therefore LiOH formation is more efficient than Li_2O_2 formation in these cells, although parasitic processes during LiOH formation still persist. As identified previously by both Kwak et al. and Liu et al.,[100-101] LiOH formation in a cell of this composition is an interesting finding, as the 4 e^-/O_2 ORR reaction is uncommon in nonaqueous Li-O_2 batteries, and on carbon electrodes in general. However, Tulodziecki et al. recently showed this LiOH formation does not follow a typical 4 e^-/O_2 reduction process such as typically observed on platinum electrodes. LiOH is likely formed via the 2 e^-/O_2 formation of Li_2O_2, followed by the chemical reactions of Li_2O_2 with water to form LiOH and the consumption of H_2O_2 via iodide, followed finally by the reduction of triiodide back to iodide. This work and mechanism is discussed further in section 6.1.

On charge, the three cells presented in Figure 5.3 exhibit very little oxygen evolution compared to the oxygen consumed during discharge. The total oxygen evolution from the nominally anhydrous battery, for example, is 2.4 μmol, or less than 13% of what would be expected assuming full oxidation of the discharge products. As the nominally anhydrous and 500 ppm water electrolytes exhibit Li_2O_2 as their dominant discharge product and the 5000 ppm water electrolyte exhibits LiOH as its dominant discharge product, the limited O_2 evolution during the cells' ~3 V charge plateaus shows

that the ~3 V charge plateau is predominantly related to electrochemical processes other than O_2 evolution, irrespective of the discharge product. Additionally, while the 5000 ppm battery exhibits a small amount of oxygen evolution during the step from the ~3 V plateau to the higher ~3.5 V plateau, DEMS shows negligible oxygen evolution otherwise. Therefore, LiOH is not reversibly oxidized to produce O_2 at these potentials. The cell chemistry on charge is extremely complex, being a function of the concentrations of I^- and H_2O, as well as the ratio of discharge capacity to total water content in the cell (and hence, the product distribution formed during discharge).

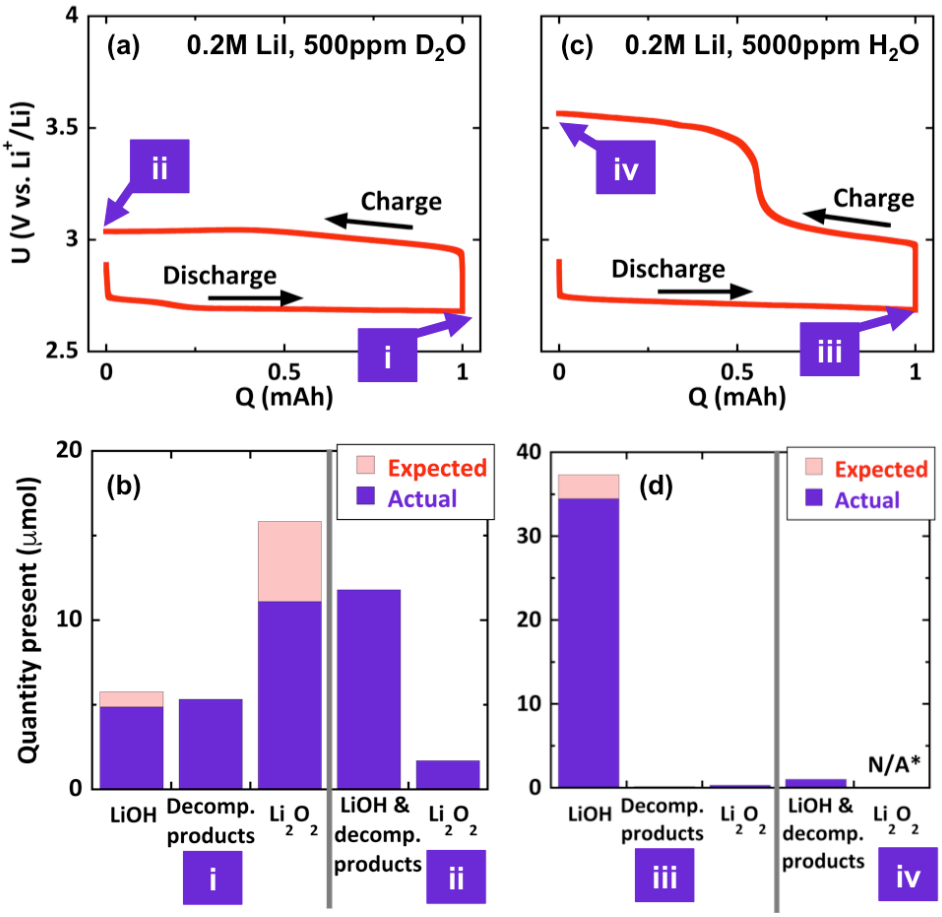

Figure 5.4. Acid/base and iodometric titration results for cells identical to those studied in Figure 5.3 d-f) (**a)** and **b)** 500 ppm H_2O) and g-i) (**c)** and **d)** 5000 ppm H_2O). The acid/base titration quantifies lithium hydroxide and other decomposition products present; these are distinguished by using the expected value of basic decomposition products formed during lithium peroxide formation. On charge, the relative fates of the decomposition products and the electrochemically formed LiOH are unknown, so they cannot be decoupled. The iodometric titration gives the lithium peroxide results. $*I_2$ formation during the 3.5V plateau in c-d interfered with the iodometric titration's ability to properly quantify Li_2O_2 at the end of charge (7.3 μmol of 'Li_2O_2' were titrated at the end of charge, even though only 0.3 μmol were produced during discharge).

Numerous processes occur during charge at the ~3 V plateau. If substantial Li_2O_2 is formed, as is the case in the low water content cells (Figure 5.3a-g), it can disappear

during this plateau, as observed from iodometric titrations presented in Figure 5.4a-b. A small fraction of Li_2O_2 disappearance is ascribed to oxidation that evolves O_2 (Figure 5.3c, f) while the remainder appears to chemically react with I_3^- to form a soluble product. I_3^- was likely formed from I^- oxidation during charge in Figure 5.4a, as the battery separator after charge was a faint yellow-red in color, indicative of I_3^- in aprotic polar media. We note that I_3^- formed during charge can result in a false positive in our iodometric titration, so that the difference in the Li_2O_2 titrated between points i and ii in Figure 5.4a (9.4 μmol difference, or 85% of the Li_2O_2 formed during discharge) represents a lower limit of the actual Li_2O_2 that disappeared on charge.

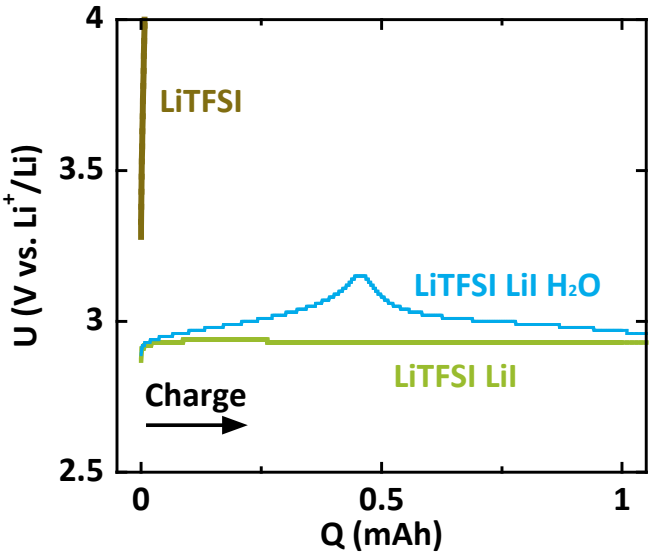

Figure 5.5. Charging cells under an argon headspace with no prior discharge (charge in this case goes left to right) containing XC72 carbon electrodes and 0.25 M LiTFSI in DME (brown line), 0.25 M LiTFSI/0.2 M LiI in DME (green line), and 0.25 M LiTFSI/0.2 M LiI/500 ppm H_2O in DME (blue line) at 100 μA/cm^2. If all I^- were converted to I_3^- in the cells containing LiI, only 0.29 mAh of charge capacity would be expected before voltage rise. The ability of the cells containing LiI to galvanostatically charge in perpetuity when no Li_2O_2 is ascribed to a redox shuttle, i.e., iodide being oxidized at the carbon positive electrode to triiodide, then diffusing to the lithium electrode, becoming electrochemically reduced back to iodide, and diffusing back to the positive electrode to repeat. Figure 5.S4 shows the current dependence of redox shuttling in cells containing 0.05M LiI, as well as an inset schematic for redox shuttling.

The Li_2O_2 disappearance cannot account for the entirety of the electrochemical charging capacity, implying that the ~3 V plateau is related in part to I^-/I_3^- redox shuttling between the anode and cathode. Figure 5.5 shows cells with an argon headspace charged at constant current with no prior discharge. A cell containing 0.25 M LiTFSI in DME exhibits immediate polarization, with the voltage rising to a cutoff of 4 V. Meanwhile, cells containing 0.2 M LiI, with and without 500 ppm H_2O, can be charged in perpetuity at a ~3 V plateau, with Figure 5.5 showing the first 1 mAh of charging. If all I^- were converted to I_3^- in this cell without any shuttling, a capacity of only 0.29 mAh would be

expected before voltage rise. This ability to "charge" without any prior formation of discharge product is ascribed to a redox shuttle mechanism, shown in the inset of Figure 5.S4, of iodide being oxidized at the carbon positive electrode, diffusing to the lithium electrode, becoming electrochemically reduced, and returning to the positive electrode to repeat. Figure 5.S4 shows similarly that a cell containing just 0.05 M LiI and 500 ppm H_2O that has yet to be discharged can be "charged" at low current densities at ~3 V in perpetuity, while Figure 5.S4b shows that an attempted charge of an identical cell without LiI exhibits an immediate sharp rise in voltage. Generally, the shuttling process is known to be strongly influenced by mediator concentration, diffusion coefficient, current density, and interelectrode distance.[106] Figure 5.5 and Figure 5.S4 are evidence that an I^-/I_3^- redox shuttle current can be maintained between the electrodes at a current density of roughly 100 $\mu A/cm^2$ which is the current density used in Figures 5.S1 and 5.3, in our typical cell geometries. Of note, analogous cells that employ higher concentrations of water, such as 5000 ppm, exhibit the two-plateau behavior as shown in Figure 5.3g. Figure 5.6 shows that a battery containing 4500 ppm H_2O charged with no prior discharge exhibits a step up to 3.5 V before subsequent perpetual charging. Complete conversion of I^- to I_3^- and I_3^- to I_2 in this cell corresponds to 0.107 mAh, near where the step occurs. This indicates water's ability, perhaps through its reaction with and subsequent passivation of the lithium metal electrode, to inhibit the system's ability to sustain the I^-/I_3^- redox shuttling between electrodes.

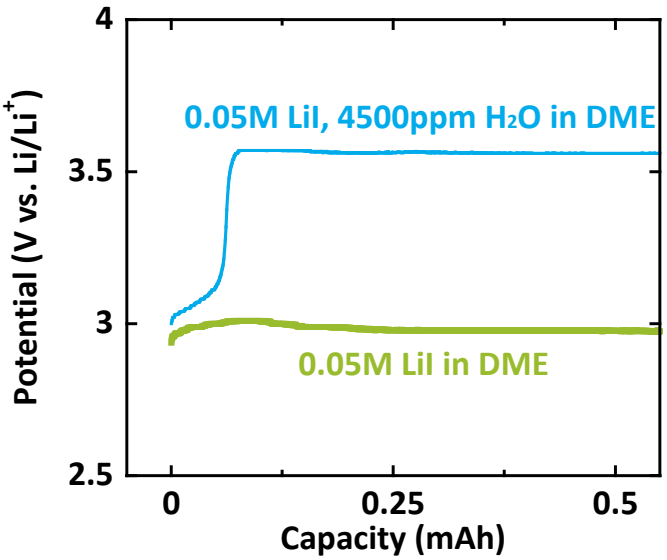

Figure 5.6 Charging cells under an argon headspace with no prior discharge (charge in this case goes left to right) containing XC72 carbon electrodes and 0.25 M LiTFSI, 0.05 M LiI, 4500 ppm H_2O in DME (blue line) or 0.25 M LiTFSI, 0.05 M LiI in DME (green line) at 50 $\mu A/cm^2$. Electrolyte volume is 80 µL. Complete conversion of I^- to I_3^- corresponds to 0.071 mAh; subsequent conversion of I_3^- to I_2 corresponds to 0.036 mAh.

When LiOH is the dominant discharge product, i.e., cells with high water content, it only disappears during the ~3.5 V plateau, and not the ~3 V plateau (e.g., Figure 5.3g), suggesting the I^-/I_3^- redox shuttle dominates at the ~3 V plateau. As shown in Figure 5.4a, acid/base titrations indicate that after a full discharge-charge cycle, cells with low water content – and thus those that exhibit the ~3 V plateau for the duration of charge – still contain all LiOH formed during discharge. This is consistent with SEM images (Figure 5.S5) showing that solid discharge products remain after charge, indicating that there is no activity for LiOH oxidation at this low charge potential. Cathodes discharged and charged in cells with high water content that reach the ~3.5 V plateau on charge, however, exhibit (after charge) only a minor fraction of the basic products formed during discharge. The ~3.5 V plateau is likely related to the I_3^-/I_2 redox couple, which is active at these potentials, and I_2 formation is clearly visible in the glass fiber separators of cells that reach this plateau. Recalling the minimal O_2 evolution exhibited at even the ~3.5 V plateau (Figure 5.3g-i), this suggests that the dominant chemistry occurring at this plateau is a non-O_2 evolving LiOH oxidation reaction involving the I_3^-/I_2 redox couple, which will be discussed later.

Isotopic labeling of O_2 and H_2O finds that no evolved O_2 originates from LiOH formed during discharge. O_2 evolution from LiOH during charge requires O-O bond reformation that occurs between statistically random oxygen atoms contained in the LiOH. LiOH forms during discharge through O_2 bond splitting and reaction with H_2O. The oxygen evolution of a cell that was charged after being discharged under a pure $^{18,18}O_2$ headspace, with $H_2{}^{16}O$ as the water impurity, is shown in Figure 5.3f (500 ppm H_2O cell). Pure $^{18,18}O_2$ is evolved during charge. This result is also consistent with a cell discharged under $^{16,16}O_2$ and containing a $H_2{}^{18}O$ impurity; Figure 5.S6 presents the oxygen evolution of a cell that was charged after being discharged to a capacity of 1 mAh in 0.2M LiI/5000 ppm $H_2{}^{18}O$ under $^{16,16}O_2$. No ^{18}O-enriched O_2 is evolved at any point during the entire charge process. Both of these cell isotope configurations (Figure 5.3f and Figure 5.S6) would be expected to evolve significant $^{16,18}O_2$ on charge (i.e., the evolved O_2 would be enriched in the H_2O O isotope) if O_2 evolution occurred from LiOH. In Figure 5.S6, the transition from I_3^- to I_2 is accompanied by the evolution of a small volume of isotopically pure $^{16}O_2$, indicating that the O-O bond in O_2 remained intact throughout the discharge-charge process, as expected with Li_2O_2 formation and oxidation. This confirms that the oxidation of LiOH to form O_2 does not occur either chemically or electrochemically, and the small amount of O_2 observed from cells containing LiOH as the primary discharge product can be ascribed to the oxidation of Li_2O_2.

Interestingly, lowering the iodide concentration enables higher rates of oxygen evolution on charge when lithium peroxide is the primary discharge product. For example, Figure 5.7 presents pressure decay (discharge) and DEMS (charge) results for batteries discharged with 0.05 M LiI (instead of 0.2 M LiI, as was used in Figure 5.3) and 2000ppm of water in 80 µl of electrolyte (corresponding to 0.5 mAh of possible LiOH formation). When discharged beyond 0.5 mAh (Figure 5.7a-c), a switch from a 4 e^-/O_2 process to a 2 e^-/O_2 process is observed on discharge, and O_2 evolution is observed on charge. The O_2 evolution coincides with a rising charge voltage above ~3.2 V, and corresponds to 63% of the expected yield based on the O_2 consumed during the 2 e^-/O_2 discharge process. This OER/ORR value is similar to (though slightly lower than) the

yield in aprotic Li-O_2 cells in the absence of LiI.[31] A battery discharged to a cutoff capacity of less than 0.5 mAh, where only a 4 e^-/O_2 process is observed (Figure 5.7d-f), exhibits only minor oxygen evolution on charge. These results further confirm that only lithium peroxide, and not LiOH, can be oxidized to evolve O_2 in aprotic electrolytes on carbon cathodes. Batteries employing lower iodide concentrations are not able to maintain the desirable ~3 V charge plateau, but do exhibit more oxygen evolution on charge than the higher LiI concentration cells, with the oxygen originating exclusively from lithium peroxide.

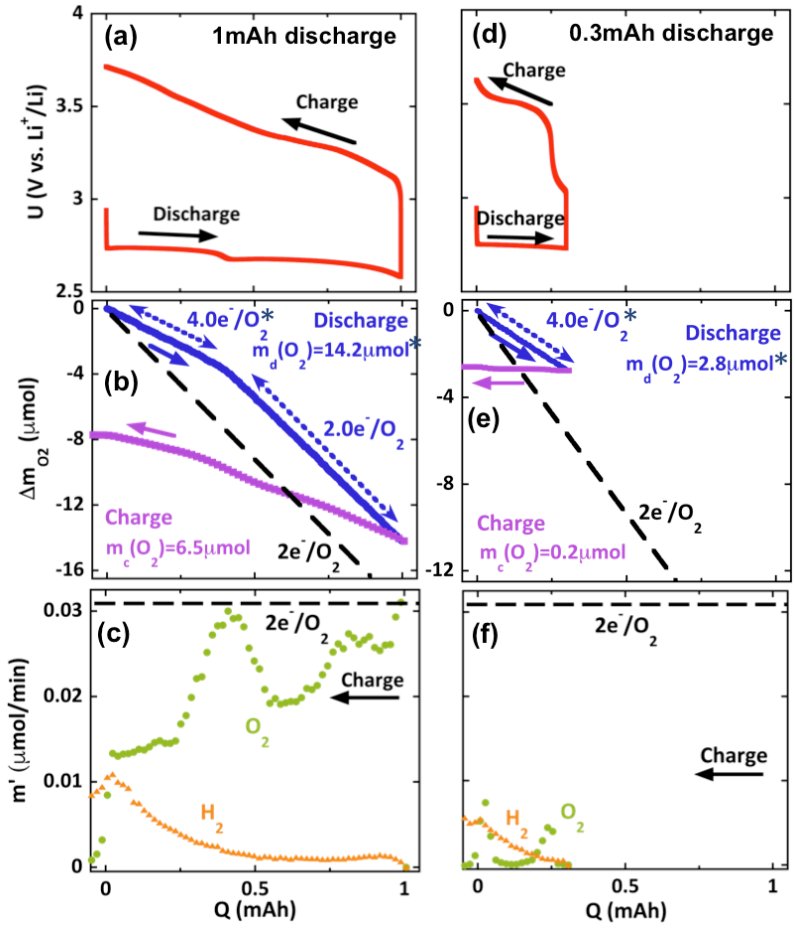

Figure 5.7. Low [LiI] DEMS results. a) and **d)** show galvanostatic discharge and charge profiles (200 μA/cm^2) from lithium-oxygen batteries employing a lithium anode, a cathode of ~2 mg XC72 carbon with PTFE binder on stainless steel mesh (12 mm diameter), and 80 μL of an electrolyte of 0.25 M LiTFSI, 0.05 M LiI, and roughly 2000 ppm H_2O in DME. The only difference between the batteries is the discharge capacity cutoff, as labeled. **b)** and **e)** show oxygen consumption on discharge and evolution on charge versus capacity. **c)** and **f)** show quantitative gas evolution throughout the charge. The asterisk (*) denotes a value adjusted for a hydrogen evolution rate at open circuit potential, which arises from water reacting with the lithium anode.

The DEMS and titration data clearly indicate that the addition of lithium iodide to a water-contaminated, nonaqueous lithium-oxygen battery enables a 4 e^-/O_2 process involving the consumption of water to form lithium hydroxide on discharge. However, on charge, lithium hydroxide is not reversibly oxidized back to oxygen. Any lithium peroxide formed during discharge is only partially oxidized to evolve oxygen on charge, with higher oxygen evolution efficiencies observed at lower iodide concentrations. Consequently, the low 3 V plateau on charge obtained in Figure 5.S1 is not due to reversible oxygen electrochemistry, but rather to a complex iodo-oxygen electrochemistry that is highly dependent on the exact cell composition and testing conditions (e.g., LiI and H_2O concentration, current density, cathode composition, and cell geometry).

This still leaves open the question of the fate of LiOH at the high, ~3.5 V charge plateau (i.e., where it is observed to disappear). Contrasting reports exist that demonstrate the removal of LiOH from the electrode surface during charge of a Li-O_2/LiI cell. Liu et al. reports that I_3^- oxidizes LiOH to evolve O_2 during the ~3 V plateau.[101] Our own results, as well as those from Kwak et al.,[100] demonstrate that LiOH does not react at the low potential plateau, but can be removed from the cathode surface at the higher (~3.5 V) voltage plateau, but without O_2 evolution. One possible explanation for this behavior is that LiOH oxidation results in $LiIO_3$ formation. In alkaline aqueous media, the following reaction occurs:[107]

$$3I_2 + 6LiOH \leftrightarrow LiIO_3 + 5LiI + 3H_2O \qquad (5.5)$$

Hence, it is possible that at high charge voltages, when the I_3^-/I_2 redox couple is actively forming I_2, LiOH reacts to form small amounts of $LiIO_3$, given that a 6 LiOH:1 $LiIO_3$ stoichiometric ratio is expected from reaction 5.5.

To prove this hypothesis, our collaborators at the University of Waterloo developed a modified version of the iodometric titration to detect small amounts of $LiIO_3$ present on various positive electrodes charged to different capacities. A detailed description of this method is in the supporting information. The fraction of $LiIO_3$ was determined for electrodes stopped at various states of charge in either 0.05 M LiI or 0.2 M LiI/5000 ppm H_2O/DME electrolyte (Figure 5.S7). This water concentration was chosen to ensure LiOH was formed as the overwhelming dominant product on discharge. For low LiI concentrations (0.05 M), it is clear that a small quantity of $LiIO_3$ is produced (< 0.5 μmol) on cell charge. The small magnitude is understandable, as at 0.05 M LiI, complete conversion of I^- to I_2 equates to a maximum of 1.5 μmol $LiIO_3$ produced via reaction 5.5, assuming the discharge product is 100% LiOH. Nonetheless, the presence of $LiIO_3$ is confirmed on extracted positive electrodes with both EDX analysis, which shows $LiIO_3$'s characteristic 3:1 ratio of O:I (Figure 5.S8), and XRD analysis, which shows diffraction patterns characteristic of $LiIO_3$ (Figure 5.S9). A similar quantity of $LiIO_3$ is also observed for the cell discharged/charged in 0.2 M LiI at voltages below 3.4 V (< 0.5 μmol). However, at high voltages and significant capacity overcharge, and thus high concentrations of I_2, approximately 3.0 μmols of $LiIO_3$ are observed on the electrode surface, clearly indicating a higher reactivity of LiOH with I_2 than I_3^-. Reaction between LiOH and I_2 (and the lack of a reaction between LiOH and I_3^-) was confirmed with mock chemical experiments, as shown in Figure 5.S10. $LiIO_3$ is very soluble in H_2O (76 g/100

mL), and hence can easily dissolve in the 5000 ppm H_2O electrolyte. Dissolution is further increased with the production of H_2O accompanying $LiIO_3$ formation. This is a plausible explanation for the removal of LiOH from the electrode surface, but does not fully explain the removal of LiOH at low voltages by Liu et al.[101] We note that the total amount of water contained in our cells is small compared to the water included in cells studied by Liu et al. (e.g., 5000 ppm H_2O in 160 μL in our cells versus 45,000 ppm H_2O in 700 μL in Liu et al.). This distinction could give rise to the discrepancy observed at low voltages in each study, as both LiOH solubility and the chemical reaction rate between LiOH and I_3^- increases with increasing water content.[104] Other factors that could play a role in this discrepancy are depth of discharge (i.e., amount of product formed) and the time delay between the end of discharge and the characterization of the discharge products.

5.4 Conclusion

In conclusion, the effect of LiI and H_2O on the Li-O_2 chemistry can be summarized as follows (Figure 5.8). On discharge, the presence of both LiI and H_2O promote a 4 e^-/O_2 process (LiOH production) instead of the normal 2 e^-/O_2 process (Li_2O_2 production) typical of an aprotic Li-O_2 cell employing an ether-based electrolyte and undoped carbon cathode. High H_2O concentrations result in almost stoichiometric 4 e^-/O_2 LiOH formation, whereas intermediate/low H_2O concentrations result in a mixture of Li_2O_2 and LiOH formation. On charge, a variety of processes occur which are dependent on the final discharge product composition and the concentrations of LiI and H_2O. I^- oxidation, in the absence of any discharge product, features two redox couples, I^-/I_3^- (E ~ 3.0 V) and I_3^-/I_2 (E ~ 3.5 V). The I^-/I_3^- shuttle between the anode and cathode substantially contributes to the cell electrochemistry at low charge potentials (2.95 – 3.10 V). LiOH does not oxidize when this I^-/I_3^- couple is active, although Li_2O_2 can react to either evolve O_2 or form unidentified iodo-oxygen species. The I_3^-/I_2 redox is observed after the initial I^-/I_3^- redox in cells with high water content in the electrolyte. This transition results in O_2 evolution from Li_2O_2, presumably promoted by the formed I_2. The I_3^-/I_2 redox is active during a second charge plateau that takes place at ~3.5 V, and LiOH is observed to disappear during this process. LiOH reacts with I_2 to form a small amount of $LiIO_3$, which is soluble in the water-filled electrolyte via reaction 5.5, but does not evolve O_2. Based on our studies, while a low charge overpotential makes the use of I^- seem appealing, the lack of O_2 evolution from Li_2O_2/LiOH oxidation in LiI-containing cells makes it a poor additive for efficient Li-O_2 cycling. Of the oxygen consumed on discharge, less than 13% is recovered on charge under the best-case ~3 V charge scenario. Hence, the low charge overpotential seen in LiI-containing Li-O_2 batteries is primarily due to iodo-oxygen electrochemistry, rather than reversible oxygen evolution. It should be noted, given our results, that other cell compositions (e.g., those with cathodes comprised of active materials other than carbon, higher water or LiI concentrations than studied here, other halide salts, etc.) may result in a substantially different electrochemistry, and more research is certainly necessary to fully understand the complex charge chemistry observed in this system.

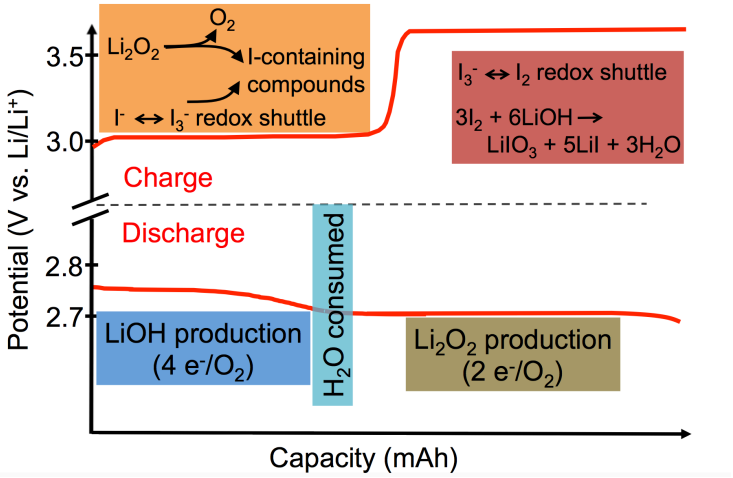

Figure 5.8. Summary of processes in typical Li-O_2 batteries employing an ether-based electrolyte, carbon cathode, LiI, and water impurities.

5.5 Acknowledgments

This work was performed in collaboration with Dr. Robert Black, Ivan Kochetkov and Professor Linda Nazar at the University of Waterloo and Dan Addison and Dr. Vincent Giordani at the private company Liox. Helpful discussions with Prof. Clare Grey are gratefully acknowledged. CMB, BDM, VG and DA gratefully acknowledge support from the U.S. Department of Energy, Energy Efficiency and Renewable Energy Vehicle Technologies Office under award No. DE-0006869, and previous support that enabled this work through the Laboratory Directed Research and Development Program of Lawrence Berkeley National Laboratory under U.S. Department of Energy Contract No. DE-AC02-05CH11231. CMB gratefully acknowledges support from a NASA Space Technology Research Fellowship under award No. NNX16AM56H. LFN is grateful for funding for this work from NRCan through their ECO-EII program, and acknowledges NSERC for partial support through the Discovery and Canada Research Chair programs.

5.6 Supporting information

Collaborators' experimental methods:

Electrode X-ray diffraction. XRD measurements were carried out using a Bruker D-8 Advance diffractometer employing Cu-Ka radiation (λ = 1.5406 Å). Samples were mounted on a silicon low-background holder using a moisture-protective barrier.

Scanning electron microscopy. Cathodes were removed from cells after cell completion. The cathodes were washed with THF, dried under vacuum and mounted onto SEM stubs with double sided carbon tape in a hermetically sealed argon-filled box. Transfer from the glovebox to the SEM was performed with minimal (*i.e.*, 1 sec) exposure to the atmosphere upon placement into the SEM load-lock chamber. Analysis was performed with a Zeiss Ultraplus FESEM.

$LiIO_3$ detection. For quantitative determination of $LiIO_3$, a modified version of the iodometric titration for Li_2O_2 was used. Once electrodes + separators were removed from the cell, washed with THF, and dried, the entire contents were placed into ~ 5 mL of H_2O (exact volume known via mass balance). Coarse MnO_2 powder was added to the solution and stirred with the cell contents for approximately 2 hours. The addition of Li_2O_2 to H_2O produces H_2O_2, which is then oxidized on the surface of MnO_2 to give O_2 + H_2O. Hence, after 2 hours, the entirety of H_2O_2 was oxidized, and what remains is LiOH and $LiIO_3$ dissolved in a known volume of H_2O. The entire contents were then filtered 3 times through a 0.2 μm syringe filter to fully remove MnO_2. MnO_2 is a false positive for this measurement, and thus mock experiments were performed to ensure that all MnO_2 is removed after three-fold filtration. The final transparent liquid (2.5 mL) was used for titration. Approximately 50 mg KI and 0.5 mL of 5 M H_2SO_4 were added which turned the solution yellow. Excess I^- and H^+ were added to ensure full conversion of the reaction $LiIO_3 + 6H^+ + 8I^- \rightarrow 3I_3^- + 3\ H_2O$. In the presence of excess I^-, I_2 converts to I_3^-, which is then titrated using a thiosulfate solution in the same manner as described previously for quantification of Li_2O_2.

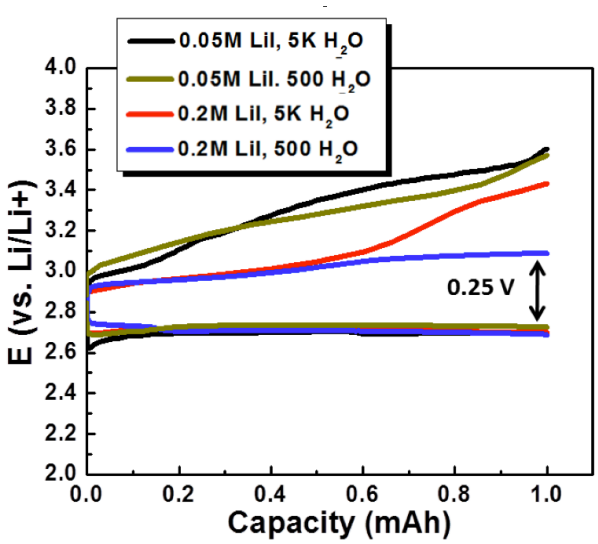

Figure 5.S1. Voltage profiles of Ketjenblack electrodes (4 mg carbon) galvanostatically discharged (lower curves, left to right) and charged (higher curves, left to right) in DME electrolyte with different LiI concentration (0.05 M and 0.2 M) and H_2O concentration (500 ppm and 5000 ppm) at 100 μA/cm^2. The total salt concentration (LiI + LiTFSI) was kept at 0.3 M. The total electrolyte volume used is 180 μL. At low LiI concentrations (0.05 M), regardless of H_2O concentration, the charge profile gradually slopes to higher voltage. At the higher LiI concentrations, an initial low voltage charge plateau (~2.95 V) is exhibited. Only at the end of charge is a rise in potential observed for 5000 ppm H_2O, while the low charge plateau continues for the low (500 ppm) H_2O concentration. Prepared by Dr. Robert Black, Ivan Kochetkov, and Professor Linda Nazar at the Univeristy of Waterloo.

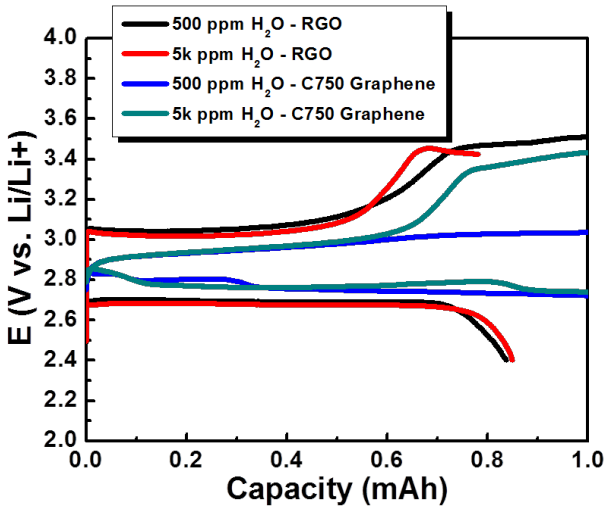

Figure 5.S2. Comparison of reduced graphene oxide and C750 graphene positive electrodes with 0.2 M LiI and either 500 ppm or 5000 ppm H_2O. This demonstrates that regardless of the positive electrode source, the electrochemistry is relatively constant. All electrodes were loaded at 4 mg. In the case of RGO, to achieve loadings of ~4 mg, a relatively thick electrode had to be constructed that resulted in poor mechanical stability. We believe this contributes to the larger overpotential observed compared to that of G750 graphene and KB electrodes. Graphene oxide was prepared via the oxidation of graphite (Alfa Aesar), followed by reduction to rGO according to the procedure previously reported by Grey et al.[101]; material was centrifuged in the initial washing steps. Prepared by Dr. Robert Black, Ivan Kochetkov, and Professor Linda Nazar at the Univeristy of Waterloo.

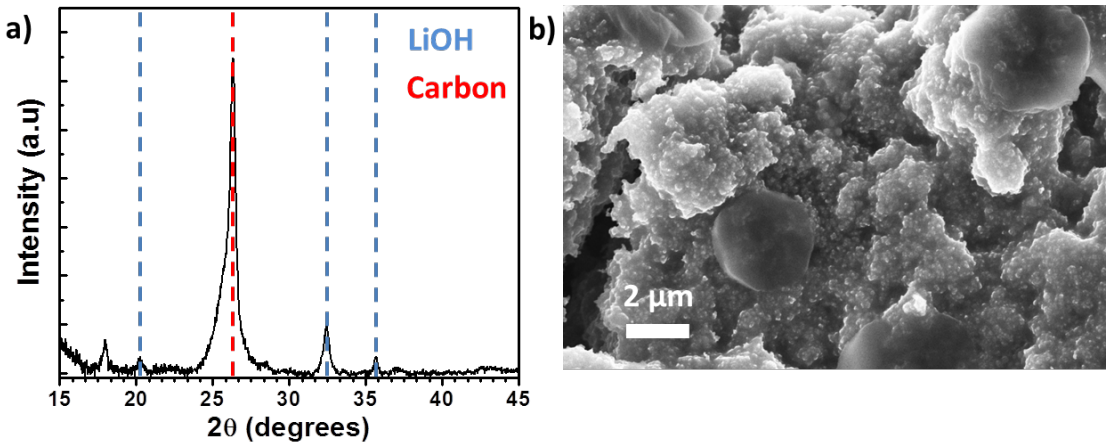

Figure 5.S3. **a)** X-ray diffraction pattern of a positive electrode after discharge in 0.2 M LiI/5000 ppm H_2O/DME. The only crystalline product is LiOH; **b)** SEM micrograph of the same discharged positive electrode. Prepared by Dr. Robert Black, Ivan Kochetkov, and Professor Linda Nazar at the Univeristy of Waterloo.

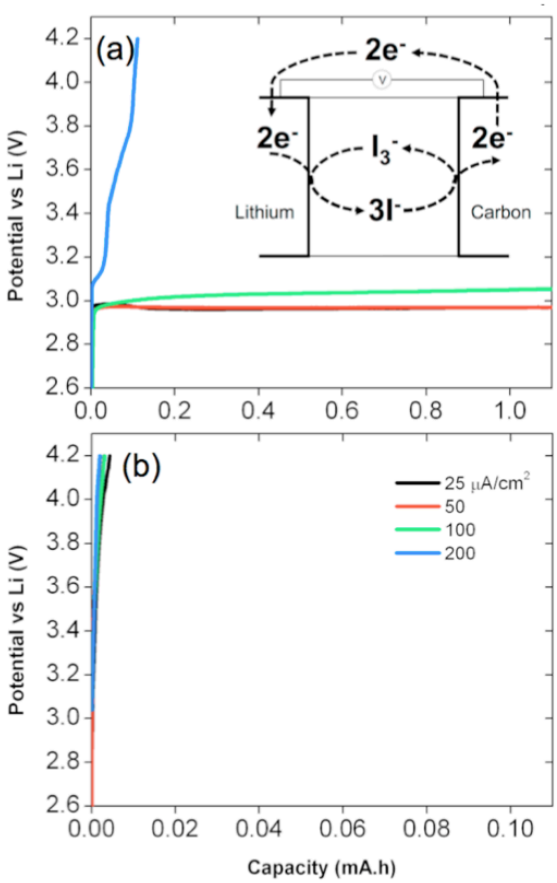

Figure 5.S4. Li-O_2 batteries charged under 1 atm argon gas with no prior discharge as a function of current density. Electrolyte is 0.25 M LiTFSI and 500 ppm H_2O in DME with 0.05M LiI (a) and no added LiI (b). These cells were constructed with two Whatman GF/D glass fiber separators, 300 μL of electrolyte, and cathodes containing 2 mg of a 95:5 mass ratio Super P carbon to PTFE on 10 mm stainless steel mesh. If all I^- were converted to I_3^- in the cells containing LiI, only 0.27 mAh of charge capacity would be expected before a voltage rise. The interelectrode distance was ~500 μm. Prepared by Dr. Vincent Giordani and Dan Addison at Liox.

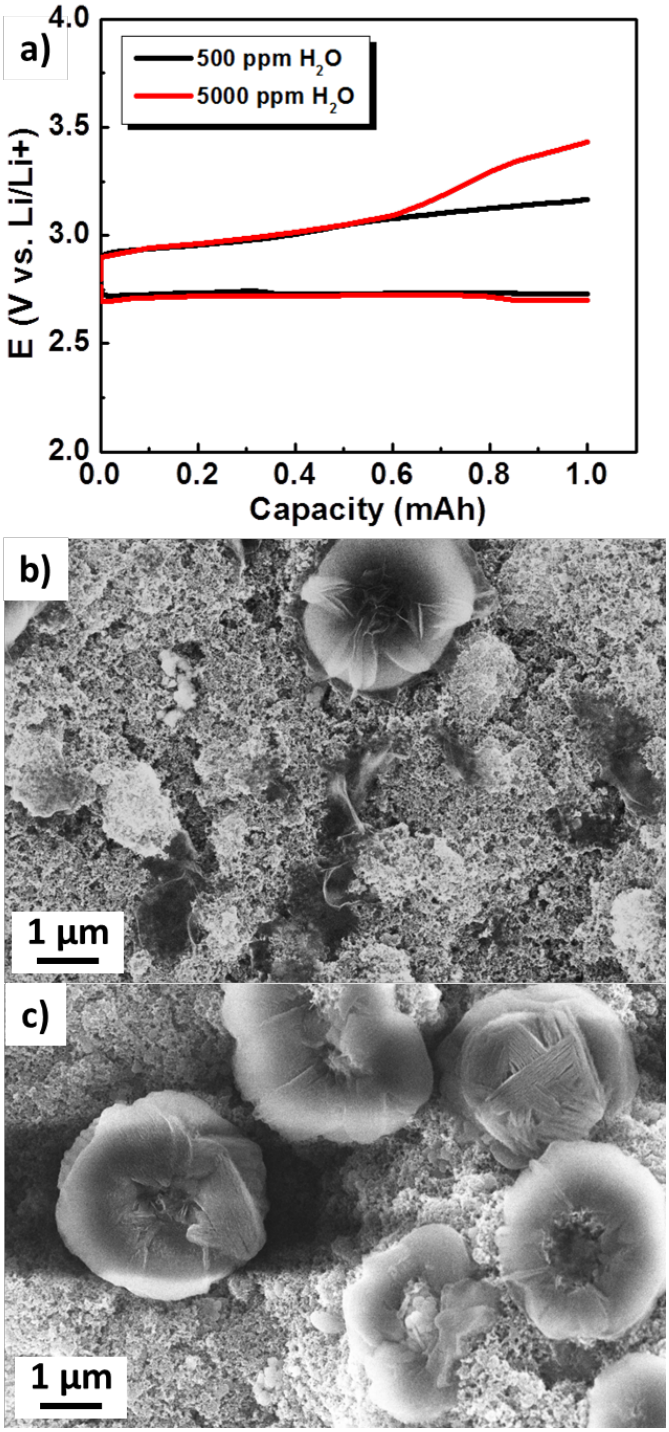

Figure 5.S5. SEM micrographs of the positive electrode surface at the end of charge. **a)** single discharge/charge profile of cells run in electrolyte with 500 ppm and 5000 ppm H_2O (0.2 M LiI/DME), and corresponding SEM micrograph at the end of charge for **b)** 500 ppm H_2O and **c)** 5000 ppm H_2O. Prepared by Dr. Robert Black, Ivan Kochetkov, and Professor Linda Nazar at the Univeristy of Waterloo.

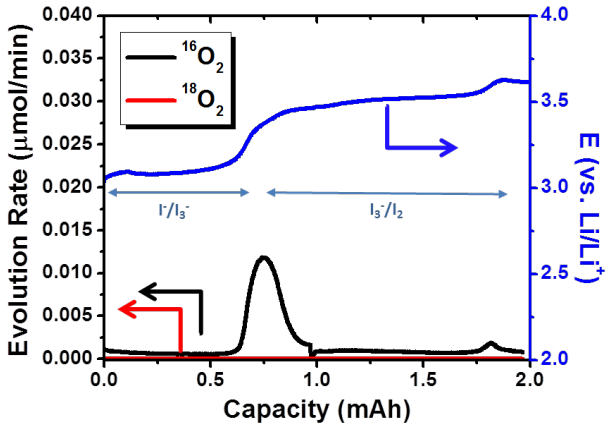

Figure 5.S6. Voltage profile and corresponding oxygen evolution profile for a cell discharged under $^{16}O_2$ and charged in 0.2 M LiI/DME with 5000 ppm $H_2{}^{18}O$. On discharge, a reasonable fraction of total produced LiOH is ^{18}O labeled (some Li_2O_2 is also produced). On charge, only $^{16}O_2$ is observed from the oxidation of Li_2O_2. No signal from $^{18}O_2$ (LiOH oxidation) is observed at either low potential (I^-/I_3^-) or high potential (I_3^-/I_2). Prepared by Dr. Robert Black, Ivan Kochetkov, and Professor Linda Nazar at the Univeristy of Waterloo.

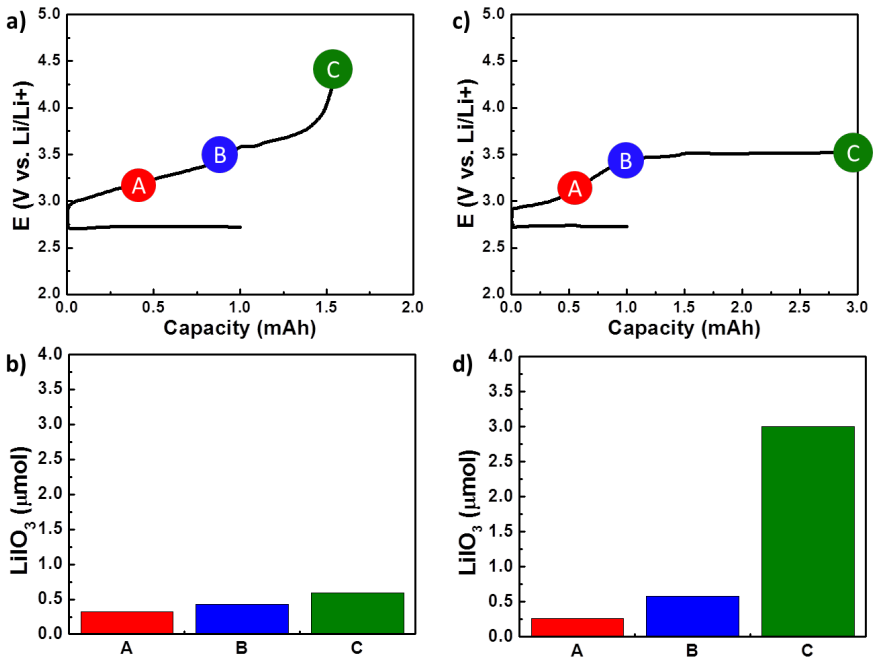

Figure 5.S7. Electrochemical curves for batteries containing **a)** 0.05 M LiI/5000 ppm H_2O/DME and **c)** 0.2 M LiI/5000 ppm H_2O/DME, and corresponding $LiIO_3$ for **b)** 0.05 M and **d)** 0.2 M LiI at the points specified. At low LiI concentrations, little $LiIO_3$ is generated due to the small concentration of I_2. At high LiI concentrations, an abundance of $LiIO_3$ is observed at V > 3.5 due to the generation of large amounts of I_2, which reacts with the LiOH to form $LiIO_3$. Batteries were cycled at 100 μA/cm^2 and cathode carbon loading was 4 mg of KB. Prepared by Dr. Robert Black, Ivan Kochetkov, and Professor Linda Nazar at the Univeristy of Waterloo.

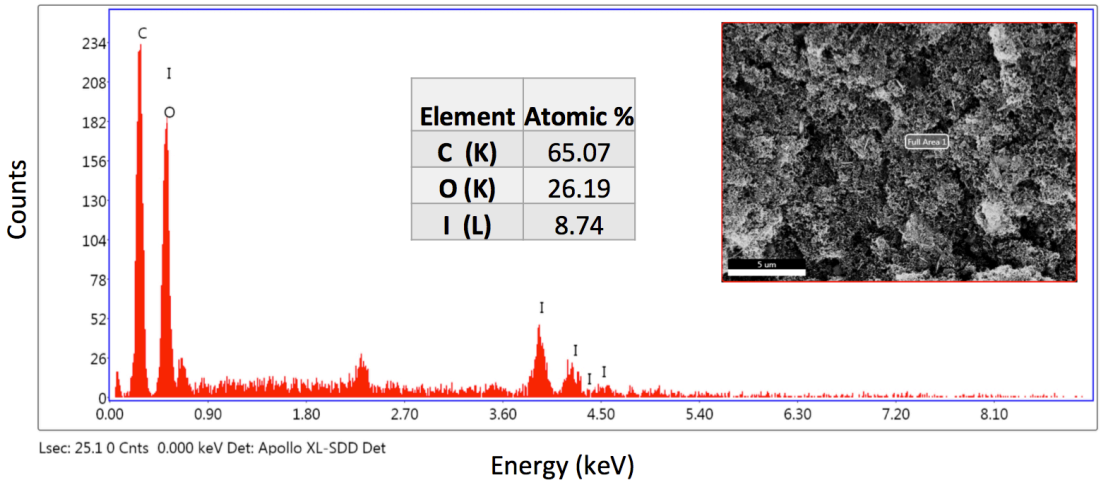

Figure 5.S8. Energy-dispersive X-ray spectroscopy spectrum of a Ketjenblack positive electrode extracted from cell containing 0.05 M LiI, 0.25 M LiTFSI, and 5000 ppm H_2O in DME after discharge at ~100 μA/cm^2 to 1 mAh and charge at ~100 μA/cm^2 to 1 mAh. As these electrolyte and cycling conditions lead to I_2 production on charge, LiOH and I_2 react to form $LiIO_3$ on the positive electrode, as exhibited by an O:I ratio of 3:1 on the positive electrode surface. Prepared by Dr. Robert Black, Ivan Kochetkov, and Professor Linda Nazar at the Univeristy of Waterloo.

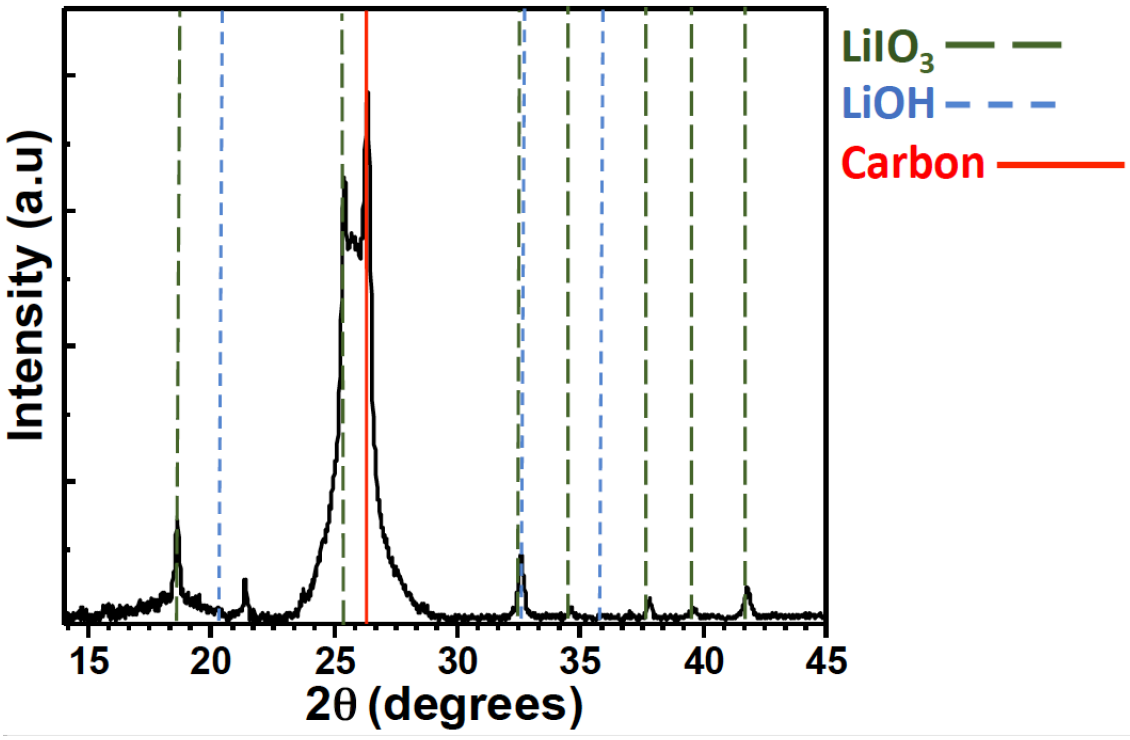

Figure 5.S9. X-ray diffraction pattern of a Ketjenblack positive electrode extracted from cell containing 0.05 M LiI, 0.25 M LiTFSI, and 5000 ppm H_2O in DME after discharge at ~100 μA/cm^2 to 1 mAh and charge at ~100 μA/cm^2 to 1 mAh. As these electrolyte and cycling conditions lead to I_2 production on charge, LiOH and I_2 react to form $LiIO_3$ on the positive electrode. Dashed lines are the major reference markers from the JCPDS database, as shown in Figure 5.S10. Prepared by Dr. Robert Black, Ivan Kochetkov, and Professor Linda Nazar at the Univeristy of Waterloo.

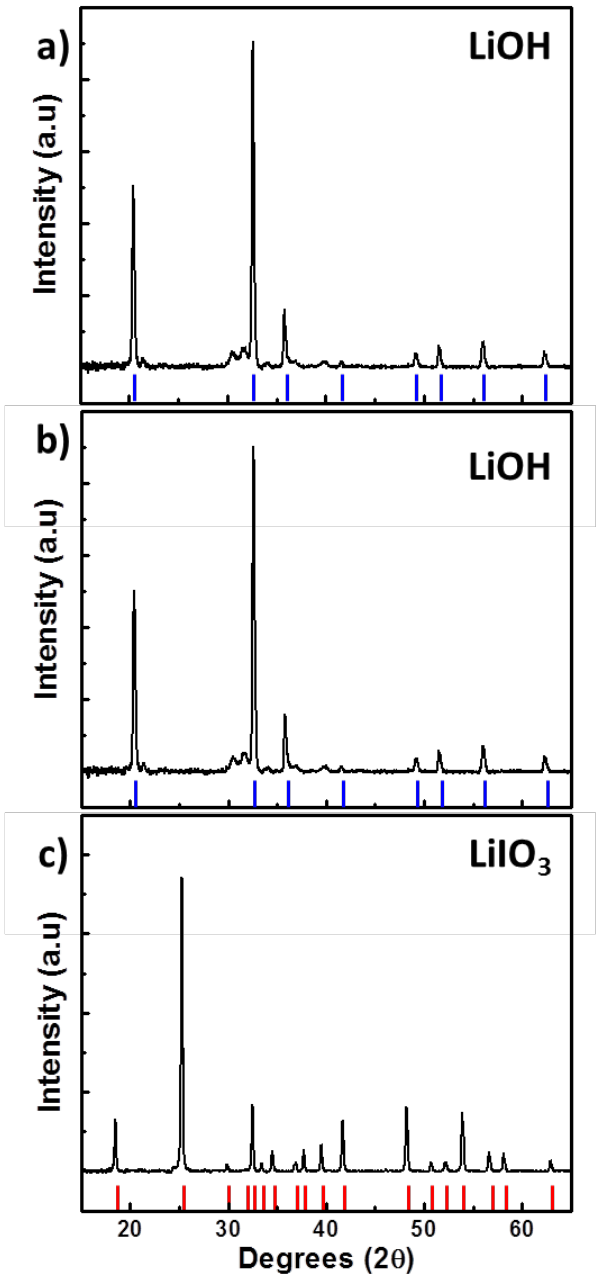

Figure 5.S10. Powder X-ray diffraction patterns of **a)** LiOH, and resulting solids after mixing 2.0 mmol LiOH with **b)** 2.5 mmol LiI and 2mmol I_2 in DME, and **c)** 4 mmol I_2 in DME. The reaction period was ~ 8 hours. Reference markers for LiOH (blue, in **a)** and **b)**) and $LiIO_3$ (red, in **c)**) are from the JCPDS database. Prepared by Dr. Robert Black, Ivan Kochetkov, and Professor Linda Nazar at the Univeristy of Waterloo.

Discussion of Figure 5.S10:

Mock chemical reactions were performed to determine the degree of reactivity between I_3^-/I_2 with LiOH. The reflections corresponding to the starting LiOH product are shown in Figure 5.S10a above. A solution of I_3^- was prepared with a mixture of 2.5 mmol LiI and 2 mmol I_2. In DME, the equilibrium $I^- + I_2 \rightarrow I_3^-$ (pKa ~ 6.5)[108] is nearly shifted 100% towards the product, creating a solution of I_3^- with excess I^- (no I_2 present). The contents were left to stir for 12 hours. The reflections of the resulting solid product are the same as the starting LiOH, leading us to conclude that no chemical reaction occurs (Figure 5.S10b). The XRD reflections of the solid product obtained from the reaction of LiOH with a solution of pure I_2 (4 mmol in DME) indicate $LiIO_3$ is formed *via* the reaction: $3I_2 + 6\ LiOH \rightarrow LiIO_3 + 5\ LiI + 3\ H_2O$. Other reactions involving I_2, reduced oxygen species (e.g., O_2^-) and the electrolyte solvent are also possible, as is shown in Figure 5.S11 below.

Of note, the lack of reaction between LiOH and I_3^- observed here is in contrast to a similar study by Liu et al.,[105] who observed slow I_3^- consumption (on the order of 10s of hours to complete consumption) when it was mixed with a DME solution containing 3-6 w% water and an excess of LiOH. The likely explanation for this discrepancy is the different water contents employed in each respective study (3-6 w% in Liu et al., <50 ppm here), as Liu et al. also suggest a fast reaction between LiOH and I_3^- in aqueous solutions, implying that H_2O acts to solubilize LiOH or I_3^-, allowing each to react more rapidly.

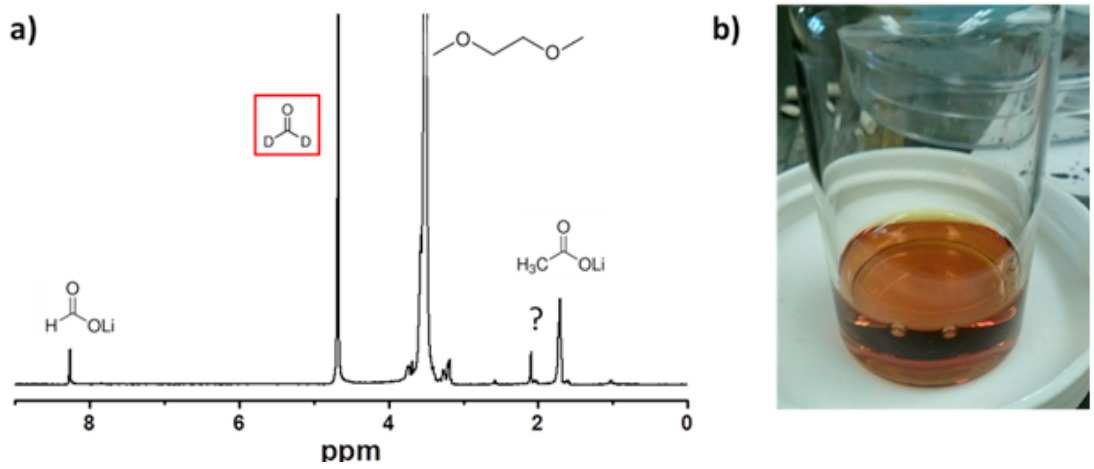

Figure 5.S11. KO_2 reaction in the presence of LiI. To determine the effect of I^- in the presence of O_2^-, a 5 mL solution of DME with 500 ppm H_2O, 0.2 M LiI and 0.1M LiTFSI was prepared, to which 1.5 mmol of KO_2 and 2.5 mmol of 18-crown-6 ether were then added to generate O_2^-. The contents were left to stir for 2 hours, after which the solid contents were removed and washed. **a)** The ^1H NMR spectrum obtained from the solids shows the clear presence of decomposition products, as expected from O_2^- in the presence of DME. **b)** After the addition of KO_2 the supernatant, turned slightly orange, and then deepened to dark orange, indicating the presence of I_3^-. Prepared by Dr. Robert Black, Ivan Kochetkov, and Professor Linda Nazar at the Univeristy of Waterloo.

Chapter 6: Considerations for redox mediators in the presence of water, including reference electrode selection

Abstract

In high-capacity lithium-oxygen (Li-O_2) batteries, lithium peroxide (Li_2O_2) forms on discharge in aggregated structures away from the carbon electrode surface. As Li_2O_2 is insoluble in the most stable, ether-based electrolyte and is an insulator, an electrolyte-soluble redox mediator is required to oxidize Li_2O_2 on charge and shuttle electrons back to the electrode surface. One promising redox mediator, iodide (I^-), has recently been shown to promote Li_2O_2 degradation to lithium hydroxide (LiOH) in the presence of water (H_2O), which is problematic because LiOH is not reversibly oxidized to lithium, oxygen, and water on charge. It therefore is important to determine the critical considerations for predicting whether a redox mediator will induce Li_2O_2 degradation to LiOH in the presence of water impurities, which are likely to be difficult to completely eliminate if lithium-air batteries are practically realized. In this study, we show via galvanostatic cycling of lab-scale Li-O_2 batteries containing LiI and H_2O in DME and DMSO that DMSO prevents Li_2O_2 degradation to LiOH. Cyclic voltammetry of these electrolytes shows DMSO exhibits a higher potential for iodide oxidation than DME, implying H_2O_2 reduction is more difficult in DMSO. Thus, the most critical consideration in predicting Li_2O_2 degradation to LiOH in the presence of water impurities is a redox mediator's ability to oxidize and subsequently reduce H_2O_2 in the electrolyte of choice. We also discuss reference electrode selection for studying redox mediators in Li-O_2 batteries, showing the study of redox mediators unstable to lithium metal – or of redox mediators in solvents unstable to lithium metal – requires the use of a lithium reference electrode with a lower lithium intercalation voltage than the redox mediator but a higher voltage than oxygen reduction.

6.1 Introduction

Redox mediators are likely necessary to enable charging of high capacity nonaqueous lithium-oxygen (Li-O_2) batteries, as the majority of the dominant discharge product lithium peroxide (Li_2O_2) forms away from the electrode surface in aggregated structures. Li_2O_2 is insoluble in common nonaqueous battery electrolytes and a wide band gap insulator,[39] such that oxidizing aggregated Li_2O_2 on charge requires electron shuttling through the electrolyte via a small molecule redox mediator.

As discussed in Chapter 5, iodide (I^-) has been studied as a possible redox mediator. However, the combination of lithium iodide and water impurities in the electrolyte leads to the formation of lithium hydroxide (LiOH) as the dominant discharge product, and LiOH is not reversibly oxidized back to its constituent components – lithium, oxygen, and water – on charge. Rather, charge current is carried via a combination of irreversible side reactions and redox shuttling between the electrodes of iodide and its oxidized forms.[41] Thus, it is important to avoid LiOH formation on discharge.

Recently, Tulodziecki et al. elucidated the mechanism for LiOH formation on discharge in a Li-O_2 battery containing an ether-based electrolyte containing lithium

iodide (LiI) and ppm quantities of added water (H_2O). By adding potassium superoxide (KO_2), a stable superoxide at ambient temperature and pressure, to an electrolyte of 0.1 M LiTFSI and 0.2 M LiI in 1,2-dimethoxyethane (DME), Tulodziecki et al. showed that rather than the typical four-electron oxygen reduction associated with catalysts like platinum:

$$4Li^+ + 4e^- + O_2 + 2H_2O \rightarrow 4LiOH \quad (6.1)$$

the formation of LiOH in an ether-based electrolyte containing LiI and ppm H_2O follows the 2 e^-/O_2 formation of Li_2O_2, chemical degradation of Li_2O_2 to LiOH and hydrogen peroxide (H_2O_2), and H_2O_2 reduction via I^- oxidation to triiodide (I_3^-):[43]

$$2Li^+ + 2e^- + O_2 \rightarrow Li_2O_2 \quad (6.2)$$

$$Li_2O_2 + 2H_2O \rightarrow 2LiOH + H_2O_2 \quad (6.3)$$

$$H_2O_2 + 3I^- + 2Li^+ \rightarrow 2LiOH + I_3^- \quad (6.4)$$

$$I_3^- + 2e^- \rightarrow 3I^- \quad (6.5)$$

This is an elegant proposal, as it essentially corresponds to an iodometric titration (described in section 2.4) occurring within the cell – water reacting Li_2O_2 to LiOH and H_2O_2 followed by iodide reducing H_2O_2. To be clear, water impurities at these concentrations without iodide do not induce the reaction of Li_2O_2 to LiOH and H_2O_2 in DME.[25] Tulodziecki et al. proposed two roles for iodide in causing this cascade of reactions. First, iodide lowers the pKa of dilute H_2O, evidenced by a downfield shift in the H_2O's ^1H NMR shift, increasing the water's reactivity. Second, iodide reduces H_2O_2 and is consequently oxidized to triiodide, as the I^-/I_3^- redox couple is at a potential only slightly above that of a discharging lithium-oxygen battery. This then enables the subsequent electrochemical reduction of I_3^- back to I^-, resulting in an overall process that is 4 e^-/O_2 as exhibited via DEMS in Chapter 5.[43]

It is important to determine if other redox mediators will cause this same Li_2O_2 degradation reaction to irreversible LiOH in the presence of water impurities. The lithium metal negative electrode currently used in Li-O_2 batteries will likely need to be protected from the electrolyte to prevent dendrite growth and/or to enable the use of organic redox mediator molecules that are unstable to lithium. With the lithium metal protected, some amount of water in the electrolyte may be tolerated in order to enable an air-breathing battery over a system including onboard oxygen storage. Thus, it is important to know the general interaction of H_2O and redox mediator molecules. This chapter discusses considerations for Li_2O_2 degradation to LiOH formation in the presence of water impurities in nonaqueous Li-O_2 batteries containing redox mediators. Our work confirms the proposed roles of iodide, with particular emphasis on the ability of iodide to reduce H_2O_2 leading to complete degradation of Li_2O_2 to LiOH. A tangential important finding during this study was the difficulty in selection of an appropriate reference electrode for studying redox mediators in Li-O_2 batteries. We discuss appropriate reference electrode selection and its importance in proper characterization of redox mediators in Li-O_2 cells.

6.2 Experimental methods

Materials. Lithium bis(trifluoromethane) sulfonimide (LiTFSI), 1,2-dimethoxyethane (DME), dimethyl sulfoxide (DMSO), Whatman QM-A glass fiber filters, poly(tetrafluoroethylene) (PTFE, 60 wt% dispersion in H_2O), Vulcan XC72, stainless steel mesh, research-grade oxygen and argon, lithium metal, lithium chloride (LiCl), deuterium oxide (D_2O), lithium nitrate ($LiNO_3$), and lithium bromide (LiBr) were all sourced as described in section 3.2. Acetonitrile (anhydrous, 99.8%), potassium dioxide, and lithium manganese (III,IV) oxide (electrochemical grade) were purchased from Sigma-Aldrich. Lithium iron phosphate-coated aluminum foil, lithium titanate spinel powder, and Super P carbon black were purchased from MTI Corp. Polyvinylidene fluoride (PVDF) was purchased from Solvay. N-methylpyrrolidone was purchased from Alfa Aesar. Water used to contaminate the electrolytes was ultrapure (18.2 MΩ cm) via a Millipore filtration system.

Electrolyte preparation. All electrolyte and cell preparation was carried out in an argon glove box with <0.1 ppm O_2 and <0.1 ppm H_2O. Water was quickly and carefully added to electrolytes in the glovebox via micropipette, with ppm quantities calculated by volume.

Electrode preparation. Cathodes of Vulcan XC72 carbon on stainless steel mesh were prepared via the spray-coating method described in Chapter 2. Electrodes of lithium iron phosphate ($LiFePO_4$) on aluminum foil were punched out as 7/16" diameter discs and used as is. Lithium titanate spinel ($Li_4Ti_5O_{12}$) and lithium manganese oxide ($LiMn_2O_4$) electrodes were prepared on stainless steel mesh via a slurry method. Either 11mm or 7/16" diameter stainless steel mesh discs were punched out, rinsed with IPA and acetone, and dried at 150 °C for at least ten minutes. Active material, Super P carbon, and polyvinylidene fluoride (PVDF) (via a 10 wt% solution in n-methylpyrrolidone (NMP)) were combined in a mass ratio of 90:5:5, typically totaling 1 g, with an additional 0.1 g NMP and mixed via a Thinky mixer for five minutes at 1500 rpm. Additional NMP was added with further mixing as needed to create a ketchup-like consistency. The slurry was then spread over the stainless steel mesh discs, which were subsequently dried at 110 °C under vacuum for ten minutes. The electrodes were then calendered to ~60% true density via an MTI rolling press, followed by further drying at 60 °C under vacuum for twelve hours. The electrodes were then transferred into the argon glovebox while hot and stored on a hot plate at 200 °C immediately prior to use. Loading was typically ~10mg for LTO and ~15-25mg for LMO.

Cell preparation. Lithium-oxygen batteries following the Swagelok design detailed in Chapter 2 were prepared with lithium metal as the negative electrode, Whatman QM-A as a separator, and Vulcan XC72 carbon on stainless steel mesh as the positive electrode, as detailed in section 3.2. Electrolyte volume was either 80 µL or 160 µL (for which two Whatman QM-A separators were used), as detailed in figure and table captions. Prior to use as the lithium source and reference electrode in Li-O_2 batteries, $Li_4Ti_5O_{12}$ and $LiMn_2O_4$ electrodes were prelithiated in cells containing a 7/16" lithium metal negative electrode, a 1/2" Whatman QM-A separator and 80 µL of 1 M LiTFSI in DME under an argon headspace.

Cell characterization. Electrochemical cycling, pressure monitoring, and titrations of discharged cathodes were performed as detailed in Chapter 2. The moles of Li_2O_2 formed on discharge are given via the iodometric titration. LiOH and basic decomposition products are both measured via the acid-base titration, and thus cannot be distinguished. The value for LiOH and basic decomposition products reported here is for that formed during discharge. LiOH formed upon reaction of Li_2O_2 with water during the titration protocol has been subtracted out as two times the moles of Li_2O_2 measured via the iodometric titration. As discussed in Chapter 5, in cells containing 1 M LiTFSI in DME as the electrolyte, which exhibits a 2.0 e^-/O_2 process on discharge, basic decomposition products are typically 24% of the quantity of Li_2O_2 formed. In cells with worse e^-/O_2, such as in 1 M LiTFSI in DMSO, this quantity is higher. Thus, even after subtracting a stoichiometric amount of LiOH formed from the reaction of Li_2O_2 with water in the titration protocol, a nonzero value for LiOH and basic decomposition products is still expected even when Li_2O_2 is formed as the dominant discharge product.

KO_2 disproportionation. Ex situ analysis of Li_2O_2 degradation in the presence of iodide and water impurities in various solvents was performed via potassium superoxide (KO_2) disproportionation experiments similar to Tulodziecki et al.[43] In an argon glovebox, electrolytes containing 0.25 M LiTFSI with and without iodide and water impurities were placed in vials. KO_2 powder was added to the electrolyte vials, resulting in immediate disproportionation upon contact with Li^+ according to:

$$2KO_2 + 2Li^+ \leftrightarrow Li_2O_2 + O_2(g) + 2K^+ \qquad (6.6)$$

with the added KO_2 massed to be the limiting reagent. Tulodziecki et al. showed this in situ formation of Li_2O_2 enables fast degradation of Li_2O_2 to LiOH by the combination of iodide and ppm water in DME, according to reactions 6.3-6.5.

X-ray diffraction. Powder X-ray diffraction was performed on the powder formed via KO_2 disproportionation via Bruker D2 phaser PXRD with CuKα radiation (λ = 1.54178 Å). To prepare the powder for XRD, the liquid was decanted and the powder rinsed three times with pure DME before drying in the glovebox antechamber.

Nuclear magnetic resonance spectroscopy. ^1H nuclear magnetic resonance spectroscopy measurements were performed on both a Bruker AM-400 magnet with a 5mm Z-gradient broad brand probe and a Bruker Avance III 500 MHz magnet with a 5mm Z-gradient broad band probe. Each electrolyte was placed in an NMR tube along with a sealed melting point capillary containing 99.9% D_2O. The D_2O was used as a deuterium lock, and its residual proton peak was used as a reference for the electrolyte's ^1H spectrum.

6.3 Results and discussion

6.3.1 Considerations for Li_2O_2 degradation to LiOH

To probe the proposed roles of iodide in causing the degradation of Li_2O_2 to LiOH in the presence of water impurities in nonaqueous Li-O_2 batteries, 1,2-dimethoxyethane (DME) typically chosen for stability,[31] was replaced with dimethyl sulfoxide (DMSO), a solvent with a higher dielectric constant and higher Gutmann Donor Number and Acceptor Number.[85] Table 6.1 gives the e^-/O_2 and titration values for typical

lab-scale Li-O_2 batteries containing 0.25 M LiTFSI, 0.2 M LiI, and 2000 ppm H_2O in pure DME, pure DMSO, and mixtures of the two by volume discharged at a constant current of 0.2 mA/cm^2. As the amount of DMSO increases, the batteries trend from a 4 e^-/O_2 process to a 2 e^-/O_2 process on discharge, and the discharge product trends from predominant LiOH to predominant Li_2O_2, along with expected basic decomposition products. Of note, 6.8 µmol Li_2O_2 after a 0.5 mAh discharge corresponds to a 73% yield of an ideal 2.0 e^-/Li_2O_2 process (9.3 µmol Li_2O_2 after 0.5 mAh), in agreement with Li_2O_2 yields in 1 M LiTFSI in DMSO.[32] These data indicate that DMSO disrupts iodide's role in the degradation of Li_2O_2 to LiOH in the presence of water.

Table 6.1 Electron per oxygen values during discharge and titration values after discharge for cells containing 160 µL of 0.25 M LiTFSI, 0.2 M LiI, and 2000 ppm H_2O in mixtures of DME and DMSO. The electrolyte volume and concentration of water correspond to sufficient water for 0.95 mAh of LiOH formation. Discharging was stopped at the labeled capacity.

Solvent	e^-/O_2	Capacity (mAh)	LiOH (and basic decomposition products) (µmol)	Li_2O_2 (µmol)
DME	4.1	0.3	10.6	0.1
1:15 (v:v) DMSO:DME	3.4	0.5	14.9	1.4
50:50 (v:v) DMSO:DME	2.3	0.5	5.2	6.0
DMSO	2.2	0.5	3.8	6.8

Confirming the stability of Li_2O_2 in the presence of LiI and H_2O in DMSO, Figure 6.1 shows oxygen consumption and gas evolution data via pressure monitoring for Li-O_2 batteries containing 0.25 M LiTFSI, 0.2 M LiI, and 2000 ppm H_2O in the labeled mixtures of DME and DMSO, galvanostatically discharged and charged at 0.25 mA/cm^2. The trend toward a 2 e^-/O_2 process on discharge coincides with increased rechargeability on charge, as observed by the larger amount of gas evolved during charge (noting that prior reports have shown that most gas evolved in a DMSO-based Li-O_2 cell is oxygen). As an additional screening, ex situ product formation analysis similar to that in Tulodziecki et al. was conducted in an argon glovebox. KO_2 was added to lithium-containing electrolytes. Figure 6.2 shows the X-ray diffraction spectra of the dried powders that precipitated from this KO_2/electrolyte mixture. The powder formed in 0.25 M LiTFSI, 0.2 M LiI, and 2000 ppm H_2O in DMSO shows Li_2O_2 signatures, similar to that formed in 0.25 M LiTFSI in DME. The powder from 0.25 M LiTFSI, 0.2 M LiI, and 2000 ppm H_2O in DME shows a distinctly different XRD spectrum, with unassigned signatures similar to, though not exactly, LiOH and $LiIO_3$.[41, 109] Additionally, the electrolyte in the vial containing 0.25 M LiTFSI, 0.2 M LiI, and 2000 ppm H_2O in DME turned yellowish orange, indicating the formation of triiodide via reaction 6.4, as described in Tulodziecki et al.,[43] while the solution in the vial containing 0.25 M LiTFSI, 0.2 M LiI, and 2000 ppm H_2O in DMSO did not exhibit a color change.

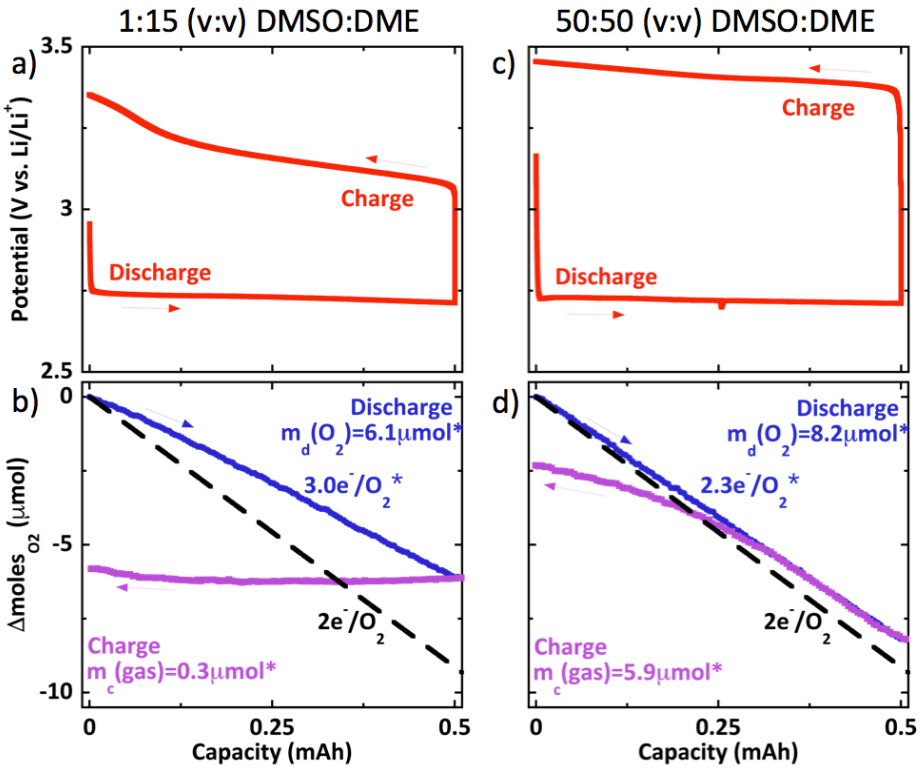

Figure 6.1 a) and **c)** Galvanostatic cycling of lithium-oxygen cells containing 160 µL of 0.25 M LiTFSI, 0.2 M LiI, and 2000 ppm H_2O in mixtures of DMSO and DME in ratios by volume of 1:15 and 50:50, respectively. **b)** and **d)** Oxygen consumption and gas evolution from pressure decay and pressure rise measurements.

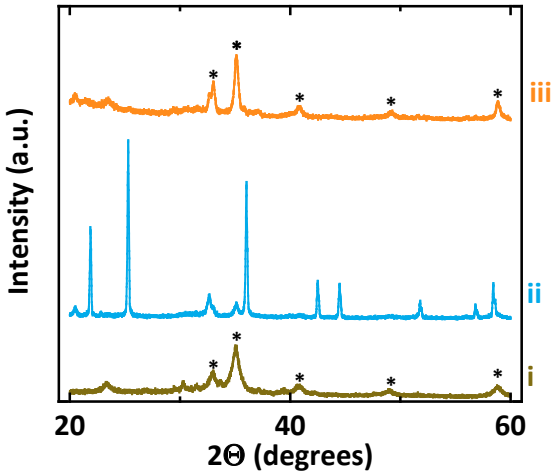

Figure 6.2 X-ray diffraction of powders formed by adding potassium superoxide as the limiting reagent to vials of lithium-containing electrolytes. Electrolytes were i) 0.25 M LiTFSI in DME, ii) 0.25 M LiTFSI 0.2 M LiI 2000 ppm H_2O in DME and iii) 0.25 M LiTFSI 0.2 M LiI 2000 ppm H_2O in DMSO. * denotes peaks expected for Li_2O_2, as seen in recent reports.[43, 109]

DMSO's effect on the iodide-induced degradation of Li_2O_2 was studied through the two roles of iodide presented by Tulodziecki et al.: 1) lowering the pKa of H_2O and 2) chemical equilibrium shift due to the continuous consumption of H_2O_2.[43]

The relative pKa of H_2O was observed via ^1H NMR. Electrolytes of DME, DMSO, and acetonitrile (MeCN) – a high dielectric constant, low Gutmann Donor Number and low Gutmann Acceptor Number solvent – with and without 0.2 M LiI and 2000 ppm H_2O were placed inside NMR tubes along with sealed melting point capillaries containing 99.9% D_2O. Figure 6.3 shows the ^1H NMR spectra, referenced to the residual proton peak (assigned 4.7 ppm in each spectra) in the D_2O capillary.

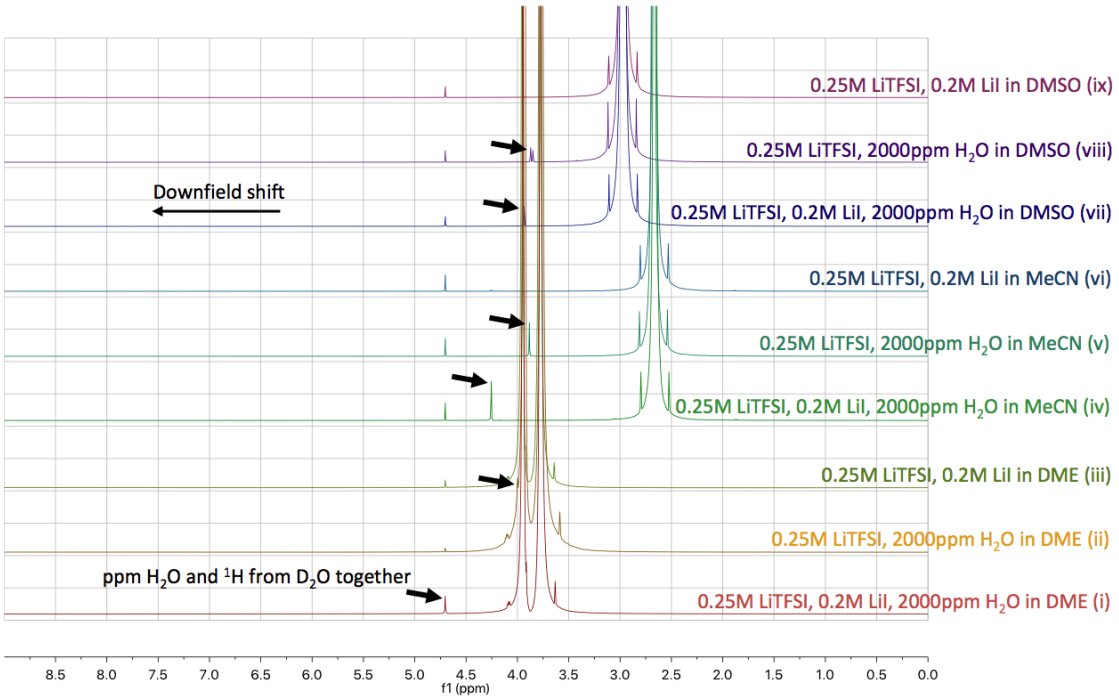

Figure 6.3 ^1H NMR of labeled electrolytes. Peak at 4.7 ppm is from residual protons in 99.9% D_2O in a sealed melting point capillary. Arrows point to peaks assigned to ppm H_2O in the electrolytes. For spectrum (i), these two peaks align, as labeled.

A large H_2O downfield shift, i.e., a strong deshielding of the proton or lowering of H_2O pKa, was observed with the addition of LiI in DME (comparing spectrum i vs. spectrum ii). In both acetonitrile and DMSO, however, the addition of LiI also moves the H_2O shift further downfield (iv vs. v and vii vs. viii respectively). Though the shifts are not as far downfield as in DME (i vs. ii), both DMSO and MeCN exhibit an iodide-induced lower pKa of H_2O, and thus predict increased LiOH formation. However, as the pressure rise and powder XRD results above show, Li_2O_2 is the predominant discharge product in 0.25 M LiTFSI, 0.2 M LiI, and 2000 ppm H_2O in DMSO. Additionally, in the absence of LiI, the proton shift of 2000 ppm H_2O is similar in the three solvents, with the shift in DME (spectrum ii) slightly further downfield than that in DMSO (viii) and MeCN (v). This

might indicate more LiOH formation in the DME electrolyte, but previous literature suggests water impurities in DMSO and acetonitrile induce more LiOH and/or lithium oxyhydroxide (LiOOH) formation than water impurities in DME, according to spectroscopic characterization of discharged cathodes.[110-112] Thus, the work herein indicates an iodide-induced lower pKa of H_2O is not the most important consideration for iodide-induced Li_2O_2 degradation.

Turning to the ability of iodide to continuously reduce H_2O_2, it is well known in the literature that iodide oxidation, i.e., triiodide and iodine (I_2) formation, is highly dependent on solvent.[113-115] To probe this solvent effect on iodide oxidation experimentally, cyclic voltammetry, beginning with an oxidative scan, was performed on batteries under an argon atmosphere containing 0.25 M LiTFSI, 0.2 M LiI, and 2000 ppm H_2O in DME and DMSO. Shown in Figure 6.4, iodide oxidation in DMSO occurs about 0.5 V vs. Li/Li^+ higher than in DME.

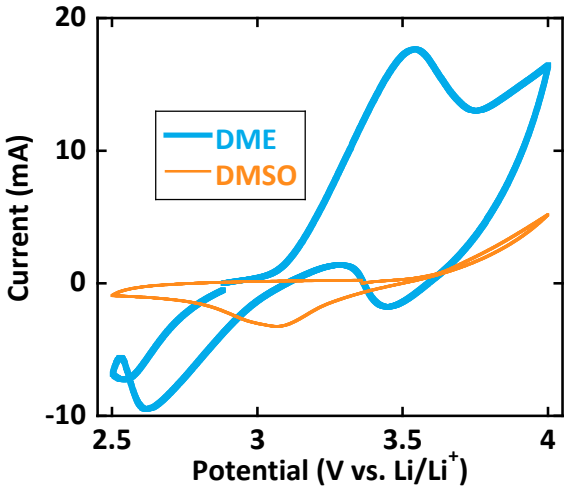

Figure 6.4 Cyclic voltammetry of batteries under an argon atmosphere containing 160 µL of 0.25 M LiTFSI, 0.2 M LiI, and 2000 ppm H_2O in DME and DMSO as labeled. Sweep rate was 20 mV/s and CVs began with oxidative scan.

Thus, iodide oxidation is more difficult in DMSO than in DME. While this is an electrochemical measurement, it points to a less favorable driving force for triiodide formation in DMSO, implying iodide-induced H_2O_2 reduction is more difficult in DMSO than in DME. This serves as an explanation for the permanence of Li_2O_2 as the predominant discharge product in LiI- and H_2O-containing electrolytes with DMSO as the solvent. Of note, this also correlates with the previously described observation that KO_2 disproportionation in LiI- and H_2O-containing DME is coupled with the electrolyte turning yellowish orange, evident of iodide oxidation, whereas KO_2 disproportionation in LiI- and H_2O-containing DMSO exhibits no color change. The higher oxidation potential of iodide in DMSO is likely linked to stronger solvation of iodide due to its higher Gutmann Acceptor Number than DME.[85]

Table 6.2 Electron per oxygen values during discharge and titration values after discharge for cells containing 160 µL of 0.25 M LiTFSI and 0.2 M LiBr with and without 2000 ppm H_2O in DME. The electrolyte volume and concentration of water correspond to sufficient water for 0.95 mAh of LiOH formation. Discharging was stopped at the labeled capacity.

Electrolyte	e^-/O_2	Capacity (mAh)	LiOH (and basic decomposition products) (µmol)	Li_2O_2 (µmol)
0.25M LiTFSI, 0.2M LiBr in DME	2.2	0.3	2.8	4.1
0.25M LiTFSI, 0.2M LiBr, 2000ppm H_2O in DME	2.3	0.3	3.1	4.1

In further support that DMSO precludes H_2O_2 reduction via more difficult iodide oxidation, electrolytes of lithium bromide (LiBr) in DME were similarly studied. Bromide oxidation is well known to occur at higher potentials than iodide oxidation in common nonaqueous electrolytes.[115-116] (Cyclic voltammetry was not performed in our laboratory to avoid bromine formation.) As expected given the higher oxidation potential of Br^- than I^-, Table 6.2 shows that LiBr- and H_2O-containing DME-based electrolytes exhibit near 2 e^-/O_2 processes on discharge. Titrations of discharged cathodes also point to Li_2O_2 as the dominant discharge product, along with basic decomposition products as expected, as 4.1 µmol Li_2O_2 after a 0.3 mAh discharge corresponds to a 73% yield of an ideal 2.0 e^-/Li_2O_2 process (5.6 µmol Li_2O_2 after 0.3 mAh).

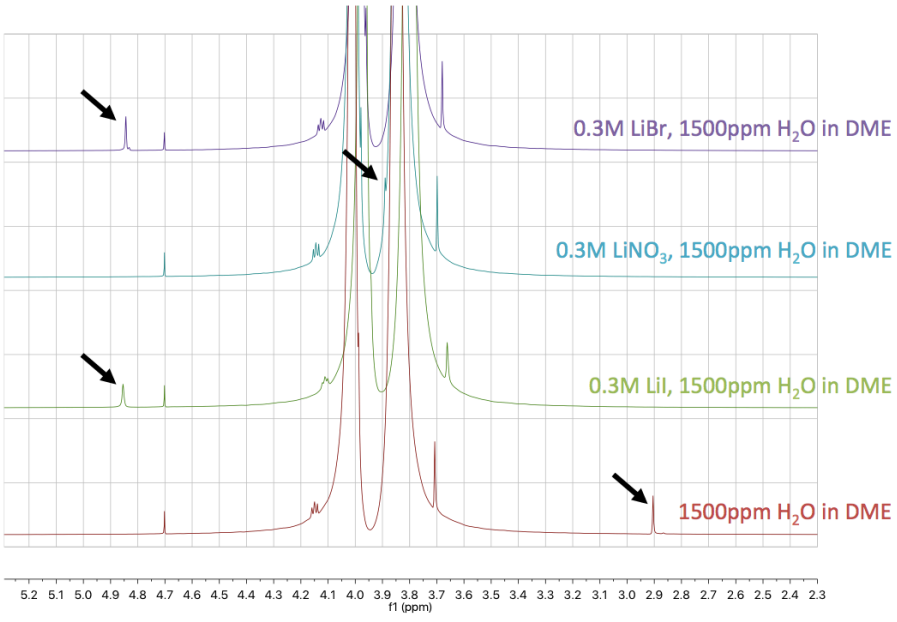

Figure 6.5 ^1H NMR of labeled electrolytes. Peak at 4.7 ppm is from residual protons in 99.9% D_2O in a sealed melting point capillary. Arrows point to peaks assigned to ppm H_2O in the electrolytes.

Meanwhile, ^{1}H NMR spectra for electrolytes with 1500 ppm H_2O with and without LiBr in DME, presented in Figure 6.5, show that the addition of LiBr to DME causes a nearly identical downfield shift in the ppm H_2O peak as with the addition of LiI. For reference, lithium nitrate ($LiNO_3$) does not induce the same downfield shift in the ppm H_2O peak, as shown in Figure 6.5. Thus, it seems the most critical consideration in predicting Li_2O_2 degradation to LiOH in the presence of water impurities is an additive's ability to oxidize and subsequently reduce H_2O_2 in the electrolyte of choice, rather than the additive's effect on the pKa of the dilute water.

6.3.2 Implications of redox mediators on reference electrode selection

A tangential important finding during this study was the difficulty in selection of an appropriate reference electrode for studying redox mediators in lithium-oxygen batteries.

In studying the effect of other solvents and other redox mediators on the degradation of Li_2O_2 to LiOH in lab-scale batteries, the use of a pure lithium metal anode limits the options. Organic redox mediators degrade quickly against lithium metal,[95, 102] and some interesting solvents do not form a stable interface on lithium, such as acetonitrile.[31]

Lithium iron phosphate ($LiFePO_4$, referred to as LFP), is commonly used as an alternative lithium source and reference electrode in lithium-oxygen studies, especially with acetonitrile.[31, 45] LFP exhibits reversible lithium intercalation near 3.5 V vs. Li/Li^+ with a stable voltage profile due to its two-phase behavior:

$$Li^+ + e^- + FePO_4 \leftrightarrow LiFePO_4 \qquad U \sim 3.5\ V\ vs.\ Li^+/Li \qquad (6.7)$$

Unfortunately, LFP's standard reduction potential for lithium intercalation is too high for use with iodide.

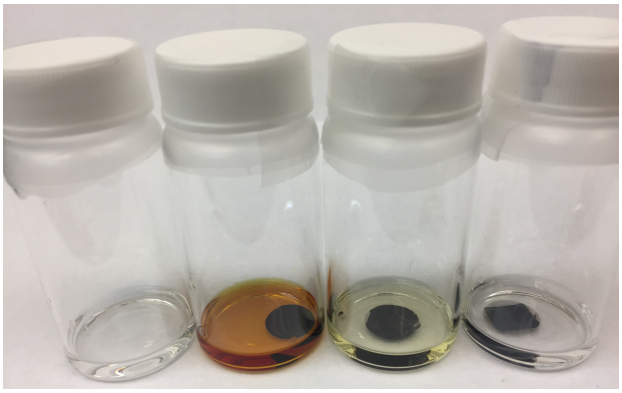

Figure 6.6 Vials containing 0.25 M LiTFSI and 0.2 M LiI in DME under an argon atmosphere and (left to right) no electrode, a lithium iron phosphate electrode, a lithiated lithium manganese oxide electrode, and a lithiated lithium titanate spinel electrode. The $LiFePO_4$ was delithiated 50% in a cell containing 1 M LiTFSI in DME and an argon headspace prior to insertion in the vial. The LMO and LTO were 50% lithiated in cells containing 1 M LiTFSI in DME and argon headspaces prior to insertion in the vial.

As iodide oxidation occurs near 3 V vs. Li/Li^+ in DME, contact between an electrolyte of LiI in DME and an LFP electrode causes immediate chemical lithiation of the LFP and oxidation of the iodide. Figure 6.6 shows vials containing 0.25 M LiTFSI and 0.2 M LiI in DME under an argon atmosphere, with the second vial from the left containing an LFP electrode that has been previously delithiated 50% in a battery containing 1 M LiTFSI in DME under argon. The electrolyte immediately has turned orange, indicating chemical oxidation of iodide, likely to iodine. This ongoing chemical reaction at the reference electrode complicates the use of LFP to study iodide redox mediation at the carbon/oxygen working electrode in a Li-O_2 battery. LFP should be avoided as a reference electrode in Li-O_2 batteries containing redox mediators with redox potentials below that of lithium intercalation in LFP, as has been recently reported.[117]

While chemical oxidation of the redox mediator provides a ceiling for possible lithium intercalation materials as reference electrodes in Li-O_2 batteries, spontaneous oxygen reduction provides a floor. As exhibited by the desired discharge reaction in the Li-O_2 battery, oxygen reduction occurs ~2.8 V vs. Li/Li^+ in DME. Lithium metal reacts spontaneously with oxygen, but forms a semi-stable passivating layer, allowing a lithium-oxygen battery employing a typical 1 M LiTFSI in DME electrolyte to rest stably under oxygen for hours. Some lower-voltage lithium intercalation materials, while avoiding chemical oxidation of the redox mediator, react spontaneously under oxygen. For example, lithium titanate spinel ($Li_4Ti_5O_{12}$, referred to as LTO), exhibits reversible lithium intercalation near 1.55 V vs. Li/Li^+ in DME with a stable voltage profile, forming lithiated lithium titanate spinel ($Li_7Ti_5O_{12}$, referred to as LLTO):

$$3Li^+ + 3e^- + Li_4Ti_5O_{12} \leftrightarrow Li_7Ti_5O_{12} \qquad U \sim 1.55\ V\ vs.\ Li^+/Li \qquad (6.8)$$

Partially delithiated LLTO is stable against iodide oxidation, as shown in the rightmost vial of Figure 6.6, where there is no color change of a 0.25 M LiTFSI and 0.2 M LiI in DME electrolyte upon insertion of the partially delithiated LLTO. However, LLTO reacts spontaneously under oxygen, losing nearly 80% state-of-charge as it undergoes the reaction:

$$Li_7Ti_5O_{12} + O_2 \leftrightarrow Li_2O_2 + Li_5Ti_5O_{12} \qquad (6.9)$$

perhaps through a lithium superoxide (LiO_2) intermediate, as shown by Piana et al.[118] Figure 6.7a shows a battery containing LLTO versus lithium metal with an O_2 headspace resting at open circuit for 10 hours before constant current charging (delithiating), discharging (lithiating), and charging again between 2 V vs. Li/Li^+ (charge) and 1.1 V (discharge) cutoffs. Pressure monitoring shows O_2 is spontaneously consumed throughout the 10 hour rest period, and only ~0.43 mAh – a fraction of the second charge – indicated with an arrow in Figure 6.7a, occurs with both a stable voltage profile and a stable pressure. Interestingly, electrochemical formation of Li_2O_2 on the surface of the lithium titanate spinel electrode seems to extend the usable capacity. Figure 6.7b shows a similar battery charged to a 4.5 V cutoff before a subsequent discharge and charge. The usable charge capacity with stable voltage and stable pressure, as indicated by the arrow, is ~0.83 mAh. Stability in both voltage and pressure when charging the electrode versus

lithium under oxygen is necessary to use the electrode as a lithium source and reference electrode in a lithium-oxygen battery.

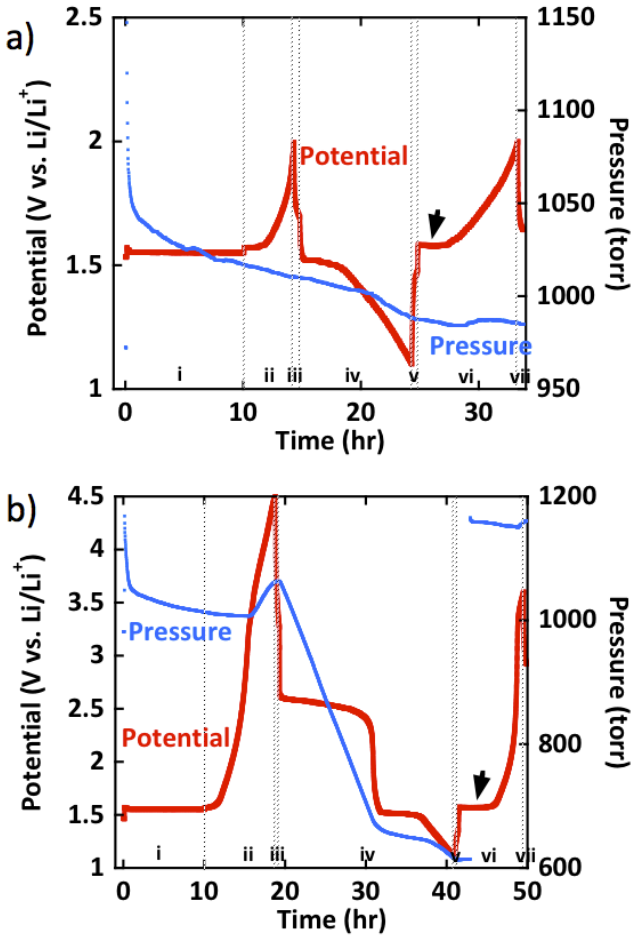

Figure 6.7 Galvanostatic cycling with pressure monitoring of lithiated lithium titanate spinel versus lithium in cells containing 1 M LiTFSI in DME and oxygen headspaces. Lithium titanate spinel electrodes were prelithiated versus lithium in cells containing 1 M LiTFSI in DME and argon headspaces before use in the exhibited cells. Labeled sections on the graphs correspond to i) open circuit for 10 hr, ii) charging at ~0.2 mA/cm^2 to **a)** 2 V and **b)** 4.5 V, iii) open circuit for 0.5 hr, iv) discharging at ~0.2 mA/cm^2 to 1.1 V, v) open circuit for 0.5 hr, vi) charging at ~0.2 mA/cm^2 to **a)** 2 V and **b)** 3.6 V (arbitrary), and vii) open circuit for 0.5 hr. The cell in **b)** was quickly refilled with oxygen at ~42 hr, resulting in the sudden increase in pressure. The arrows point to the usable capacity as a lithium reference electrode with stable voltage and stable pressure: **a)** ~0.43 mAh and **b)** ~0.84 mAh.

Between the two challenges of chemical oxidation of the redox mediator and spontaneous oxygen reduction, a possible mid-voltage option for a lithium reference electrode is lithium manganese oxide ($LiMn_2O_4$, referred to as LMO). LMO has been

shown to withstand overlithiation of ~0.7 Li^+ to $Li_{1.7}Mn_2O_4$ at ~3 V vs. Li/Li^+ in carbonates,[119] presenting a lithium intercalation voltage slightly above oxygen reduction.

$$0.7Li^+ + 0.7e^- + LiMn_2O_4 \leftrightarrow Li_{1.7}Mn_2O_4 \qquad U \sim 3\ V\ vs.\ Li^+/Li \quad (6.10)$$

Figure 6.8a shows the galvanostatic discharge profile and pressure data for a battery containing LLMO versus lithium metal with an O_2 headspace resting at open circuit for 10 hours before charging (delithiating), discharging (lithiating), and charging again at constant current between 3.6 V vs. Li/Li^+ (charge) and 2.7 V (discharge) cutoffs.

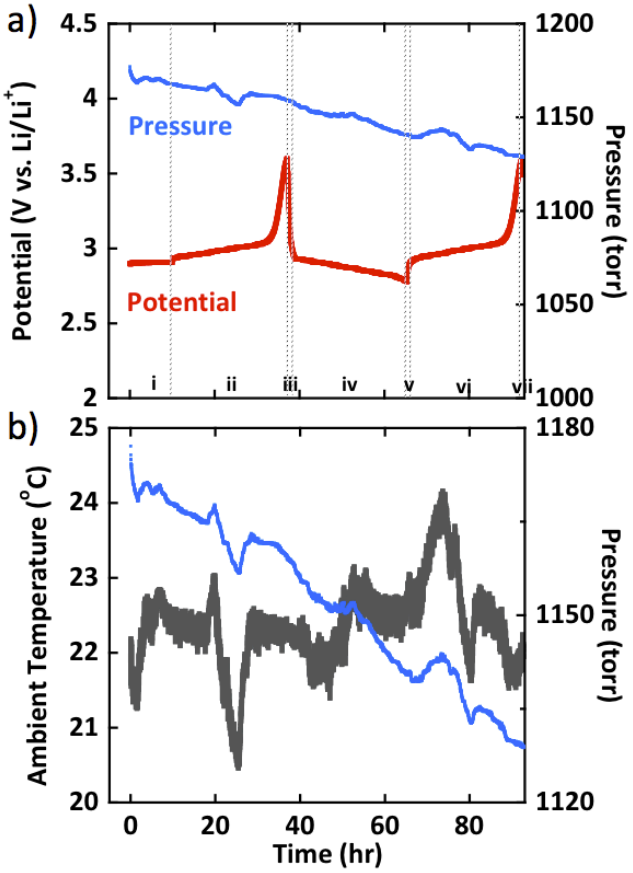

Figure 6.8 a) Galvanostatic cycling with pressure monitoring of lithiated lithium manganese oxide versus lithium in cells containing 1 M LiTFSI in DME and oxygen headspaces. Lithium manganese oxide electrodes were prelithiated versus lithium in cells containing 1 M LiTFSI in DME and argon headspaces before use in the exhibited cells. Labeled sections on the graphs correspond to i) open circuit for 10 hr, ii) charging at ~0.076 mA/cm^2 to 3.6 V vs. Li/Li^+, iii) open circuit for 0.25 hr, iv) discharging at ~0.076 mA/cm^2 to 2.7 V, v) open circuit for 0.25 hr, vi) charging at ~0.076 mA/cm^2 to 3.6 V (arbitrary), and vii) open circuit for 0.25 hr. **b)** Comparison of the pressure of this cell with the ambient temperature, measured via a thermocouple near the cell exterior.

This electrode shows 1.7 mAh of delithiation capacity with a stable voltage plateau before a sudden voltage rise on the first charge, as well as repeatability on the next cycle. Pressure monitoring of the cell shows a pressure decay of 0.5 torr/hr, with fluctuations due to temperature as shown in Figure 6.8b. While this is not ideal for use as a lithium reference electrode, its steady nature means it could be accounted for, and a 2.0 e^-/O_2 process and a 4.0 e^-/O_2 process in this cell would consume 13.4 torr/hr and 6.7 torr/hr, respectively, or more than ten times this consumption. Unfortunately, additionally, an electrolyte of 0.25 M LiTFSI and 0.2 M LiI in DME shows a color change to faint yellow with the addition of 50% delithiated LLMO electrode, shown in the second vial from the right in Figure 6.6. The partially delithiated electrode reaches an open circuit potential just above 3 V vs. Li/Li^+, and iodide to triiodide onset, as shown in Figure 5.2, occurs at ~2.95 V vs. Li/Li^+. Thus, LLMO might work best as a lithium source and reference electrode for redox mediators with higher redox potentials than iodide, such as tetrathiafulvalene (TTF), which exhibits a redox couple at ~3.5 V vs. Li/Li^+.

6.4 Conclusion

In conclusion, the most critical consideration in predicting Li_2O_2 degradation to LiOH in the presence of water impurities is an additive's ability to oxidize and subsequently reduce H_2O_2 in the electrolyte of choice. Galvanostatic cycling of lab-scale Li-O_2 batteries containing LiI and H_2O in DME and DMSO shows that DMSO prevents Li_2O_2 degradation to LiOH, and cyclic voltammetry of these electrolytes show DMSO exhibits a higher potential for iodide oxidation than DME, implying H_2O_2 reduction is more difficult in DMSO. As the low pKa of dilute water in DMSO via ^1H NMR would predict LiOH formation, an additive's effect on the pKa of the dilute water likely plays a minor role in final product formation.

The use of a lithium metal negative electrode limits the options of solvents and redox mediators for studying the degradation of Li_2O_2 to LiOH, so we investigated other possible lithium reference electrodes for use in lab-scale Li-O_2 batteries. High voltage lithium intercalation materials like lithium iron phosphate are unsuitable with most redox mediators, as their lithium intercalation voltages are higher than the redox potentials of most Li-O_2 redox mediators, leading to chemical oxidation of the redox mediator upon contact with the intercalation material. Low voltage lithium intercalation materials like lithiated lithium titanate spinel are unstable to oxygen, though after significant exposure to O_2, LLTO can provide some usable capacity – a stable voltage profile and stable O_2 headspace pressure – for use in a lab-scale Li-O_2 battery. Overlithiated lithium manganese oxide is a possible mid-voltage option that is stable to O_2, though it exhibits slow oxygen consumption, and its intercalation voltage (~3 V vs. Li^+/Li) is slightly too high for use with iodide.

6.5 Acknowledgments

I gratefully acknowledge Kyle Diederichsen for helping with ^1H NMR measurements and helpful discussions on NMR theory, Joe Papp for helping with powder XRD measurements, and Byungchun Park for helping with LMO and LTO electrode

preparation. This work was supported by a NASA Space Technology Research Fellowship.

Chapter 7: Summary

In this work, the nonaqueous electrolyte of the lithium-oxygen (Li-O_2) battery was engineered toward achieving a high-capacity, rechargeable battery.

Toward inducing a high-capacity solution mechanism of lithium peroxide (Li_2O_2) growth, the typical lithium battery salt lithium bis(trifluoromethane) sulfonimide (LiTFSI) was partially exchanged for lithium nitrate ($LiNO_3$), as NO_3^- is a stronger electron donor than $TFSI^-$ and therefore provides enhanced stability of Li^+, and hence the superoxide intermediate, in the electrolyte. Li-O_2 batteries employing electrolytes of both $LiNO_3$ and LiTFSI in 1,2-dimethoxyethane (DME), totaling 1.0 M lithium cation (Li^+) concentration, displayed increasing capacity with increasing $LiNO_3$ concentration. Titrations of cathodes extracted from discharged batteries confirmed Li_2O_2 formation as the dominant discharge process, and scanning electron microscopy (SEM) of discharged cathodes showed increasing toroid formation with increasing $LiNO_3$ concentration, confirming the solution mechanism. ^{7}Li nuclear magnetic resonance (NMR) spectroscopy was used to attribute this increase in the solution mechanism to enhanced Li^+ stability in solution, which in turn induces solubility of lithium superoxide (LiO_2), the intermediate to Li_2O_2 formation. In addition, an Ising model was developed with collaborators to predict Li^+ stability as a function of its solvation shell composition. Differential electrochemical mass spectrometry (DEMS), via a custom-built instrument, was used to show the addition of $LiNO_3$ did not deleteriously affect battery rechargeability.

As anion selection induces the solution mechanism by lowering the free energy of Li^+ in solution, non-Li alkali metal cations and alcohols were studied as methods of inducing the solution mechanism by lowering the free energy of the superoxide anion (O_2^-) in solution. The addition of non-Li alkali metal salts induced a minimal increase in the achievable discharge capacity of Li-O_2 batteries. Gas analysis of the addition of lithium salt to a sodium-oxygen battery showed Li^+ quickly scavenges any non-Li alkali metal cation-associated O_2^- in electrolytes containing both Li^+ and non-Li alkali metal cations. This corroborates a recent report that a capacity increase is only expected at high currents when oxygen reduction occurs quickly enough that some O_2^- temporarily avoids Li^+ and solubilizes as non-Li alkali metal cation-associated O_2^-. The addition of ppm quantities of methanol, ethanol, or 1-propanol to ether-based Li-O_2 battery electrolytes induced a two-fold increase in battery capacity with little trend in the capacity as a function of the additive's Acceptor Number, highlighting the complexity of interactions between the constituent species in an electrolyte in terms of their Lewis basicities, Lewis acidities, and other physicochemical properties.

As the high-capacity solution mechanism of Li_2O_2 causes some Li_2O_2 to form in aggregated structures away from the electrode surface, the addition of small molecule redox mediators to the electrolyte was studied as a means of charging Li_2O_2. The effect of water (H_2O) contamination in the electrolyte on the promising redox mediator lithium iodide (LiI) was studied. DEMS and titrations of cathodes extracted from discharged batteries confirmed recent reports that lithium hydroxide (LiOH) formed as the dominant discharge product via a 4 e^-/O_2 process. However, isotopic labeling and DEMS were used to show LiOH is not reversibly oxidized back to its reactants (Li^+, O_2, H_2O). With the help of collaborators, titrations, SEM energy-dispersive X-ray spectroscopy (SEM EDX), and galvanostatic cycling of batteries under an argon atmosphere were used to show

charge current in batteries containing both LiI and H_2O is a complex mixture of side reactions and redox shuttling.

With LiOH identified as an undesirable side product, the mechanism for Li_2O_2 degradation to LiOH in the presence of LiI and H_2O was studied. Galvanostatic cycling of lab-scale Li-O_2 batteries containing LiI and H_2O in DME and dimethyl sulfoxide (DMSO) showed that DMSO prevents Li_2O_2 degradation to LiOH. Cyclic voltammetry of these electrolytes showed DMSO exhibits a higher potential for iodide oxidation than DME, implying iodide-mediated H_2O_2 reduction is more difficult in DMSO. This points to the ability of an additive to reduce H_2O_2 as a key consideration in Li_2O_2's stability in the presence of an additive and water impurities.

As some redox mediators and solvents are unstable with a lithium metal negative electrode, other possible lithium-containing electrodes were investigated for use in lab-scale Li-O_2 batteries. Placement of a lithium iron phosphate (LFP) electrode in a vial of an iodide-containing electrolyte showed a color change attributed to chemical oxidation of iodide to triiodide, indicating LFP's lithium intercalation voltage is too high for stable use in a LiI-containing Li-O_2 battery. Meanwhile, DEMS of lithiated lithium titanate spinel (LLTO) showed spontaneous oxygen consumption, indicating its lithium intercalation voltage is too low for use in Li-O_2 batteries. A possible mid-voltage option was shown to be lithiated lithium manganese oxide, though it exhibits slow oxygen consumption, and its intercalation voltage (~3 V vs. Li^+/Li) is better suited for redox mediators with slightly higher first oxidation potentials than iodide.

References

1. McCloskey, B. D.; Burke, C. M.; Nichols, J. E.; Renfrew, S. E., Mechanistic Insights for the Development of Li-O_2 Battery Materials: Addressing Li_2O_2 Conductivity Limitations and Electrolyte and Cathode Instabilities. *Chemical Communications* **2015,** *51* (64), 12701-12715.
2. Abraham, K. M., Prospects and Limits of Energy Storage in Batteries. *Journal of Physical Chemistry Letters* **2015,** *6* (5), 830-844.
3. Goodenough, J. B.; Kim, Y., Challenges for Rechargeable Li Batteries. *Chemistry of Materials* **2010,** *22* (3), 587-603.
4. Wagner, F. T.; Lakshmanan, B.; Mathias, M. F., Electrochemistry and the Future of the Automobile. *Journal of Physical Chemistry Letters* **2010,** *1* (14), 2204-2219.
5. *2015 NASA Technology Roadmaps TA 3: Space Power and Energy Storage*; National Aeronautics Space Administration: 2015; pp 1-97.
6. Van Noorden, R., The Rechargeable Revolution: A Better Battery. *Nature* **2014,** *507* (7490), 26-28.
7. Obrovac, M. N.; Chevrier, V. L., Alloy Negative Electrodes for Li-Ion Batteries. *Chemical Reviews* **2014,** *114* (23), 11444-11502.
8. Whittingham, M. S., Ultimate Limits to Intercalation Reactions for Lithium Batteries. *Chemical Reviews* **2014,** *114* (23), 11414-11443.
9. Luntz, A. C.; McCloskey, B. D., Nonaqueous Li–Air Batteries: A Status Report. *Chemical Reviews* **2014,** *114* (23), 11721-11750.
10. Manthiram, A.; Fu, Y.; Chung, S.-H.; Zu, C.; Su, Y.-S., Rechargeable Lithium–Sulfur Batteries. *Chemical Reviews* **2014,** *114* (23), 11751-11787.
11. Ji, X.; Nazar, L. F., Advances in Li-S Batteries. *Journal of Materials Chemistry* **2010,** *20* (44), 9821-9826.
12. Shterenberg, I.; Salama, M.; Gofer, Y.; Levi, E.; Aurbach, D., The Challenge of Developing Rechargeable Magnesium Batteries. *MRS Bulletin* **2014,** *39* (5), 453-460.
13. Muldoon, J.; Bucur, C. B.; Gregory, T., Quest for Nonaqueous Multivalent Secondary Batteries: Magnesium and Beyond. *Chemical Reviews* **2014,** *114* (23), 11683-11720.
14. Fergus, J. W., Recent Developments in Cathode Materials for Lithium Ion Batteries. *Journal of Power Sources* **2010,** *195* (4), 939-954.
15. Li, Z.; Chernova, N. A.; Feng, J.; Upreti, S.; Omenya, F.; Whittingham, M. S., Stability and Rate Capability of Al Substituted Lithium-Rich High-Manganese Content Oxide Materials for Li-Ion Batteries. *Journal of The Electrochemical Society* **2011,** *159* (2), A116-A120.
16. Bettge, M.; Li, Y.; Gallagher, K.; Zhu, Y.; Wu, Q.; Lu, W.; Bloom, I.; Abraham, D. P., Voltage Fade of Layered Oxides: Its Measurement and Impact on Energy Density. *Journal of The Electrochemical Society* **2013,** *160* (11), A2046-A2055.
17. Ohzuku, T.; Takeda, S.; Iwanaga, M., Solid-State Redox Potentials for $Li[Me_{1/2}Mn_{3/2}]O_4$ (Me: 3d-Transition Metal) Having Spinel-Framework Structures: A Series of 5 Volt Materials for Advanced Lithium-Ion Batteries. *Journal of Power Sources* **1999,** *81-82*, 90-94.
18. Lin, F.; Markus, I. M.; Nordlund, D.; Weng, T.-C.; Asta, M. D.; Xin, H. L.; Doeff, M. M., Surface Reconstruction and Chemical Evolution of Stoichiometric Layered Cathode Materials for Lithium-Ion Batteries. *Nature Communications* **2014,** *5*, 3529.
19. Girishkumar, G.; McCloskey, B.; Luntz, A. C.; Swanson, S.; Wilcke, W., Lithium−Air Battery: Promise and Challenges. *Journal of Physical Chemistry Letters* **2010,** *1* (14), 2193-2203.
20. Bruce, P. G.; Freunberger, S. A.; Hardwick, L. J.; Tarascon, J.-M., Li-O_2 and Li-S Batteries with High Energy Storage. *Nature Materials* **2012,** *11* (1), 19-29.

21. Christensen, J.; Albertus, P.; Sanchez-Carrera, R. S.; Lohmann, T.; Kozinsky, B.; Liedtke, R.; Ahmed, J.; Kojic, A., A Critical Review of Li / Air Batteries. *Journal of The Electrochemical Society* **2012,** *159* (2), R1-R30.
22. Lu, J.; Li, L.; Park, J.-B.; Sun, Y.-K.; Wu, F.; Amine, K., Aprotic and Aqueous Li–O_2 Batteries. *Chemical Reviews* **2014,** *114* (11), 5611-5640.
23. Gallagher, K. G.; Goebel, S.; Greszler, T.; Mathias, M.; Oelerich, W.; Eroglu, D.; Srinivasan, V., Quantifying the Promise of Lithium-Air Batteries for Electric Vehicles. *Energy & Environmental Science* **2014,** *7* (5), 1555-1563.
24. Cho, M. H.; Trottier, J.; Gagnon, C.; Hovington, P.; Clement, D.; Vijh, A.; Kim, C. S.; Guerfi, A.; Black, R.; Nazar, L.; Zaghib, K., The Effects of Moisture Contamination in the Li–O_2 Battery. *Journal of Power Sources* **2014,** *268*, 565-574.
25. Aetukuri, N. B.; McCloskey, B. D.; Garcia, J. M.; Krupp, L. E.; Viswanathan, V.; Luntz, A. C., Solvating Additives Drive Solution-Mediated Electrochemistry and Enhance Toroid Growth in Non-Aqueous Li-O_2 Batteries. *Nature Chemistry* **2015,** *7* (1), 50-56.
26. Gowda, S. R.; Brunet, A.; Wallraff, G. M.; McCloskey, B. D., Implications of CO_2 Contamination in Rechargeable Nonaqueous Li–O_2 Batteries. *Journal of Physical Chemistry Letters* **2013,** *4* (2), 276-279.
27. Abraham, K. M.; Jiang, Z., A Polymer Electrolyte - Based Rechargeable Lithium/Oxygen Battery. *Journal of The Electrochemical Society* **1996,** *143* (1), 1-5.
28. Ogasawara, T.; Débart, A.; Holzapfel, M.; Novák, P.; Bruce, P. G., Rechargeable Li_2O_2 Electrode for Lithium Batteries. *Journal of the American Chemical Society* **2006,** *128* (4), 1390-1393.
29. Freunberger, S. A.; Chen, Y. H.; Drewett, N. E.; Hardwick, L. J.; Barde, F.; Bruce, P. G., The Lithium-Oxygen Battery with Ether-Based Electrolytes. *Angewandte Chemie-International Edition* **2011,** *50* (37), 8609-8613.
30. McCloskey, B. D.; Bethune, D. S.; Shelby, R. M.; Girishkumar, G.; Luntz, A. C., Solvents' Critical Role in Nonaqueous Lithium–Oxygen Battery Electrochemistry. *Journal of Physical Chemistry Letters* **2011,** *2* (10), 1161-1166.
31. McCloskey, B. D.; Bethune, D. S.; Shelby, R. M.; Mori, T.; Scheffler, R.; Speidel, A.; Sherwood, M.; Luntz, A. C., Limitations in Rechargeability of Li-O_2 Batteries and Possible Origins. *Journal of Physical Chemistry Letters* **2012,** *3* (20), 3043-3047.
32. McCloskey, B. D.; Valery, A.; Luntz, A. C.; Gowda, S. R.; Wallraff, G. M.; Garcia, J. M.; Mori, T.; Krupp, L. E., Combining Accurate O_2 and Li_2O_2 Assays to Separate Discharge and Charge Stability Limitations in Nonaqueous Li-O_2 Batteries. *Journal of Physical Chemistry Letters* **2013,** *4* (17), 2989-2993.
33. Chen, Y.; Freunberger, S. A.; Peng, Z.; Barde, F.; Bruce, P. G., Li–O_2 Battery with a Dimethylformamide Electrolyte. *Journal of the American Chemical Society* **2012,** *134* (18), 7952-7957.
34. McCloskey, B. D.; Speidel, A.; Scheffler, R.; Miller, D. C.; Viswanathan, V.; Hummelshøj, J. S.; Nørskov, J. K.; Luntz, A. C., Twin Problems of Interfacial Carbonate Formation in Nonaqueous Li–O_2 Batteries. *Journal of Physical Chemistry Letters* **2012,** *3* (8), 997-1001.
35. Mahne, N.; Renfrew Sara, E.; McCloskey Bryan, D.; Freunberger Stefan, A., Electrochemical Oxidation of Lithium Carbonate Generates Singlet Oxygen. *Angewandte Chemie-International Edition* **2018,** *57* (19), 5529-5533.
36. McCloskey, B. D.; Scheffler, R.; Speidel, A.; Bethune, D. S.; Shelby, R. M.; Luntz, A. C., On the Efficacy of Electrocatalysis in Nonaqueous Li-O_2 Batteries. *Journal of the American Chemical Society* **2011,** *133* (45), 18038-41.
37. McCloskey, B. D.; Scheffler, R.; Speidel, A.; Girishkumar, G.; Luntz, A. C., On the Mechanism of Nonaqueous Li–O_2 Electrochemistry on C and Its Kinetic Overpotentials:

Some Implications for Li–Air Batteries. *Journal of Physical Chemistry C* **2012,** *116* (45), 23897-23905.
38. Albertus, P.; Girishkumar, G.; McCloskey, B.; Sanchez-Carrera, R. S.; Kozinsky, B.; Christensen, J.; Luntz, A. C., Identifying Capacity Limitations in the Li/Oxygen Battery Using Experiments and Modeling. *Journal of The Electrochemical Society* **2011,** *158* (3), A343-A351.
39. Viswanathan, V.; Thygesen, K. S.; Hummelshoj, J. S.; Norskov, J. K.; Girishkumar, G.; McCloskey, B. D.; Luntz, A. C., Electrical Conductivity in Li_2O_2 and Its Role in Determining Capacity Limitations in Non-Aqueous Li-O_2 Batteries. *Journal of Chemical Physics* **2011,** *135* (21), 214704.
40. Burke, C. M.; Pande, V.; Khetan, A.; Viswanathan, V.; McCloskey, B. D., Enhancing Electrochemical Intermediate Solvation through Electrolyte Anion Selection to Increase Nonaqueous Li–O_2 Battery Capacity. *Proceedings of the National Academy of Sciences of the United States of America* **2015,** *112* (30), 9293-9298.
41. Burke, C. M.; Black, R.; Kochetkov, I. R.; Giordani, V.; Addison, D.; Nazar, L. F.; McCloskey, B. D., Implications of 4 e^- Oxygen Reduction Via Iodide Redox Mediation in Li-O_2 Batteries. *ACS Energy Letters* **2016,** *1* (4), 747-756.
42. Knudsen, K. B.; Luntz, A. C.; Jensen, S. H.; Vegge, T.; Hjelm, J., Redox Probing Study of the Potential Dependence of Charge Transport through Li_2O_2. *Journal of Physical Chemistry C* **2015,** *119* (51), 28292-28299.
43. Tulodziecki, M.; Leverick, G. M.; Amanchukwu, C. V.; Katayama, Y.; Kwabi, D. G.; Barde, F.; Hammond, P. T.; Shao-Horn, Y., The Role of Iodide in the Formation of Lithium Hydroxide in Lithium-Oxygen Batteries. *Energy & Environmental Science* **2017,** *10* (8), 1828-1842.
44. Papp, J. K.; Forster, J. D.; Burke, C. M.; Kim, H. W.; Luntz, A. C.; Shelby, R. M.; Urban, J. J.; McCloskey, B. D., Poly(Vinylidene Fluoride) (PVDF) Binder Degradation in Li-O_2 Batteries: A Consideration for the Characterization of Lithium Superoxide. *Journal of Physical Chemistry Letters* **2017,** *8* (6), 1169-1174.
45. Johnson, L.; Li, C.; Liu, Z.; Chen, Y.; Freunberger, S. A.; Ashok, P. C.; Praveen, B. B.; Dholakia, K.; Tarascon, J.-M.; Bruce, P. G., The Role of LiO_2 Solubility in O_2 Reduction in Aprotic Solvents and Its Consequences for Li–O_2 Batteries. *Nature Chemistry* **2014,** *6* (12), 1091-1099.
46. Giordani, V.; Tozier, D.; Tan, H.; Burke, C. M.; Gallant, B. M.; Uddin, J.; Greer, J. R.; McCloskey, B. D.; Chase, G. V.; Addison, D., A Molten Salt Lithium–Oxygen Battery. *Journal of the American Chemical Society* **2016,** *138* (8), 2656-2663.
47. Garcia, J. M.; Horn, H. W.; Rice, J. E., Dominant Decomposition Pathways for Ethereal Solvents in Li-O_2 Batteries. *Journal of Physical Chemistry Letters* **2015,** *6* (10), 1795-1799.
48. Meini, S.; Piana, M.; Beyer, H.; Schwämmlein, J.; Gasteiger, H. A., Effect of Carbon Surface Area on First Discharge Capacity of Li-O_2 Cathodes and Cycle-Life Behavior in Ether-Based Electrolytes. *Journal of The Electrochemical Society* **2012,** *159* (12), A2135-A2142.
49. Gerbig, O.; Merkle, R.; Maier, J., Electron and Ion Transport in Li_2O_2. *Advanced Materials* **2013,** *25* (22), 3129-3133.
50. Højberg, J.; McCloskey, B. D.; Hjelm, J.; Vegge, T.; Johansen, K.; Norby, P.; Luntz, A. C., An Electrochemical Impedance Spectroscopy Investigation of the Overpotentials in Li–O_2 Batteries. *ACS Applied Materials & Interfaces* **2015,** *7* (7), 4039-4047.
51. Meini, S.; Piana, M.; Tsiouvaras, N.; Garsuch, A.; Gasteiger, H. A., The Effect of Water on the Discharge Capacity of a Non-Catalyzed Carbon Cathode for Li-O_2 Batteries. *Electrochemical and Solid-State Letters* **2012,** *15* (4), A45-A48.
52. Schwenke, K. U.; Metzger, M.; Restle, T.; Piana, M.; Gasteiger, H. A., The Influence of Water and Protons on Li_2O_2 Crystal Growth in Aprotic Li-O_2 Cells. *Journal of The Electrochemical Society* **2015,** *162* (4), A573-A584.

53. Mayer, U.; Gutmann, V.; Gerger, W., The Acceptor Number — a Quantitative Empirical Parameter for the Electrophilic Properties of Solvents. *Monatshefte für Chemie* **1975,** *106* (6), 1235-1257.
54. Gutmann, V.; Wychera, E., Coordination Reactions in Non Aqueous Solutions - the Role of the Donor Strength. *Inorganic and Nuclear Chemistry Letters* **1966,** *2* (9), 257-260.
55. Herranz, J.; Garsuch, A.; Gasteiger, H. A., Using Rotating Ring Disc Electrode Voltammetry to Quantify the Superoxide Radical Stability of Aprotic Li-Air Battery Electrolytes. *Journal of Physical Chemistry C* **2012,** *116* (36), 19084-19094.
56. Black, R.; Oh, S. H.; Lee, J.-H.; Yim, T.; Adams, B.; Nazar, L. F., Screening for Superoxide Reactivity in Li-O_2 Batteries: Effect on Li_2O_2/LiOH Crystallization. *Journal of the American Chemical Society* **2012,** *134* (6), 2902-2905.
57. Leskes, M.; Drewett, N. E.; Hardwick, L. J.; Bruce, P. G.; Goward, G. R.; Grey, C. P., Direct Detection of Discharge Products in Lithium–Oxygen Batteries by Solid-State NMR Spectroscopy. *Angewandte Chemie* **2012,** *124* (34), 8688-8691.
58. McCloskey, B. D.; Bethune, D. S.; Shelby, R. M.; Mori, T.; Scheffler, R.; Speidel, A.; Sherwood, M.; Luntz, A. C., Limitations in Rechargeability of Li-O_2 Batteries and Possible Origins. *Journal of Physical Chemistry Letters* **2012**, 3043-3047.
59. Khetan, A.; Luntz, A.; Viswanathan, V., Trade-Offs in Capacity and Rechargeability in Nonaqueous Li–O_2 Batteries: Solution-Driven Growth Versus Nucleophilic Stability. *Journal of Physical Chemistry Letters* **2015**, 1254-1259.
60. Schmeisser, M.; Illner, P.; Puchta, R.; Zahl, A.; van Eldik, R., Gutmann Donor and Acceptor Numbers for Ionic Liquids. *Chemistry – A European Journal* **2012,** *18* (35), 10969-10982.
61. Walker, W.; Giordani, V.; Uddin, J.; Bryantsev, V. S.; Chase, G. V.; Addison, D., A Rechargeable Li–O_2 Battery Using a Lithium Nitrate/N,N-Dimethylacetamide Electrolyte. *Journal of the American Chemical Society* **2013,** *135* (6), 2076-2079.
62. Uddin, J.; Bryantsev, V. S.; Giordani, V.; Walker, W.; Chase, G. V.; Addison, D., Lithium Nitrate as Regenerable SEI Stabilizing Agent for Rechargeable Li/O_2 Batteries. *Journal of Physical Chemistry Letters* **2013,** *4* (21), 3760-3765.
63. Laoire, C. O.; Mukerjee, S.; Abraham, K. M.; Plichta, E. J.; Hendrickson, M. A., Influence of Nonaqueous Solvents on the Electrochemistry of Oxygen in the Rechargeable Lithium-Air Battery. *Journal of Physical Chemistry C* **2010,** *114* (19), 9178-9186.
64. Laoire, C. O.; Mukerjee, S.; Abraham, K. M.; Plichta, E. J.; Hendrickson, M. A., Elucidating the Mechanism of Oxygen Reduction for Lithium-Air Battery Applications. *Journal of Physical Chemistry C* **2009,** *113* (46), 20127-20134.
65. Peng, Z.; Freunberger, S. A.; Hardwick, L. J.; Chen, Y.; Giordani, V.; Barde, F.; Novak, P.; Graham, D.; Tarascon, J.-M.; Bruce, P. G., Oxygen Reactions in a Non-Aqueous Li^+ Electrolyte. *Angewandte Chemie-International Edition* **2011,** *50* (28), 6351-6355.
66. Lu, Y. C.; Gallant, B. M.; Kwabi, D. G.; Harding, J. R.; Mitchell, R. R.; Whittingham, M. S.; Shao-Horn, Y., Lithium-Oxygen Batteries: Bridging Mechanistic Understanding and Battery Performance. *Energy & Environmental Science* **2013,** *6* (3), 750-768.
67. Iliksu, M.; Khetan, A.; Yang, S.; Simon, U.; Pitsch, H.; Sauer, D. U., Elucidation and Comparison of the Effect of LiTFSI and $LiNO_3$ Salts on Discharge Chemistry in Nonaqueous Li-O_2 Batteries. *ACS Applied Materials & Interfaces* **2017,** *9* (22), 19319-19325.
68. Adams, B. D.; Radtke, C.; Black, R.; Trudeau, M. L.; Zaghib, K.; Nazar, L. F., Current Density Dependence of Peroxide Formation in the Li-O_2 Battery and Its Effect on Charge. *Energy & Environmental Science* **2013,** *6* (6), 1772-1778.
69. Erlich, R. H.; Popov, A. I., Spectroscopic Studies of Ionic Solvation. X. Study of the Solvation of Sodium Ions in Nonaqueous Solvents by Sodium-23 Nuclear Magnetic Resonance. *Journal of the American Chemical Society* **1971,** *93* (22), 5620-5623.
70. Cretzmeyer, J. W. Process for Producing Anhydrous Lithium Perchlorate. 1963.

71. Cahen, Y. M.; Handy, P. R.; Roach, E. T.; Popov, A. I., Spectroscopic Studies of Ionic Solvation. XVI. Lithium-7 and Chlorine-35 Nuclear Magnetic Resonance Studies in Various Solvents. *Journal of Physical Chemistry* **1975,** *79* (1), 80-85.
72. Linert, W.; Jameson, R. F.; Taha, A., Donor Numbers of Anions in Solution: The Use of Solvatochromic Lewis Acid-Base Indicators. *Journal of the Chemical Society, Dalton Transactions* **1993,** (21), 3181-3186.
73. Gal, J.-F.; Laurence, C., Comment on the Article "Gutmann Donor and Acceptor Numbers for Ionic Liquids" by M. Schmeisser, P. Illner, R. Puchta, A. Zahl, and R. Van Eldik (Chem. Eur. J. 2012, 18, 10969–10982). *Chemistry – A European Journal* **2013,** *19* (49), 16832-16834.
74. Marcus, Y., Thermodynamics of Solvation of Ions. Part 5.-Gibbs Free Energy of Hydration at 298.15 K. *Journal of the Chemical Society, Faraday Transactions* **1991,** *87* (18), 2995-2999.
75. Bryantsev, V. S.; Diallo, M. S.; Goddard Iii, W. A., Calculation of Solvation Free Energies of Charged Solutes Using Mixed Cluster/Continuum Models. *Journal of Physical Chemistry B* **2008,** *112* (32), 9709-9719.
76. Ising, E., Beitrag Zur Theorie Des Ferromagnetismus. *Zeitschrift fur Physik* **1925,** *31* (1), 253-8.
77. Sethna, J., *Statistical Mechanics: Entropy, Order Parameters, and Complexity*. Oxford University Press: 2006; Vol. 14.
78. Sharon, D.; Hirsberg, D.; Afri, M.; Chesneau, F.; Lavi, R.; Frimer, A. A.; Sun, Y.-K.; Aurbach, D., Catalytic Behavior of Lithium Nitrate in Li-O_2 Cells. *ACS Applied Materials & Interfaces* **2015**.
79. McCloskey, B. D.; Garcia, J. M.; Luntz, A. C., Chemical and Electrochemical Differences in Nonaqueous Li-O_2 and Na-O_2 Batteries. *Journal of Physical Chemistry Letters* **2014**, 1230-1235.
80. Landa-Medrano, I.; Olivares-Marín, M.; Bergner, B.; Pinedo, R.; Sorrentino, A.; Pereiro, E.; Ruiz de Larramendi, I.; Janek, J.; Rojo, T.; Tonti, D., Potassium Salts as Electrolyte Additives in Lithium–Oxygen Batteries. *Journal of Physical Chemistry C* **2017,** *121* (7), 3822-3829.
81. Ding, F.; Xu, W.; Chen, X.; Zhang, J.; Shao, Y.; Engelhard, M. H.; Zhang, Y.; Blake, T. A.; Graff, G. L.; Liu, X.; Zhang, J.-G., Effects of Cesium Cations in Lithium Deposition Via Self-Healing Electrostatic Shield Mechanism. *Journal of Physical Chemistry C* **2014,** *118* (8), 4043-4049.
82. Ding, F.; Xu, W.; Graff, G. L.; Zhang, J.; Sushko, M. L.; Chen, X.; Shao, Y.; Engelhard, M. H.; Nie, Z.; Xiao, J.; Liu, X.; Sushko, P. V.; Liu, J.; Zhang, J.-G., Dendrite-Free Lithium Deposition Via Self-Healing Electrostatic Shield Mechanism. *Journal of the American Chemical Society* **2013,** *135* (11), 4450-4456.
83. Matsuda, S.; Kubo, Y.; Uosaki, K.; Nakanishi, S., Potassium Ions Promote Solution-Route Li_2O_2 Formation in the Positive Electrode Reaction of Li-O_2 Batteries. *Journal of Physical Chemistry Letters* **2017,** *8* (6), 1142-1146.
84. Landa-Medrano, I.; Ruiz de Larramendi, I.; Rojo, T., Modifying the Orr Route by the Addition of Lithium and Potassium Salts in Na-O_2 Batteries. *Electrochimica Acta* **2018,** *263*, 102-109.
85. Wypych, G., Knovel Solvents - a Properties Database. ChemTec Publishing.
86. Haskins, J. B.; Bauschlicher, C. W.; Lawson, J. W., Ab Initio Simulations and Electronic Structure of Lithium Doped Ionic Liquids: Structure, Transport, and Electrochemical Stability. *Journal of Physical Chemistry B* **2015**.
87. Haskins, J. B.; Wu, J. J.; Lawson, J. W., Computational and Experimental Study of Li-Doped Ionic Liquids at Electrified Interfaces. *Journal of Physical Chemistry C* **2016,** *120* (22), 11993-12011.

88. Sharon, D.; Afri, M.; Noked, M.; Garsuch, A.; Frimer, A. A.; Aurbach, D., Oxidation of Dimethyl Sulfoxide Solutions by Electrochemical Reduction of Oxygen. *Journal of Physical Chemistry Letters* **2013,** *4* (18), 3115-3119.
89. Ottakam Thotiyl, M. M.; Freunberger, S. A.; Peng, Z.; Bruce, P. G., The Carbon Electrode in Nonaqueous Li–O_2 Cells. *Journal of the American Chemical Society* **2012,** *135* (1), 494-500.
90. Bryantsev, V. S.; Giordani, V.; Walker, W.; Blanco, M.; Zecevic, S.; Sasaki, K.; Uddin, J.; Addison, D.; Chase, G. V., Predicting Solvent Stability in Aprotic Electrolyte Li-Air Batteries: Nucleophilic Substitution by the Superoxide Anion Radical ($O_2^{\bullet-}$). *Journal of Physical Chemistry A* **2011,** *115* (44), 12399-12409.
91. Bryantsev, V. S.; Uddin, J.; Giordani, V.; Walker, W.; Addison, D.; Chase, G. V., The Identification of Stable Solvents for Nonaqueous Rechargeable Li-Air Batteries. *Journal of The Electrochemical Society* **2013,** *160* (1), A160-A171.
92. Adams, B. D.; Black, R.; Williams, Z.; Fernandes, R.; Cuisinier, M.; Berg, E. J.; Novak, P.; Murphy, G. K.; Nazar, L. F., Towards a Stable Organic Electrolyte for the Lithium Oxygen Battery. *Advanced Energy Materials* **2015,** *5* (1), 1400867.
93. Kundu, D.; Black, R.; Adams, B.; Harrison, K.; Zavadil, K.; Nazar, L. F., Nanostructured Metal Carbides for Aprotic Li-O_2 Batteries: New Insights into Interfacial Reactions and Cathode Stability. *Journal of Physical Chemistry Letters* **2015,** *6* (12), 2252-2258.
94. Adams, B. D.; Black, R.; Radtke, C.; Williams, Z.; Mehdi, B. L.; Browning, N. D.; Nazar, L. F., The Importance of Nanometric Passivating Films on Cathodes for Li-Air Batteries. *ACS Nano* **2014,** *8* (12), 12483-12493.
95. Chase, G. V.; Zecevic, S.; Walker, W. T.; Uddin, J.; Sasaki, K. A.; Giordani, V.; Bryantsev, V.; Blanco, M.; Addison, D. D. Soluble Oxygen Evolving Catalysts for Rechargeable Metal-Air Batteries. US 20120028137 A1, 2012.
96. Chen, Y. H.; Freunberger, S. A.; Peng, Z. Q.; Fontaine, O.; Bruce, P. G., Charging a Li-O_2 Battery Using a Redox Mediator. *Nature Chemistry* **2013,** *5* (6), 489-494.
97. Bergner, B. J.; Schurmann, A.; Peppler, K.; Garsuch, A.; Janek, J., Tempo: A Mobile Catalyst for Rechargeable Li-O_2 Batteries. *Journal of the American Chemical Society* **2014,** *136* (42), 15054-15064.
98. Kundu, D.; Black, R.; Adams, B.; Nazar, L. F., A Highly Active Low Voltage Redox Mediator for Enhanced Rechargeability of Lithium-Oxygen Batteries. *ACS Central Science* **2015,** *1* (9), 510-515.
99. Sun, D.; Shen, Y.; Zhang, W.; Yu, L.; Yi, Z. Q.; Yin, W.; Wang, D.; Huang, Y. H.; Wang, J.; Wang, D. L.; Goodenough, J. B., A Solution-Phase Bifunctional Catalyst for Lithium-Oxygen Batteries. *Journal of the American Chemical Society* **2014,** *136* (25), 8941-8946.
100. Kwak, W.-J.; Hirshberg, D.; Sharon, D.; Shin, H.-J.; Afri, M.; Park, J.-B.; Garsuch, A.; Chesneau, F. F.; Frimer, A. A.; Aurbach, D.; Sun, Y.-K., Understanding the Behavior of Li-Oxygen Cells Containing LiI. *Journal of Materials Chemistry A* **2015,** *3* (16), 8855-8864.
101. Liu, T.; Leskes, M.; Yu, W.; Moore, A. J.; Zhou, L.; Bayley, P. M.; Kim, G.; Grey, C. P., Cycling Li-O_2 Batteries Via LiOH Formation and Decomposition. *Science* **2015,** *350* (6260), 530-533.
102. Lim, H. D.; Song, H.; Kim, J.; Gwon, H.; Bae, Y.; Park, K. Y.; Hong, J.; Kim, H.; Kim, T.; Kim, Y. H.; Lepro, X.; Ovalle-Robles, R.; Baughman, R. H.; Kang, K., Superior Rechargeability and Efficiency of Lithium-Oxygen Batteries: Hierarchical Air Electrode Architecture Combined with a Soluble Catalyst. *Angewandte Chemie-International Edition* **2014,** *53* (15), 3926-3931.
103. Kwak, W.-J.; Hirshberg, D.; Sharon, D.; Afri, M.; Frimer, A. A.; Jung, H.-G.; Aurbach, D.; Sun, Y.-K., Li-O_2 Cells with LiBr as an Electrolyte and a Redox Mediator. *Energy & Environmental Science* **2016**.

104. Liu, T.; Kim, G.; Carretero-González, J.; Castillo-Martínez, E.; Grey, C. P., Response to Comment on "Cycling Li-O_2 Batteries Via LiOH Formation and Decomposition". *Science* **2016,** *352* (6286), 667-667.
105. Liu, T.; Kim, G.; Carretero-González, J.; Castillo-Martínez, E.; Bayley, P. M.; Liu, Z.; Grey, C. P., Response to Comment on "Cycling Li-O_2 Batteries Via LiOH Formation and Decomposition". *Science* **2016,** *352* (6286), 667-667.
106. Narayanan, S. R.; Surampudi, S.; Attia, A. I.; Bankston, C. P., Analysis of Redox Additive-Based Overcharge Protection for Rechargeable Lithium Batteries. *Journal of The Electrochemical Society* **1991,** *138* (8), 2224-2229.
107. Kulyukhin, S. A., Fundamental and Applied Aspects of the Chemistry of Radioactive Iodine in Gas and Aqueous Media. *Russian Chemical Reviews* **2012,** *81* (10), 960-982.
108. Datta, J.; Bhattacharya, A.; Kundu, K. K., Relative Standard Electrode Potentials of I_3-/I-, I_2/I_3-, and I_2/I- Redox Couples and the Related Formation Constants of I_3- in Some Pure and Mixed Dipolar Aprotic Solvents. *Bulletin of the Chemical Society of Japan* **1988,** *61* (5), 1735-1742.
109. Li, Z.; Ganapathy, S.; Xu, Y.; Heringa, J. R.; Zhu, Q.; Chen, W.; Wagemaker, M., Understanding the Electrochemical Formation and Decomposition of Li_2O_2 and LiOH with Operando X-Ray Diffraction. *Chemistry of Materials* **2017,** *29* (4), 1577-1586.
110. Ma, S.; Wang, J.; Huang, J.; Zhou, Z.; Peng, Z., Unveiling the Complex Effects of H_2o on Discharge–Recharge Behaviors of Aprotic Lithium–O_2 Batteries. *Journal of Physical Chemistry Letters* **2018,** *9* (12), 3333-3339.
111. Tomita, K.; Noguchi, H.; Uosaki, K., Effect of Water and HF on the Distribution of Discharge Products at Li-O_2 Battery Cathode. *ACS Applied Energy Materials* **2018**.
112. Kwabi, D. G.; Batcho, T. P.; Feng, S.; Giordano, L.; Thompson, C. V.; Shao-Horn, Y., The Effect of Water on Discharge Product Growth and Chemistry in Li-O_2 Batteries. *Physical Chemistry Chemical Physics* **2016,** *18* (36), 24944-24953.
113. Iwamoto, R. T., Solvent Effects on the Electro-Oxidation of Iodide Ion. *Analytical Chemistry* **1959,** *31* (5), 955-955.
114. Hanson, K. J.; Tobias, C. W., Electrochemistry of Iodide in Propylene Carbonate: I . Cyclic Voltammetry Monitored by Optical Spectroscopy. *Journal of The Electrochemical Society* **1987,** *134* (9), 2204-2210.
115. Bentley, C. L.; Bond, A. M.; Hollenkamp, A. F.; Mahon, P. J.; Zhang, J., Voltammetric Determination of the Iodide/Iodine Formal Potential and Triiodide Stability Constant in Conventional and Ionic Liquid Media. *Journal of Physical Chemistry C* **2015,** *119* (39), 22392-22403.
116. Vojinovic, V.; Mentus, S.; Komnenic, V., Bromide Oxidation and Bromine Reduction in Propylene Carbonate. *Journal of Electroanalytical Chemistry* **2003,** *547* (1), 109-113.
117. Yang, H.; Wang, Q.; Zhang, R.; Trimm, B. D.; Whittingham, M. S., The Electrochemical Behaviour of TTF in Li-O_2 Batteries Using a TEGDME-Based Electrolyte. *Chemical Communications* **2016**.
118. Piana, M.; Wandt, J.; Meini, S.; Buchberger, I.; Tsiouvaras, N.; Gasteiger, H. A., Stability of a Pyrrolidinium-Based Ionic Liquid in Li-O_2 Cells. *Journal of The Electrochemical Society* **2014,** *161* (14), A1992-A2001.
119. Ohzuku, T.; Kitagawa, M.; Hirai, T., Electrochemistry of Manganese Dioxide in Lithium Nonaqueous Cell: III . X ‐ Ray Diffractional Study on the Reduction of Spinel ‐ Related Manganese Dioxide. *Journal of The Electrochemical Society* **1990,** *137* (3), 769-775.